Inaugural Dissertation

Submitted to

Combined Faculty of Mathematics, Engineering and Natural Siences

of the

Ruprecht - Karls - University

Heidelberg , Germany

Presented by **Maryam Najafian Jazi**

Born in: Isfahan, Iran

Oral examination: 16th of December 2022

Hippocampal representations of homing based on path integration

Referees:

Prof. Hannah Monyer
Dr. Alexander Groh
Dr. Amit Agarwal
Dr. Kevin Allen

Declaration

Declaration according to § 8 (3) b and c of the doctoral degree regulations. a. I hereby declare that I have written this dissertation myself, and while writing it, I have not used any other sources or materials except the ones mentioned in the reference section. b. I hereby declare that I have not applied to be examined at any other institution. I also have not used this dissertation in this or any other form at any other institution as an examination paper or any other faculty as a dissertation.

Table of Contents

Summary

The ability to plan and execute a journey to a specific destination is essential for the survival of individuals of different species. Purposeful navigation can be achieved using landmark-based navigation and path integration. During path integration, the animal integrates self-motion information to estimate its location. Path integration is needed when external landmarks, such as visual landmarks, odour or auditory cues, are unavailable or when the animal visits unfamiliar environments. The study of the neuronal basis of path integration has been hampered by the lack of behavioural paradigm assessing path integration that allows simultaneous *in vivo* electrophysiological recordings in freely moving animals. Lesion studies have shown that the hippocampus and parahippocampal area are involved in path integration but the firing activity of the spatially selective cells, such as place cells, during path integration is unknown.

Here, we developed a new behavioural paradigm (Automated Path Integration or AutoPI) to study homing behaviour based on path integration. In this task, a mouse finds a movable lever on the arena, presses it and returns to its home base to collect a food reward. Using the AutoPI task, we could record the firing pattern of the neurons in a large arena and investigate their spatial properties during homing behaviour. We used silicon probes to record the activity of hippocampal pyramidal cells when mice were running in AutoPI.

By comparing the firing activity of neurons in the AutoPI task and during random foraging, we detected a complete reorganisation of hippocampal ensembles. We also found that several hippocampal pyramidal cells were firing when the animal was close to the lever (lever-anchored cells), independently of the lever's location on the arena. The spatial stability of lever-anchored cells was reduced during the trials with inaccurate homing. Moreover, the firing activity of lever-anchored cells also predicted the homing direction of the mice. These findings describe how hippocampal neurons with object-anchored firing fields contribute to homing behavior based on path integration.

Zusammenfassung

Die Fähigkeit, einen Weg zu einem bestimmten Ziel zu planen und durchzuführen, ist für das Überleben von Individuen verschiedener Arten von entscheidender Bedeutung. Eine zielgerichtete Navigation kann mit Hilfe der landmarkenbasierten Navigation und der Pfadintegration erreicht werden. Bei der Pfadintegration integriert das Tier Informationen über die Eigenbewegung, um seinen Standort in der Umgebung zu bestimmen. Die Pfadintegration ist erforderlich, wenn externe Landmarken wie visuelle Orientierungspunkte, Geruchs- oder Hörzeichen nicht zur Verfügung stehen oder wenn das Tier eine ihm unbekannte Umgebung aufsucht. Die Untersuchung der Pfadintegration war dadurch limitiert, dass es bisher kein Verhaltensparadigma gab, das elektrophysiologische *In-vivo*-Aufzeichnungen ermöglichte, während ein Tier eine große Umgebung erkundet. Der Hippocampus und das parahippocampale Areal sind an der Pfadintegration beteiligt. Allerdings ist die Aktivität der räumlich selektiven Zellen, wie z. B. der Ortszellen, während der Pfadintegration unbekannt.

Hier haben wir ein neues Verhaltensparadigma (Automated Path Integration oder AutoPI) entwickelt, um das auf der Pfadintegration basierende Homing-Verhalten zu untersuchen. Bei dieser Aufgabe müssen die Mäuse einen beweglichen Hebel in der Arena finden, ihn betätigen und zur Belohnung zur Ausgangsbasis zurückkehren. Mit Hilfe der AutoPI-Aufgabe können wir das Feuerungsmuster der Neuronen in einer großen Arena aufzeichnen und ihre räumlichen Eigenschaften während des Homings in Licht und Dunkelheit untersuchen. Mit Hilfe von Silizium-Elektroden haben wir die Aktivität von Pyramidenzellen im Hippocampus während AutoPI und bei der zufälligen Futtersuche aufgezeichnet.

Durch den Vergleich der Zellaktivität bei der AutoPI-Aufgabe und bei der zufälligen Futtersuche konnten wir eine vollständige Reorganisation der Hippocampus-Ensembles feststellen. Wir konnten auch beobachten, dass mehrere Pyramidenzellen im Hippocampus feuern, wenn sich das Tier in der Nähe des Hebels befindet (Hebel-verankerte Zellen), unabhängig von der Position des Hebels in der

Arena. Die räumliche Stabilität der Hebel-verankerten Zellen war reduziert in Versuchen, die ungenaues Homing aufzeigten. Dadurch konnte die Zielrichtung der Mäuse durch die Aktivität der Hebel-verankerten Zellen vorhergesagt werden. Diese Ergebnisse beschreiben wie hippocampale Neuronen, die Objekt-verankerte Feuermuster aufweisen, zum Homing-Verhalten mittels Pfadintegration beitragen.

1. Introduction

1.1 Path integration

Navigation is the ability to plan and execute a route toward a goal. Navigational strategies include landmark-based navigation and path integration (PI). During landmark-based navigation, the animal uses external cues to navigate toward a place. PI, on the other hand, allows the animal to return to their starting point without external cues. PI, or 'dead-reckoning', was first described by Charles Darwin in 1873. Darwin argued that both vertebrates and invertebrates could return to their starting point using the integration of self-motion information. During PI, the animal integrates information from the self-motion cues (such as vestibular information, optic flow and copies of motor commands) to calculate its current location and orientation relative to a starting point. This constant update enables the animal to estimate the direct way back to its home at any time during an exploratory journey (Walker, 1992; Gallistel & Cramer, 1996).

Since Darwin, PI has been observed in species ranging from insects to humans (Ariane S Etienne & Jeffery, 2004, Ariane S. Etienne et al., 1996). For example, desert ants can return to their nest after an outward journey of hundred of meters in a featureless desert (Wehner & Srinivasan, 1981). In addition, night-active rodents use PI to navigate during the night when they can not rely on external landmarks (Ariane S. Etienne et al., 1996). Finally, humans can accomplish navigational tasks that require the estimation of active or passive displacements using self-motion cues (Wan et al., 2012; Segen et al., 2021).

PI is an essential mechanism for the animal who has to return home without external cues. However, when the external landmarks are absent, PI suffers from an important limitations: it accumulates error with time. Its been shown that animals estimate their position using multiple sensory modalities such as proprioceptive,

vestibular, and visual optic flow signals. Each of these signals is processed in their respective sensory systems. They are then integrated in different brain areas, including brain stem nuclei and cortical regions. The integration of this multi-sensorial information leads to estimations of linear and angular velocity (Bassett & Taube, 2001; Britten, 2008). PI-related computations accumulate error in estimating the velocity (due to the systematic or unbias noise), the time elapsed from the previous events, and the velocity factor that is required to estimate the following displacement (Stangl et al., 2020). Because of this accumulation of noise, it has been proposed that during long-distance journeys the animal uses both path integration and landmark-base navigation to return home (Ariane S. Etienne et al., 1996; McNaughton et al., 2006; Etienne & Jeffery, 2004).

1.2 Path Integration In Mammals

Path integration is usually studied through homing behaviour. For instance, during the food-carrying task, the animal must search for a large amount of food in an arena and then return to its nest. One of the difficulties in studying path integration is confirming that the animal are not using external landmarks such as olfactory, visual or auditory cues while performing a PI task. Three methods are used to encourage the animal to rely on PI during homing. These methods includes 1) masking external landmarks (allocentric cues), 2) using an unfamiliar environment, and 3) creating conflict between idiotethic (self-motion cues) and external landmarks.

For example Etienne in 190 used the masking method to ensure that hamsters were using PI. The task of the hamsters was to find their pups in a random place in an arena, visit a fixed location to get a reward and return to their nest. While hamsters performed this homing task, Etienne used infrared light, pink noise and sawdust to mask the potential visual, auditory and olfactory cues (**Figure 1**, Ariane S. Etienne, 1980). The second method was to perform the homing experiment in an unfamiliar environment (Etienne et al., 1985). The third method was to create a conflict between

external cues such as proximal or distal cues and PI (A. S. Etienne et al., 1995; Ariane S. Etienne et al., 1986; A. S. Etienne et al., 1985; Etienne et al., 1990). For example, Etienne and her colleagues designed a circular arena surrounded by a symmetrical enclosure. Specific visual landmark panoramas were presented against the wall of the enclosure during the experiment. The arena and the animal's nest were rotated 90 degrees relative to the visual landmark before the start of the test trial. In this situation, the external panoramic landmarks associated with the nest entrance led the animal to the previous nest location. However, path integration directed the animal toward the new location of the nest (A. S. Etienne et al., 1995). Another way to creat a conflict between PI and external landmarks is to perform rotations of the animal that cannot be detected by the vestibular system. For example, gerbils were tested to retrieve their pups from the centre of an arena to their nest located at the border of the arena. The arena was rotated slowly when the gerbil was in the arena to manipulate the input to the path integration system. The arena was rotated with a very slow acceleration that is below the detection threshold of the vestibular system, so that the animal did not perceive the arena rotation. After the rotation, gerbils returned to their home in a direction that deviated from the nest by an angle equal to the arena rotation, indicating that their behavior was guided by path integration (Mittelstaedt & Mittelstaedt, 1980).

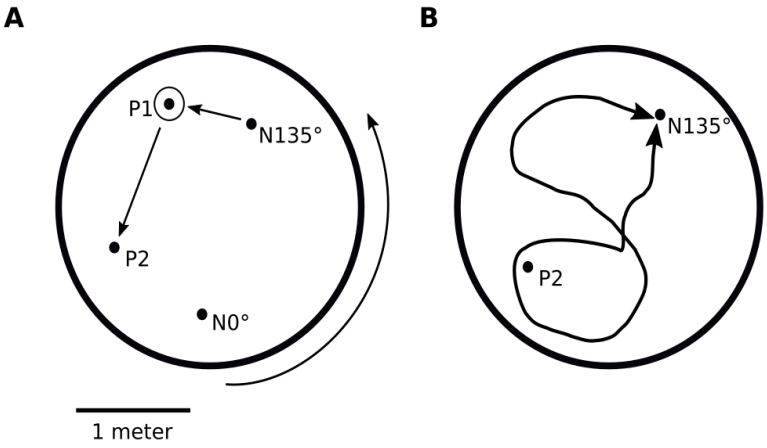

Figure 1. Homing through PI in the golden hamster A: Outward journey. Before the trial started, the arena with the nest under the arena was rotated 135 degrees. The nest moved from position N0° to position N135°. The hamster left the nest from position N135°, and searched for the pups under infrared light. The animal proceeded to point P1 and then goes to P2, where it is offered food and fills its pouches. B: Return paths. Only one return path is represented in which the animal did not reach the arena wall. This figure is adapted from Etienne and K. Jeffery 2004.

1.3 Neuronal Circuits Supporting Path Integration

Lesion studies were the first experiments investigating the brain areas essential for PI (Whishaw & Tomie, 1997). Previous works showed that damage to the hippocampus could result in behavioural deficit during spatial navigation paradigms such as Morris water maze and radial-arm maze tasks (O'Keefe et al., 1971; Morris et al., 1982; Jarrard, 1995, 1993; O'Keefe & Nadel, 1978). The animal uses the visual landmark navigation mechanism in the Morris water maze and radial-arm maze. O'Keefe and Nadel (1978) were probably the first to propose that the hippocampus could integrate self-motion cues during path integration. Wishaw and his colleagues were the first to test this hypothesis.

In a first study, Whishaw and Tomie (1997) performed fimbria-fornixlesions in rats to investigate whether homing behaviour depended on hippocampal formation. The fornix is a C-shape bundles that acts as one of the major outputs of the hippocampus (**Figure 2**). It was previously shown that fimbria-fornix lesions produce memory impairments typically observed after hippocampal lesions (Gaffan, 1974; Swanson and Cowan, 1977, 1979, Olton & Papas, 1979).

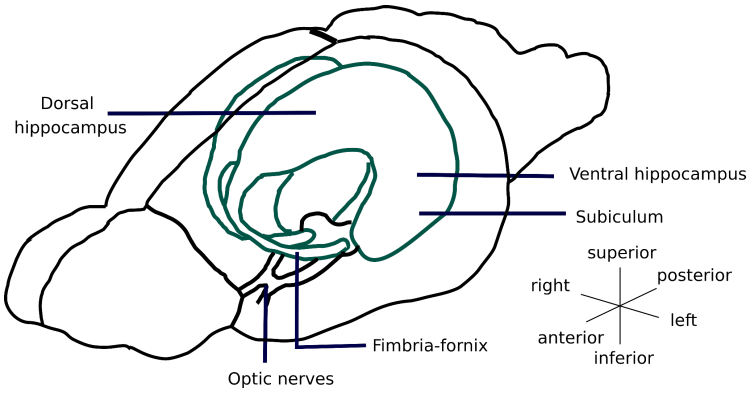

Figure 2. Fimbria fornix in the rodent brain. Fibmria are C-shape bundles that are part of the limbic system and provide the major input and output to the hippocampus. The C-shape bundles that seperate the two hippocampus are calles fimbria which are joining together again in the midbrain (called fornix body). The figrue is adapted from Cheung & Cardinal, 2005.

.

In the study by Whishaw and Tomie (1997), rats had to leave their nest under the arena and search for food in one of the 23 food wells. Rats would carry the large food pieces to their nest to eat (Whishaw, 1990; Whishaw & Dringenberg, 1992). During the training phase, the location of the home base remained the same. During the test session, the home base moved to a new location. Therefore, rats needed to use path integration to return to the new location of the home base. The experimental apparatus in this experiment, called food-carrying task, is shown in **Figure 3**. Rats with fimbria-fornix lesions were returning to the previous but incorrect home base location. Control rats could directly return to the new location of their nest. The data from this study suggested that fimbria-fornix lesioned rats were using visual landmarks to return to the previous location of the home base. However, they could not use PI to return to the new location of the home base. In the next experiment, Maaswinkel and his colleagues (1999) used masks and blindfolds on the control and hippocampal lesioned rats in the test phase (Maaswinkel et al., 1999). Control and hippocampus-lesioned rats returned to the familiar and incorrect home base location using visual cues. When

blindfolded, only control rats returned to the new location of the refuge cage. The author concluded that rats with hippocampal lesions could not use PI to return to the new location of the refuge cage in the absence of visual landmarks.

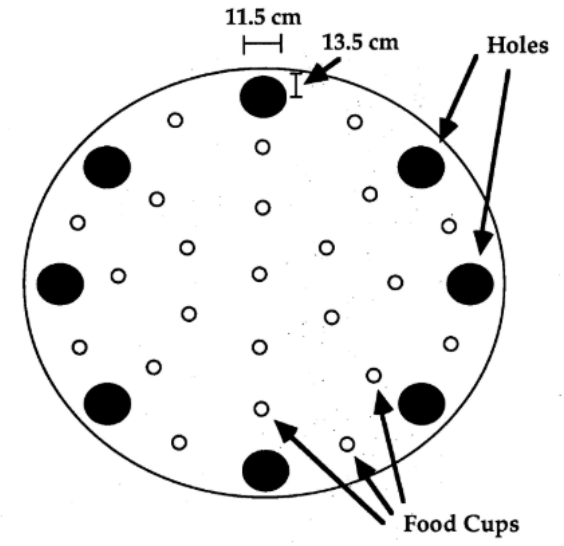

Figure 3. The food-carrying apparatus. The refuge cage is hidden beneath the surface of the circular open table, and the rat can enter and exit through a hole in the table surface. There are eight potential entrance and exit holes spaced equidistantly around the table. Locations of food cups are indicated by open circles (not drawn to scale). This figure is adapted from Whishaw & Tomie (1997).

The next step to test the neural basis of the path integration was to investigate whether the brain areas projecting to the hippocampus could also be involved in PI. It was shown that the vestibular and self-motion information reaches the hippocampus via the entorhinal, parietal and retrosplenial cortex (Save & Moghaddam, 1996; Smith, 1997). The role of the entorhinal cortex in path integration was first investigated by Parron and Save (2004). They tested homing accuracy of rats with lesions of the entorhinal or parietal cortex during a food-carrying task similar to that of Whishaw and Tomie (1997). To assess the homing accuracy of the animal during homing, they defined a variable called homing error. *Homing error* was defined as the angle between the

home base and the point at which the animal reached the arena's edge. Rats with entorhinal or parietal lesions had more homing errors (less accurate) during homing compared to control rats with sham lesions. These findings indicated that the entorhinal and parietal cortex contribute to homing behaviour. Further studies from Save and Poucet's laboratory showed that rats with medial entorhinal cortex lesions reduced their performance during homing. These results highlighted the essential role of the medial entorhinal cortex in PI (Van Cauter et al., 2012).

Another brain area connected to the hippocampus and entorhinal cortex is the medial septum. Inactivation of the medial septum strongly reduces the theta oscillation (6-10 HZ) in the hippocampus and entorhinal cortex (Rawlin et al., 1979; Mizumori et al., 1990; Koenig et al., 2011) and alters the firing activity of neurons in both regions (Koenig et al., 2011; Brandon et al., 2011). To test whether the medial septum plays a role in PI, Jacob and colleagues (2017) inactivated medial septum in rats during a new distance estimation task on a linear track. In this task, rats had to leave one end of the track to reach a Plexiglas platform and return to the starting point to receive a food reward. Rats had to estimate the distance run and return the same distance to get the reward. During the dark trial, the animal had to estimate the distance run based on self-motion cues and repeat this behaviour during returning. Besides, Injections of muscimol into the medial septum increased the variability of the responses when rats had to run 60 cm. Therefore, the authors suggested that the medial septum is involved in estimating the distance run and potentially PI (Jacob et al., 2017).

Later studies also showed that the retrosplenial cortex is involved in PI. For instance, Elduayen and Save (2014) tested rats with a lesion in the retrosplenial cortex in the food-carrying task. The lesioned rats and the control groups could return to the home base when the task was conducted in light. However, the performance of the rats with the retrosplenial lesion dropped when the task was performed in darkness (Elduayen & Save, 2014). In another study by Cooper and Mizomuri (1999), the

inactivation of the retrosplenial cortex impaired the performance of the rats in a radial arm maze during darkness. These results suggested that the retrosplenial cortex has an essential role in PI.

1.4 Hippocampus anatomy

Hippocampus formation is part of the limbic system in the medial temporal lobe in the shape of a curved tube similar to the seahorse (see **Figure 4**). The hippocampus formation includes the hippocampus proper containing CA1, CA2 and CA3, dentate gyrus, subicular complex and entorhinal cortex. The major input to the hippocampus is via the perforant path (major input of the hippocampus) that transfers information from layer II of the entorhinal cortex to the dendate gyrus. Axons in the perforant path have synaptic contact with the dendrites of granular cells. The granule cells in the dentate gyrus then project through their axons (mossy fibres) to the pyramidal cells in CA3. The pyramidal cells in CA3 then project ipsilaterally to CA1 pyramidal cells through Schaffer collaterals. The contralateral CA3 and CA1 cells transfer information through commissural connections. Pyramidal CA1 neurons project to the layer V of the entorhinal cortex forming the major output of the hippocampus. Neurons in layer II of the entorhinal cortex connect to the CA1 pyramidal neurons via temporoammonic pathway which then projects back their axons to the layer V of the enthrinal cortex.

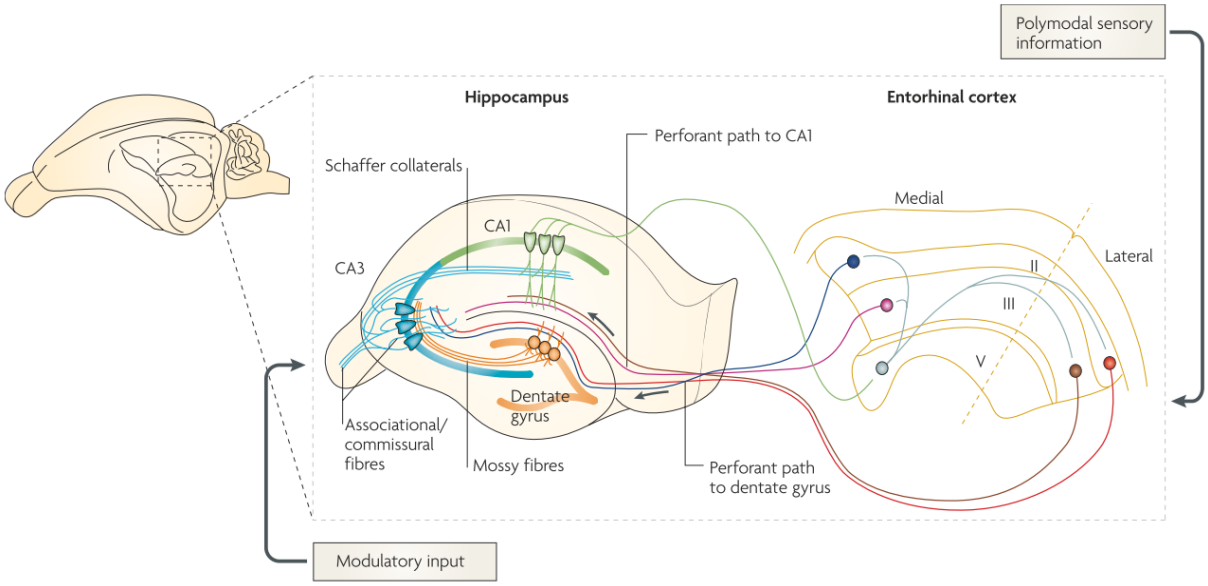

Figure 4. The basic anatomy of the Hippocampus. Basic anatomy of the hippocampus. The wiring diagram of the hippocampus is traditionally presented as a trisynaptic loop. In addition to the sequential trisynaptic circuit, there is a dense associative network interconnecting CA3 cells on the same side. CA3 pyramidal is also innervated by direct input from layer II cells of the entorhinal cortex (not shown). The distal apical dendrites of CA1 pyramidal neurons receive direct input from layer III cells of the entorhinal cortex. There is also substantial modulatory input to hippocampal neurons. The three major subfields have an elegant laminar organization in which the cell bodies are tightly packed in an interlocking C-shaped arrangement, with afferent fibres terminating on selective regions of the dendritic tree. The hippocampus is also home to a rich diversity of inhibitory neurons that are not shown in the figure. Adapted from Neves et al., 2008.

1.5 Spatial selective neurons contributing to path integration

1.5.1 Place cells

O'Keefe and Dostrovsky (1971) discovered the first spatially selective cells while recording from the dorsal part of the hippocampus. In this experiment, the spontaneous activity of the cells was recorded during behaviours such as eating, walking, grooming, drinking, sniffing or when the animal was restrained in a specific direction of the arena. Some cells in the hippocampus exhibited place-dependent activity in the arena independent of animal behaviour. Eight units from the 76 units recorded showed place-dependent activity in the arena. These cells were active when the animal was restrained in a particular part of the arena (place field) or faced in a specific direction (see **Figure 5**) (O'Keefe & Dostrosvky, 1976). These cells were later called place cells. It was afterwards suggested that the animal's location in its environment could be inferred from the joint activity of a small sample of place cells (Wilson & McNaughton, 1996). Therefore, place cells are the essential elements of a spatial internal cognitive map (O'Keefe & Dostrosvky, 1976; 1976; O'Keefe & Nadel, 1979; Moser et al., 2017).

Further studies in the late 1970s and 1980 were dedicated to investigating what causes the place cells to fire in a special location in the environment. These studies showed that place cells had a robust directional selectivity when the animal frequently ran on a restricted path in a radial arm maze with only one arm openned at a time (McNaughton et al., 1983). This study investigated the spatial properties of pyramidal cells recorded from the dorsal hippocampus (CA1 and CA3). The correlation between the firing activity of the cells with the animal’s direction, position and velocity was observed in this experiment. Pyramidal cells recorded from the CA1 region of the hippocampus illustrated a higher spatial/directional tuning than cells recorded from CA3

of the hippocampus. Also, the place fields of neurons recorded from the CA1 region were larger than that of the CA3 pyramidal cells.

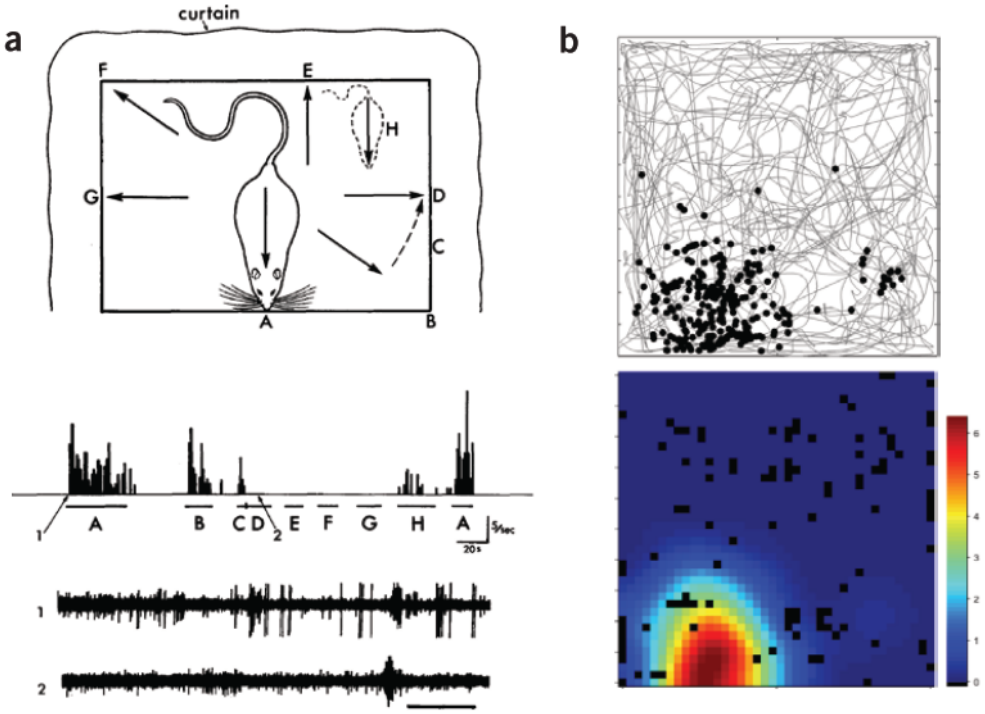

Figure 5. Discovery of place cells. (**a)** The first place cell that O'Keef and Dostrosvky recorded. Arrows and letters show positions at which the animal was restrained as it was pushed or coaxed around the test platform. Letters correspond to positions, and lines indicate periods of restraint. The firing rate of the cell is illustrated by the frequency histograms at the bottom of the figure. The bottom lines show spikes at the onset of the unit response at A (1) and during the absence of response at D (2). Calibration bar, 400 ms. (**b)** A place field as typically displayed today. Top: the animal trajectory is shown in grey lines, and the spike locations are displayed as black dots. Bottom: colour-coded rate map of the same cell; Dark red is the maximum firing rate, and dark blue is the minimum firing rate in this plot. Adapted from Moser et al. (2017).

Muller and Kubie (1987) later tested the effect of environmental changes on the firing activity of place cells. The experimental apparatus in this experiment was a

cylinder with a diameter of 76 cm and a height of 51 cm. The inferior wall of the cylinder was grey except for a white cue card attached to the wall of the arena. The first sets of manipulation showed that rotation of the cue card (in absence of the animal in the arena) would result in rotation of the place field with an equal angle. However, changing the cue card size did not affect the place field's size, shape or radial position in the arena. Removing the cue card from the cylinder wall had similar effects with no change in the place field's size, shape and radial position. However, it rotated the angular position of the fields unpredictably. When the arena's size was scaled, some cells increased their firing fields. Also, changing the shape of the environment from a circle to a rectangle increased the size of the place field on 36% of active cells in both environments. These results demonstrated that the place cells respond to the abstract features of the environment rather than the raw sensory changes in the environment (Muller et al., 1987).

Foraging studies were soon followed by studies investigating the external origins of place cell activity. For example, Gothard and his colleagues recorded a population of hippocampal place cells while a rat was running between a fixed reward site on one side and a movable reward site mounted on a sliding box (Gothard et al., 1996). First, rats were trained to run in a shuttle between a box at one end and a fixed reward site at the other. In the recording session, while the rat ran toward the fixed reward site, the other box was moved to a new location. The movement of the box created a mismatch between the initially learned relationship of the boxes and external landmarks in the rat's environment. Place cells were active at a fixed distance from the origin on the initial part of the journey. In contrast, place cells firing was more related to the fixed distance to the journey's destination on the final part of the trial. These results demonstrated that the position representation of the place cells was updated using path integration on the outward part of the journey where the box was located behind the animal. However, the field of the place cells aligned to the external stimulus farther along the journey.

Together the data suggested that path integration and external sensory information interact to update the animal's spatial representation.

In another study, O'Keefe and Burgess (1996) recorded the activity of place cells in four rectangular boxes. The difference between these boxes was in the length of one of two axes of the rectangle. Place cells fired at a fixed distance from one wall or a proportion of the distance from opposite walls. These results were similar with previous studies on linear track or open field representing the effect of PI in defining the firing activity of the place cells (Gothard et al., 1996a; Gothard et al., 1996b). Subsequently, Bjerknes and his colleagues (2018) recorded place cells in adults and premature rats (17th-34th days after birth; P17-P34) running on a linear track. Place cell firing patterns can be observed in premature rats from when they leave the nest (P16). However, other spatial selective cells in medial enthorinal cortex such as grid cells with period spatial firing patterns were not identified until the fourth week of life. Bjerknes and colleagues tested the distance-dependent firing activity of place cells in a linear track with different lengths. Both young and adult rats had place fields with a fixed distance from the start position of the track in light and dark. This result suggested that self-motion cues can be used to determine the position of the fields when the input from grid cells is unavailable (Bjerknes et al., 2018).

1.5.2 Head direction cells

Head-direction (HD) cells fire as a function of animal’s head direction in a horizontal plane independent of animal location or behaviour. HD cells were first discovered in the presubiculum (Taube et al., 1990a,b). Taube and his colleagues (1990) recorded HD cells from the dorsal-presubiculum in rats while running in a cylinder with a white cue card attached to the arena's wall (Taube et al., 1990). They found that some cells only fired when the animal's head faced a particular angle in

allocentric (map-based) coordinates called the cell preferred firing direction. The firing rate of the HD cells was near zero when the head of the animal was not toward the preferred head direction of the cell (see **Figure 6, b-c**). However, the firing rate of the HD cell increased linearly from zero if the animal shifted his head toward the preferred direction from either side in an angular range of 90 degrees away (Taube, 2007). HD cells later found also in the anterior dorsal thalamic nucleus (ADN) (Taube, 1995), lateral mammillary nuclei (Stackman & Taube, 1998), retrosplenial cortex and entorhinal cortex (Chen et al. 1994, Cho and Sharp 2001, Sargolini et al., 2006), dorsal striatum, medial precentral cortex (Wiener 1993, Mizumori et al. 2000), CA1 hippocampus (Leutgeb et al., 2000) and dorsal tegmental nucleus (DTN) (Taube, 2007).

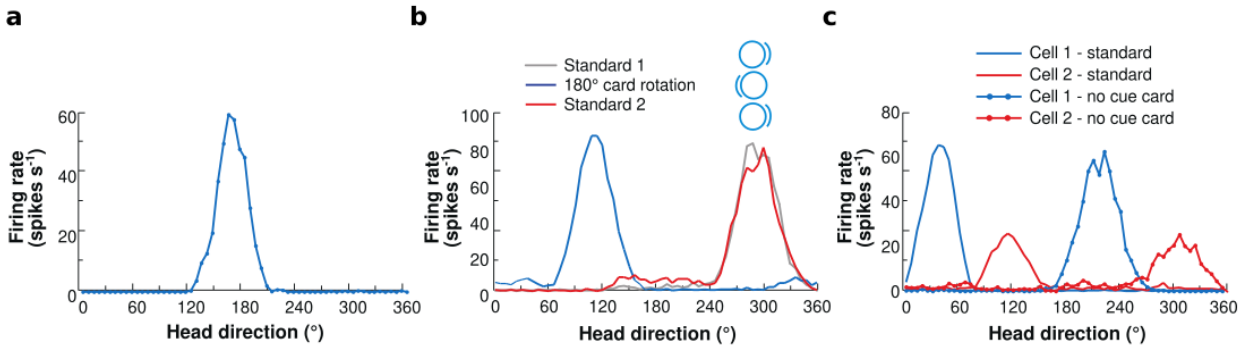

Figure 6. Discovery of head direcion cells. a: Firing rate versus head direction plot for a typical HD cell. Firing rates are shown plotted in 6◦ bins. **b:** Responses of an HD cell following a 180◦ rotation of the visual cue card. The cell's preferred firing direction shifted similarly to the cue rotation (blue line). It returned to its original orientation when the cue card was returned to its initial position (red line). The initial recording session is shown as a grey line. **c:** Responses of two HD cells were recorded simultaneously after removing the visual cue card. Both cells retained direction-specific firing without the visual cue, but their preferred firing directions shifted equally and remained in register with one another. Adopted from (Taube, 2007).

Taube and his colleagues performed sets of experiments to determine the environmental factors influencing the firing rate of HD cells. In the first set of

experiments, the environmental manipulation was to rotate the cue card attached to the cylinder wall as Muller and Kubie did for place cells (1987). The rotation of the cue card by 45 degrees caused a rotation in the preferred direction of the HD cells by an approximately equal amount. Rotation of the cue card for 90, 180, and 270 degrees induced the same rotation in the preferred direction of the HD cells. After the rotation of the cue card to its initial location, the preferred direction of the HD cells also returned to their initial values. Removal of the cue card caused only an unpredictable shift in the preferred direction of HD cells. Next, they tested whether the shape of the environment changed the prefered direction of HD cells. Changing the shape of the environment from a circular arena to a rectangular one, followed by a counter-clockwise rotation in a preferred direction of the HD (Taube et al., 1990b; Taube et al., 1990b; Taube, 1995). These results suggested that external landmarks in a familiar environment predominate over the PI mechanism and affect the preferred direct of the HD cells.

Some studies also investigated how HD cells fired when the visual landmarks conflicted with the idiothetic information (self-motion cues). For example, Goodridge and Taube (1995) recorded the activity of HD cells while rats were running in a cylinder with a cue card attached to the arena's wall. Afterwards, the rat was returned to the cylinder with the cue card removed from the arena's wall. The preferred direction of the HD cells shifted 30° in the absence of the cue card. The authors later argued that during the sessions without no cue card, the rat used PI resulted in an accumulation of errors in estimating the direction of the movement. The reintroduction of the familiar cue card to the cylinder caused an immediate shift from the preferred direction of the HD cells to their original established orientations. Together, these results suggested that the directional information from the idiothetic cues can be corrected in the presence of a salient visual landmark (Goodridge & Taube, 1995).

1.5.3 Grid cells

The entorhinal cortex is part of the neocortex in the medial temporal lobe. The entorhinal cortex is usually divided into the medial entorhinal cortex (MEC) and the lateral entorhinal cortex (LEC). In rodents, the MEC is located in the ventrocaudal region of the entorhinal cortex and is connected to the LEC and parasubiculum laterally and rostrally. The subiculum and presubiculum are anterior to the MEC, while the postrhinal cortex is adjusted dorsally. The MEC sends projections to the cortical and subcortical regions of the brain, such as the retrosplenial cortex, hippocampus, amygdala and medial septum (human: Witter et al., 2000; monkey: Witter and Amaral, 1991; rat: Naber et al., 2001; van Strien et al., 2009; Witter et al., 2017). The MEC has six principle layers (I-VI) that are divided into the superficial layers (I-III) and the deep layers (layer IV-VI). Layer II and III of the MEC provides the primary spatially modulated input to the hippocampus formation. Layer II preferentially projects to the dentate gyrus and CA3, but layer III provides inputs to CA3 and CA1 of the hippocampus. Spatial firing properties of the cells in superficial layers of the MEC were not studied until the 1990s (Fyhn et al., 2004).

Quirk and his colleagues (1992) recorded neurons from the superficial layers of the MEC to search for the origins of the place fields outside of the hippocampus. The cells recorded from the superficial layers of the MEC showed spatial-specific properties similar to what was recorded from CA1 hippocampal cells but with a smaller signal-to-noise ratio. Further experiments also showed that external visual cues could also control the spatial properties of the MEC cells, like place cells recorded from the hippocampus. Further studies on the spatial properties of cells in MEC were continued on 2005 when Hafting and his colleagues targeted tetrodes at the dorsal part of the MEC, which is the origin of most of the inputs to the dorsal hippocampus (McNaughton et al., 2006; Hafting et al., 2005). They found that a subset of neurons in dorsal MEC had multiple separated firing fields (**Figure 7**). These cells were later called grid cells

with firing fields that formed a regularly tessellating triangular (hexagons) covering the

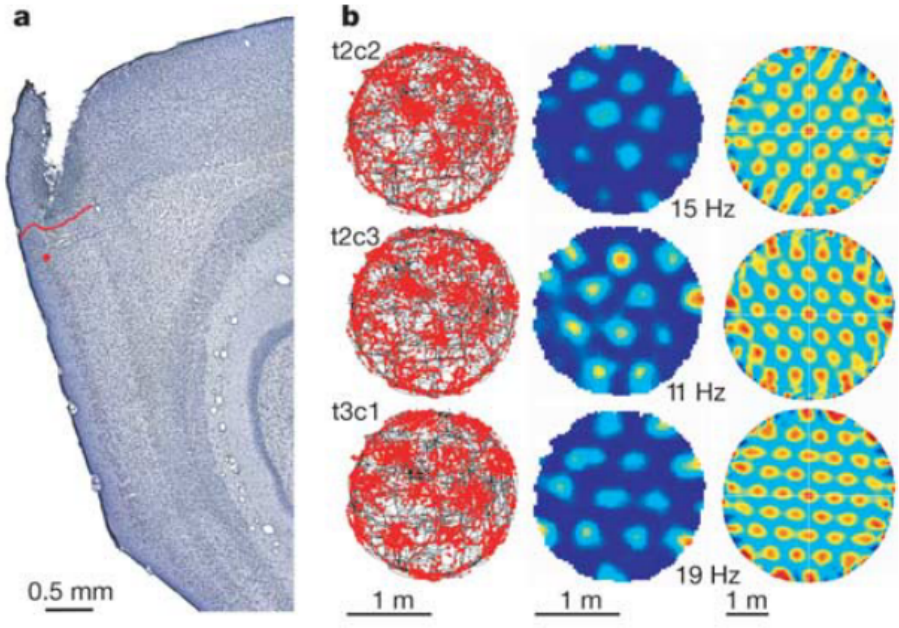

entire recording environment.

Figure 7. Grid cells have hexagonal firing fields. (a) Sagittal Nissl-stained section indicating the recording location (red dot) in layer II of the dMEC. The red line indicates the border to the postrhinal cortex. **(b)** Firing fields of three simultaneously recorded cells during 30 min of running in a large circular enclosure. Cell names refer to tetrode (t) and cell (c). The rat's trajectory (black) with superimposed spike locations (red) is left. Middle, colour-coded rate map with the peak rate indicated. Red is maximum; dark blue is zero. Right, spatial autocorrelation for each rate map. Adapted from Hafting et al., (2005).

Hafting and his colleagues calculated the grid cell's autocorrelogram to identify the cell's spatial properties. The autocorrelogram is the correlation of the signal with a shifted copy of itself. The autocorrelogram is usually used to identify the repeated pattern of a signal and its frequency. The autocorrelogram analysis of grid cells on the same tetrode suggested that the nearby grid cells share properties such as spacing, orientation and size of the field. The distance between the central peak and the inner hexagon's vertices in the autocorrelogram (spacing) was around 2.1 for the cells on the

same tetrode. The orientation of the grid pattern in the autocorrelogram was defined as the angle between the reference line (0 degrees) and the nearest vertex of the inner hexagon in the counterclockwise direction. The grid cell's orientations were minimally varied across cells recorded on the same tetrode. The last feature was the field's size, defined as the area covered by the central peak of the autocorrelogram.

The rotation of the cue card by 90 degrees caused the rotation with the same angle in the phase and orientation of the grid cell pattern. In the next set of experiments, Hafting and colleagues tested whether removing the external cues would change the grid pattern of the cells recorded from dorsal MEC. For this purpose, they recorded the activity of the cells in dorsal MEC in total darkness for 30 minutes after a baseline session of 10 minutes which was recorded in light in the same arena. Darkness did not change the spacing, field size or the average firing rate of the cells. In contrast, from the beginning of the dark trial, most grid cells showed a drift in the grid pattern, suggesting that the external cues may determine the phase of the grid pattern to align with the external reference frame. The persistence of the grid pattern in darkness also suggested that the cells in dorsal MEC might have a role in PI. The authors later declared that dorsal MEC potentially performs the computation for the PI since the convergence of the directional input from the dorsal presubiculum and visuospatial input from the postrihnal cortex happens in dorsal MEC. This hypothesis was later confirmed by Gil et al., 2018 and Allen et al., 2014; where disrupted grid cells impaired PI.

1.5.4 Speed cells

Previous studies showed that the hippocampal neuronal activity is coupled with the running speed during locomotion. For example, Vanderwolf and colleagues showed that the amplitude of the theta rhythm (slow oscillatory activity within 3-10 Hz) in the CA1 region of the hippocampus increased linearly with running speed (Vanderwolf et al., 1969). Later, it was also shown that the firing rate of the pyramidal hippocampal and interneurons was affected by running speed (Terrazas et al., 2005; Góis & Tort, 2018).

Moreover, the activity of the place cells in the unrestrained situation was abolished when the restrained animal was moved passively through the environment (Foster et al., 1989). This result highlighted the importance of self-motion movement for generating the firing activity of hippocampal neurons (Bruce L. McNaughton et al., 2006b). Attenuating the self-motion signal also made the size of the place fields large (Maurer et al., 2005). Later, the movement-speed signal affecting the scale of the place fields in the hippocampus should be generated outside of the hippocampus (Bruce L. McNaughton et al., 2006b).

Grid cells were hypothesised to be a good candidate for the computation of path integration-based navigation. During PI, the instantaneous displacement of the animal (running speed) is also calculated across short windows to update the animal's current location in the environment. Therefore, it was suggested that grid cells need information from the animal's running speed to perform the path integration computations. Previous studies showed that the running speed correlated with the entorhinal theta frequency and the firing rate of some of the MEC neurons (Jeewajee et al., 2008). However, it was unclear whether there is a separate population of cells in MEC that encode the animal's speed. To test this hypothesis, Kropff and colleagues recorded cells from all layers of the MEC while rats were running on a 4-meter-long linear track with a computer-driven bottomless frame (called bottomless car). Using this setup, they could pre-set the animal's speed while the rat had to run alongside the track (**Figure 8**). In this experiment, rats were trained to run fast on the first half of the track and then slow on the second half of the linear track. There was a fast transition between the two speeds in the middle. The firing rate of some cells recorded from MEC showed a speed profile with a firing rate as a function of the animal's speed. Recording the cells in random foraging showed that 51% percent of the neurons recorded from MEC increased their firing rate linearly with speed. The data suggested that the speed modulation is similar in the random foraging task and the bottomless car experiment (Kropff et al., 2015).

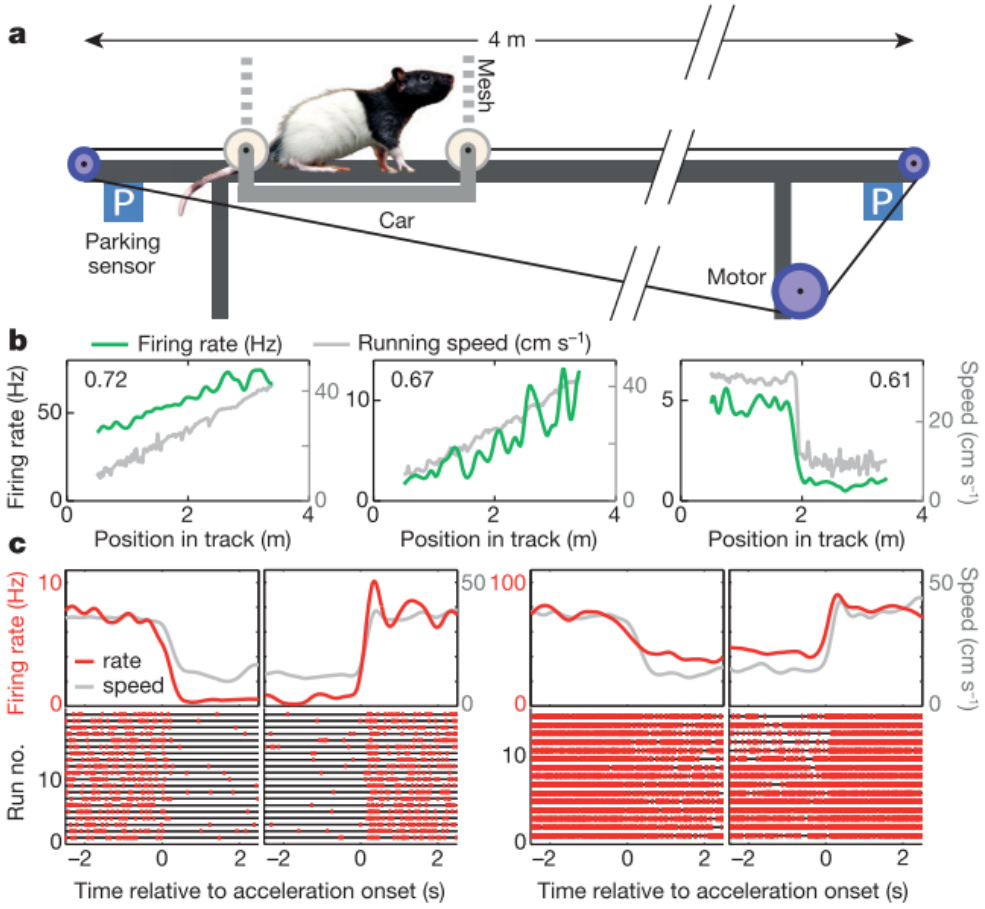

Figure 8. Speed cells in MEC. a: Bottomless car. **b:** Mean firing rate (green) and running speed (grey) as a function of position for three representative speed cells in the MEC. Left and middle linear speed protocol; right, step protocol. Pearson correlations between instantaneous running speed and firing rate are indicated. **c:** Representative speed cells during decelerating and accelerating events of the step protocol (left and right subpanels, respectively). Top, firing rate (red, left axis) and running speed (grey, right axis) as a function of time relative to the event onset. Bottom, spike raster plots. This figure is adapted from (Kropff et al., 2015).

The next set of experiments was performed to test whether the speed cells could be used for path integration. If the speed cells are involved in PI, the animal's running speed could be obtained by decoding the cells' firing pattern independent of the experiment's context. MEC cells were recorded when rats were running in an open field

trial either in the same room or two different rooms. The construction of the running speed from this data was highly correlated with the track speed of the animal in both environments. Likewise, the speed cells were recorded in an open field with the light on-off-on sequence. The speed profile of the cells was invariant across different light conditions suggesting that speed cells in MEC present a context-independent speed code and can be used to decode the animal's speed in different sets of experimental manipulations (Kropff et al., 2015).

1.5.5 Neurons with object-related reference frames

Most of the studies that have been described so far investigated the firing activity of the cells in an empty open field. However, the natural world is full of irregular and different geometrical structures. The previous finding demonstrated that the hippocampal cell firing activity is affected by distal cues (O'Keefe & Nadel, 1978; Jarrard, 1993). However, how pyramidal hippocampal cell activity can by controlled by proximal landmark was not studied until 1996. In this experiment, Gothard and her colleagues investigated the firing activity of place cells in a navigational task that required the animal to find the reward location relative to the position of two objects within the open field (Gothard et al., 1996a). The experimental paradigm was a circular arena surrounded by a black curtain. Five distinct objects were close to the curtain and act as static background cues. Two objects were located withing the open field and determined the location of the reward. The position of these two objects changed between trials. The task of the animal was to find the location of the reward in relation to the two movable objects. The animal was released from a box in the arena; the animal then needed to navigate toward the goal location and return to the box, which was then located in a new location in the arena (**Figure 9**).

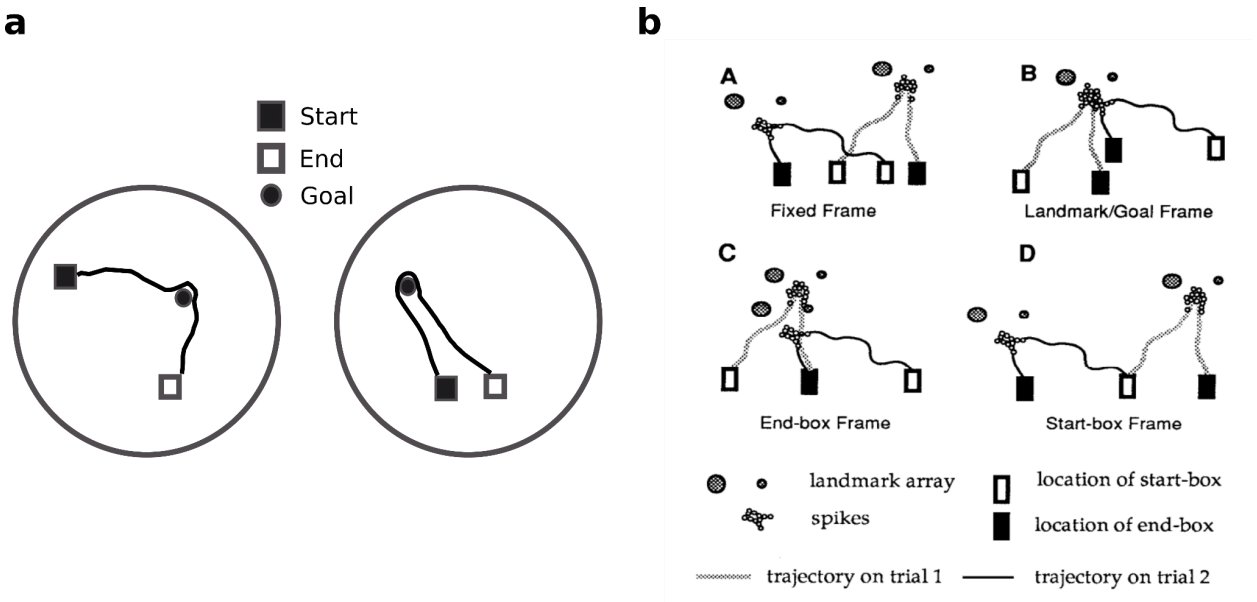

Figure 9. Hippocampal cells are firing in a global or local reference frames. a. The two consecutive trials of the task. Note that the box's position changed both at the start and end of the trial. **b.** Four possible reference frames that could explain the firing activity of the cells. Two trial on each reference frame are shown here (stippled line and solid line). The cells rpresented in this figure is active when the animal is close to the goal and its silence in other part of the environment. To better present how these cells are binfing to a particular reference frame, four different ways was used to aligne the trials. In (A) you see the fixed (arena frame). (B) Represents the landmark reference frame. (C) shows the end-box reference frame and in (D) the start-box reference frame is shown. All of the spiking firing are concentrated in a single arena in the landmark/goal reference frame. However, the spikes are distributed in two seperate areas in other reference frames. The classification of the cells was based on alignment that resulted in the tightest concentration of firing (i.e., the largest spatial information per spike). Adapted from Gothard et al., 1996.

Gothard and colleagues characterized three different types of hippocampal cells in this experiment. 1. Pyramidal cells with fixed place fields in the arena. 2. goal/landmark-related cells are firing close to the goal independent of the goal's location or the landmark in the arena. 3. Box-related cells fire when the animal enters or leaves

the box independent of the box in the arena. Landmark/goal-related cells and box-related cells fire at a fixed distance from the landmarks, independent of the box's location relative to the global reference frame. The results from this experiment suggested that both the fixed landmarks (global reference frame) and movable landmarks (local reference frames) can define the reference frame encoded by different subsets of hippocampal cells. Furthermore, the authors also suggested that task-relevant landmarks or locations can control the firing activity of a subset of hippocampal place cells.

1.5.6 Object vector cells

Collet and his colleagues (1986) showed that gerbils could restore information about their distance and orientation from a specific landmark and later use it to return to their goal. Later theoretical studies suggested that there should be some cells with vector-coding properties in the hippocampus and subiculum (Collet et al., 1986). However, it was unclear how the vectorial information was implemented to help navigation in a natural environment until the early 2010s. For instance, in 2012, Deshmukh and his colleagues tested the firing activity of the cells in the lateral entorhinal cortex (LEC) and perirhinal cortex (PRC) in an open field with objects. In contrast to the study by Gothard et al. (1996), the rats performed a random foraging task, and the location of the objects was not task-relevant. Data analysis showed that LEC and PRC contain object-responsive neurons, increasing their firing rate close to the object. The spatial stability of the cells recorded in LEC was more than spatial stability of cells recorded in PRC. In addition, some LEC cells presented stable firing fields away from the object, similar to place cells recorded in the hippocampus. Authors later suggested that the cells in the PCR represent more non-spatial information while the cells in LEC display a combined spatial and non-spatial representation of the space (Deshmukh et al., 2012).

The activity of hippocampal pyramidal cells in the present of an object was not studied until 2013 (Deshmukh & Knierim, 2013). Deshmukh and Knierim studied the activity of pyramidal cells (CA1 and CA3) when the rat explored an arena with multiple discrete objects (see **Figure 10**). Some place cells called landmark-vector cells encode the animal's spatial location as a vector relationship to local landmarks. A minority of recorded place cells developed a new place field located at a similar distance and direction from the object. Also, a small number of cells in CA1 and CA3 increased their firing rate in the absence of the object in the location where it used to be. Results from this experiments suggested that hippocampal place cells encode multiple types of information regarding the location of the animal and the relationship between the animal's location and the location of landmarks in the environment (Deshmukh & Knierim, 2013).

Later in 2019, another study showed that a significant fraction of cells located in the MEC fire when the animal is located at a specific distance or orientation from an object. The cells recorded in this study, called object-vector cells, are tuned to an object independent of the object's location in the arena (Høydal et al., 2019). In this experiment, mice ran in a square or circular arena with one or more objects located in the arena. On the first trial of the recording session, the mice explored the arena without the object. In the subsequent trial, an object was located on the floor of the arena and in the third trial, the object was moved to a different location. The results showed that MEC object-vector cells fire at a similar distance across objects. This property of the MEC object-vector cells is similar to that observed in landmark-vector cells in hippocampus.

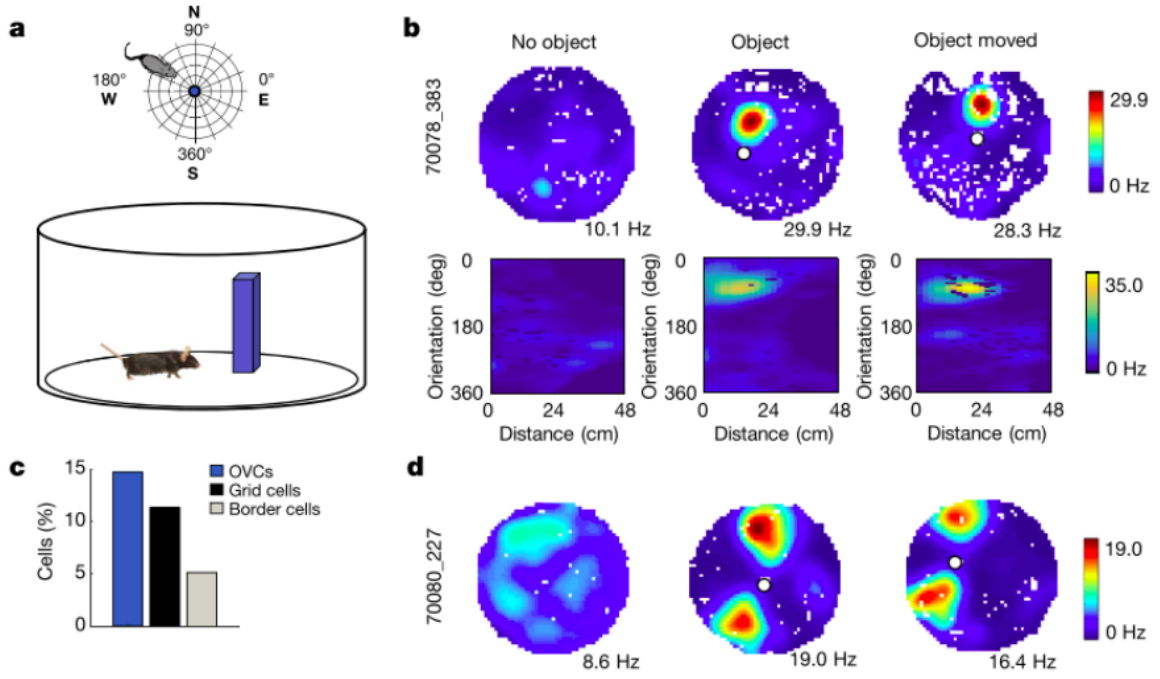

Figure 10. Object-vector cells fire at fixed distances and directions from the object. a: Schematics of recording environment (bird's-eye view). Distance and direction (orientation) are defined in an allocentric frame concerning the object's centre (central circle). East is 0°. **b:** Top, colour-coded firing rate maps (with peak rates) showing an example cell that expressed a new firing field when an object (white circle) was introduced into the recording enclosure (middle). When the object was moved, the firing field moved accordingly (right). Mouse and cell identifier numbers are indicated (5 and 3 digits in length, respectively). Bottom, colour-coded vector maps showing firing rate for cell in the top row as a function of distance (x-axis) and allocentric orientation (y-axis) from the object's centre. The vector map for the non-object trial is referred to the object position on the object trial. **c:** Fractions of grid cells, object-vector cells and border cells in the entire population of recorded MEC cells. **d:** A subset of object-vector cells had two object-vector fields. Symbols as in **b.** Adapted from Hoydal et al., 2019

Moreover, Høydal and his colleagues recorded the activity of MEC cells in a familiar (A) and novel environment (B). All the object-vector cells recorded in A also had object-vector fields in B. The data suggested that the object-vector cells in MEC are tuned to an object from the first time of exposure to the new object or new environment.

Therefore, object-vector cells in MEC maintain their distance metrics across the environment. The data from this experiment suggested that object-vector cells in MEC are coding the animal's position in the allocentric vector coding system, which is different from cells observed in the hippocampus and subiculum. Also, the object-vector cells in MEC differ from object cells in LEC. The object cells in the LEC respond to the object when the animal is at the object but not when the animal perceives the object from a distance. Object-vector cells recorded in MEC use stable landmarks as reference frames in their environment to navigate. Therefore, object-vector cells, unlike object cells, provide information for the position mapping of the animal in space between the objects in the environment (Høydal et al., 2019).

1.6 Spatial reference frames in the cognitive map

The hippocampus can encode the animal's position in the environment in relation to the external landmark (McNaughton et al., 1991). During navigation, the distance and direction of the animal are updated using self-motion information relative to an external landmark. The information about the direction and speed of movement is then encoded by a set of activated place cells relative to a local or global reference frame. In other words, place cells provide information about the distance and direction (vector) from an arbitrary point in the frame within a reference frame. Repetitive visits with a constant internal orientation reference would update the place representation and establish an association between the visual stimuli and path integrator. Therefore, visual inputs could realign the system when reference frame mismatches occur (McNaughton et al., 1991).

In an experiment in 1995, Gothard and his colleagues trained a rat to obtain food in a linear track with one box at each end while recording from CA1 hippocampal cells. One of the boxes was fixed, and the other could move in 5 different equally spaced locations on the track. The rat had to run between the boxes to get the reward. While the rat was in the fixed box, the other box was randomly moved to one of the five

locations along the track. Two sets of place cells in this experiment were found. The first one represented a fixed relationship to the static box (global reference frame), and the other responded in a fixed relationship to the last-experience location of the box (local reference frame). Many of the box-related cells shifted their place field according to the new position of the box. Other cells displayed an interaction between the box's distance and the track's exact location. This data suggested that box-related cells were influenced by the local spatial cues of the static reference frame (Gothard et al., 1995).

As the rat explores the new environment, the information from external landmarks is associated with the current reference frame. This information can then be used to update the animal's position within the reference frame in later visits (McNaughton et al., 1996). Without visual input or in total darkness, the reference frame gets updated using the integration of self-motion information, resulting in an accumulation of errors. However, during light conditions, the association between the landmark and the path integrator results in the correction of cumulative error (McNaughton et al., 1996).

1.7 Experimental paradigms to study PI

Food-carrying task has been one of the paradigms used most frequently to study path integration in rodents. One limitation of this paradigm is that the animal can performe a limited number of trials per session (up to 10). Therefore, this paradigm is not ideal for 1. obtaining a reliable performance estimation for each subject and 2. recording the cell's spatial properties in a relatively large environment. The only study that investigated the spatial properties of the cells during the food-carrying task was by Valerio and Taube (2012). They recorded the activity of HD cells while rats were performing the food-carrying task. Investigating the spatial properties of HD cells does not require long recording, where the animal needs to explore a large 2D arena thoroughly. Recording the HD's firing activity in angles ranging between 0 to 360 is enough for this purpose. Valerio and Tabe recorded the activity of the HD cells in the

rest box before and after each trial to compare the HD drifts on each trial. The data showed that the preferred direction of the head-direction cells had a robust correlation with the heading error of the animal during the homing behaviour in each trial (Valerio & Taube, 2012). The activity of the other spatial selective neurons during the path integration task is unknown.

The L maze task is another paradigm used to study path integration. (Allen et al., 2014, Gil et al., 2018). In this paradigm, the mouse was trained to swim toward a hidden platform at the end of the L shape corridor during the initial sample trial. Later during test trials, the mice had to use path integration in total darkness to find the platform. This paradigm is not very suitable for *in vivo* electrophysiological recording since it would involve recording the activity of mice swimming in water which may interfere with the quality of the recording signal or damage the electrical device (like the amplifire) on the head of the animal.

The virtual reality (VR) platform is another paradigm used to study path integration. In this paradigm, the mouse is typically head-fixed or harnessed on a ball that can be rotated. The optical sensors tracking the optical ball movement can be used to update the visual display in front of the animal. One of the advantages of head-fixed virtual setups is that They allow the manipulation of the environment in a way that is not easy in the real world. Plus, it is possible to perform intracellular recording and two-photon imaging while the mouse head is fixed. However, there are several critical disadvantages of VR systems. Lack of translational vestibular input and sensory-motor feedback modalities are two disadvantages that may be more behavioural relevant than the visual inputs used in VR setups (Ravassard et al., 2015). Another available head-fixed setup is the track floating on air (Kislin et al., 2014; Nashaat et al., 2016). These setups provide the possibility of sensory feedback modalities during the navigation, besides providing an opportunity for two-photon imaging (Go et al., 2021). However, the lack of translational vestibular information remains the same.

1.8 Aims of the thesis

As mentioned before, the firing activity of place are getting updated by PI information (Gothard el al., 1996). Studies with lesions of hippocampus and enthorinal cortex also affected the homig behavior based on PI (Whishaw & Tomie, 1997; Save & Moghaddam, 1996; Parron & save, 2004). However, the firing pattern of place and grid cells duing a homing behavior based on PI are still unkown due to the lack of a suitable behavioral paradigm that allow the characterization of the firing activity of place and grid cells.

During my PhD, I developed a new PI paradigm suitable to perform *in vivio* recording during PI behaviour. To study the spatial properties of spatially selective cells, it is necessary to record the activity of the cells in a large arena. Therefore, it is necessary to ensure that the animal visits all parts of the environment during navigation. In the traditional food-carrying task, it is only possible to record a limited number of trials per session, making it less likely that the animal would explore all parts of the arena. To overcome the limitations of current PI tasks, I adapted a classic operant conditioning paradigm (lever press) for the study of homing based on path integration. In the *automated path integration* (*AutoPI*) task, I can record at least 100 trials per session without human intervention. In this task, the mouse has to leave the home base, search and press a lever located on the arena and return to the home base to get one small pellet. Many trials per session, in combination with the variable position of the lever, ensure that the animal explores all parts of the arena. In the darkness, the ability of the mouse to return directly to the home base depends on the PI.

We then used our newly developed task to characterize the activity of hippocampal neurons during a path-integration-dependent homing task for the first time. I tested whether place cells encode the animal's position in the object-centre reference frame or the world-centre coordinate system (reference frame anchored to distal landmarks). I hypothesized that some place cells encode the animal's location in the object-reference

frame and others within the world-centre reference frame. Therefore, I expect that the field of the firing rate for some cells is anchored to the task-relevant object rather than the world-centre reference frame. I also tested whether the activity of hippocampal neurons correlates with the homing performance of the animal.

2. Material and Methods

The material and method is adapted from the manuscript with the title of “Hippocampal firing fields anchored to a moving object predict homing direction during path-integration-based behavior” currently in progress.

2.1 Apparatus

The AutoPI apparatus had two parts (see **Figure 12.a**): a home base (20 x 30 x 30.5 cm) and a circular arena (diameter: 80 cm) that was elevated 45 cm above the floor. The home base was connected to the arena via a bridge (10 x 10 cm). A sliding door in front of the home base controlled the mouse's access to the bridge and arena. The mouse received one pellet as a reward in the food-magazine inside the home base. The food magazine was equipped with an infrared LED and a receiver to detect the animal's presence. A costumed pellet dispenser was located behind the home base and delivered one pellet (AIN-76A Rodent tablets 5 mg, TestDiet) to the magazine on each trial. The arena was mounted on a taper roller bearing to rotate the arena during the task. Eight walls were fixed to the arena's edge, creating 1.6 cm high walls along the arena's edge. There was a 10 cm wide opening between the wall inserts. These openings were located at multiple of 45° on the arena edge, creating eight potential exit points to access the home base and the bridge. The arena could always orient to have one of the eight exit points aligned with the position of the bridge on each trial.

The lever was built on a 2-wheel-drive mobile platform containing two servo motors and an Arduino Nano with a radio frequency module (NRF24L01). The lever assembly has a 2000mAh lithium battery with a dimension of 13x10 mm. Pressing the lever down broke an infrared beam located inside the lever assembly. Using a radio frequency module, I established a bi-directional communication between the Arduino nano of the lever assembly and a second Arduino Uno that was connected to the microcomputer controlling the task (Jetson Xavier Nx or Raspberry Pi 4). The lever

assembly could move to any position and orientation on the arena. Two other Arduino Unos controlled arena rotation and movement of the door using stepper motors. Two cameras, one above the circular arena and one above the home base, were used to monitor the animal behaviour during the AutoPI task. The cameras were connected to a microcomputer Jetson Xavier Nx or (Raspberry PI 4) and recorded a video at 30 Hz (640 x 480 pixels) for further offline processing.

To facilitate the communication between different programs (nodes) controlling individual parts of the system (door, arena, pellet dispenser, cameras, log), the Robot Operating System (ROS) was used. ROS allowed coordinating computer programs on different computers, microcomputers, and Arduinos. The task was controlled by a python script running on a microcomputer. During the task, a log file containing task-related events (lever press, food delivery, magazine IR beam break, door operation, arena rotation, etc.) with their respective timestamps was created.

A closed-loop navigation system moved the lever to a different location. Before any movement, the current location and orientation of the lever were estimated using DeepLabCut. The next lever position and orientation were randomly selected within a circle centred on the arena centre and a radius of 75% of the arena. The movement vector was then calculated between the current and future pose of the lever. Using radio frequency communication, the lever was later moved along the movement vector to the new location and orientation. DeepLabCut was used to confirm the current location with the estimated pose that was generated before to prevent possible errors in the position and orientation of the lever.

Lights and white noise: LED stripes above the arena and the home base were the only visible light source around the setup. I used an Arduino Uno equipped with a relay module to turn the visible light on and off. Besides the visible LED stripes, there was one long infrared LED stripe on the arena and another on top of the home base, which

remained turned on during the training and testing. A white noise (70 dB) was generated from a speaker directly above or below the arena.

2.2 Subjects

The subjects were 3- to 6-month-old male wild-type C57BL/6 mice. Mice were singly housed in 26 cm x 20 cm x 14 cm high cages containing 2 cm of sawdust and 2-3 facial tissues. Mice were kept on a 12 hr light-dark schedule with all procedures performed during the light phase. All experiments were carried out under the European Committees Directive (86/609/EEC) and were approved by the Governmental Supervisory Panel on Animal Experiments of Baden Württemberg in Karlsruhe (G-236/20). Before starting the familiarization with the home base, the experimenter handled each mouse for 10 minutes per day for three days. Thirteen mice were included in the behavioural experiments without electrophysiological recordings.

Food restriction: Three days before the familiarization with the home base started, mice were put on a diet to reduce their weight to approximately 85 % of their normal weight. Water was available for mice throughout the day. During the food restriction period, mice were weighed and fed daily. The food restriction continued until the end of the experiment.

2.3 Training procedure

Familiarization with the home base: To train mice to get rewards inside the food magazine, I had three days of familiarization step inside the home base. In these three days there is no lever inside the home base.The animal was placed in the home base for 20 minutes per day while the home base door remained closed. The animal received one food pellet inside the food magazine every 30 seconds. The home base familiarisation was performed under the standard illumination in the light phase.

Lever training: Lever training started after three days of familiarization with the home base. In this step, the lever was placed at one of the six potential positions inside the home base (**Figure. 11.a**) and remained in the same position for the entire session. The lever training session was only 30 minutes unless the mouse pressed the lever 100 times earlier. To obtain the next reward, the mouse had to break the infrared beam of the food magazine between lever presses. This procedure ensured that the mouse learned to visit the food magazine after pressing the lever. The lever position in the home base changed between days.

After the sixth day of the lever training inside the home base, the sliding door was opened, and the lever was moved to the bridge and remained there for the whole session. Once the mouse readily pressed the lever at the six possible positions in the home base, the sliding door was open, and the lever was placed on the bridge at the beginning of the next session. The lever was gradually moved toward the arena by approximately 2 cm every two days. If a mouse stopped pressing the lever, the lever was moved back towards the home base by a few cm until the lever press response reappeared. If a mouse received fewer than 50 rewards during a 30-minute session, the lever was at the same position during the next session. Once the lever reached the arena, the same training procedure continued until the lever was at the centre of the arena. The lever training from where the lever is at the homebase to the time where the lever is at the centre of the arena took approximately 16-20 training days.

Arena rotations and door operations: In this step, the home base's sliding door was closed between trials (when the mouse returned to the baited magazine), and the session time was extended to 60 minutes. During the first two sessions, no arena rotations were performed. Subsequently, rotations of the arena by multiples of 45° were introduced between trials. For two sessions, the lever was at the centre of the arena, and the arena angle varied between -45° to 45°. The range was then increased to -90° to 90° for two sessions, and all eight possible orientations were used during the last two sessions. This training ensured the mice learned to press the lever independently of its

orientation. White noise (approximately 65 dB) was also introduced at that point and played throughout the sessions.

Lever movement: In this step, the lever movement to the random locations were added alongside the area's rotation to one of the possible eight rotations between trials. This procedure ensured that the mouse could press the lever independently of its orientation and position. The home base's sliding door was closed between the trials to confine the mouse in the home base during the arena rotation and lever movements. Mice were trained in this protocol for five days. All training steps described so far took place with the visible light sources turned on.

2.4 AutoPI task

There were seven light trials at the beginning of the AutopI task (**Figure 12.c**). From the eight trial, the visible light switch was flipped after every trial, creating a trial sequence alternating between light and dark trials in one session. Note that the white noise was played throughout the whole session. Each trial started when the home base door opened. The mouse had to search for the lever, press it and return to the magazine in the home base to collect the reward. When the mouse broke the infrared (IR) beam inside the food magazine, the sliding door of the home base got closed, and the trial ended. If the IR beam was not broken within 240 seconds in a dark trial, the visible light turned on, and the trial ended in the following food magazine IR beam break. Each AutoPI session ended after 60 minutes or if the lever was pressed 100 times earlier. The arena rotated to one of the eight possible orientations (multiple of 45°) and the lever moved to a new random pose every fourth trial. Note that the arena rotation changed the lever position between the other three trials. This procedure ensured that the search and homing paths were different across trials.

2.5 Analysis of behavioural data

The data analysis was performed in Python, using the following packages: NumPy, Pandas, Scipy, Scikit-Learn, OpenCV, Deeplabcut, Matplotlib, and Seaborn. The code will be made available on GitHub upon publication.

Object detection from the video: The arena centre and arena radius was calculated using the *houghCircles* function from the OpenCV library. I trained convolutional neural networks (DeepLabCut) to detect the position of the bridge, lever and mouse in the videos (Mathis et al., 2018). Four body parts were tracked offline to extract the mouse's position on each video frame. The body parts were the nose, two ears and the base of the tail. The midpoint between the ears was calculated as the animal position on each frame.

Trial segmentation: The time stamps from the door opening and closing were obtained from the event log file of each session. Then I established whether the mouse was in the home base, on the bridge, on the arena or at the lever. A trial was divided into journeys, which started each time the mouse ran from the bridge to the arena. If the mouse pressed the lever during a journey, the mouse running path was divided into search and homing paths.

To separate the search and homing path of the animal on each trial, I needed to estimate whether the mouse was at the lever. The contour of the lever was first obtained and generated in two lever areas by scaling up the lever contour by factors of 1.65 and 2.0. When the mouse’s head entered the smaller (x1.65) lever area, It was considered that the mouse had reached the lever. The search path ranged from the journey's beginning until the animal reached the lever. Likewise, the homing path ranged from when the mouse left the lever until it reached the periphery of the arena. It was considered that the mouse reached the arena periphery if the mouse was less than 3 cm away from the border of the arena. The length, duration, average speed, and

complexity were then calculated to characterize animal behaviour on each search and homing path. Trials in which the centre of the lever box was at a distance larger than 30 cm from the centre of the arena were not used in the analysis.

The path complexity was estimated by first calculating the mean vector length of the movement direction vector within each path. A logarithmic transformation was applied to this score (natural logarithm of one plus) to reduce the skewness of the distribution. I referred to the transformed score as path complexity.

2.6 Surgical procedure

Mice were implanted with one, two or four Buzsaki32 silicon probes (NeuroNexus) aimed at the CA1 region of the dorsal hippocampus. The probes were mounted on customised microdrives that allowed independent movement in the dorso-ventral axis. For the surgery, mice were anaesthetised with isoflurane (1–3%) and fixed to the stereotaxic instrument. The skull was exposed, and two miniature screws were inserted into the skull. One of the screws was implanted on top of the cerebellum, and the other one was implanted anterior to the bregma. The screw located above the cerebellum served as ground electrodes. Next, the skull and dura above the hippocampus were removed, and the probes were implanted at the following coordinates (ML: ±1.8 mm from the midline, AP: 2.0 mm posterior to bregma and DV: 0.6 mm from the surface of the brain). The dental cement was used to fix the microdrive to the skull. During the first 72 hr post-surgery, mice received a subcutaneous injection of Carprofen (0.1 mg/kg; Rymadil) every 8 hours. Mice were given a week to recover after surgery.

2.7 Electrophysiological recordings, spike extraction and spike clustering

Mice were connected to the data acquisition system (RHD2000-Series Amplifier Evaluation System, Intan Technologies, analogue bandwidth 0.09–7603.77 Hz, sampling rate 20 kHz) via a lightweight cable (RHD 6-ft (1.8 m) ultra-thin SPI cable). The recording was controlled using ktan software (https://github.com/kevin-allen/ktan). Kilosort2 (https://github.com/jamesjun/Kilosort2) was used for spike extraction and clustering. Automatically generated clusters were visually inspected and manually refined with Phy (https://github.com/cortex-lab/phy).

Clusters' quality was estimated from the spike-time autocorrelation. A refractory period ratio was calculated from the spike-time autocorrelation from 0 to 25 ms (bin size: 0.5). The mean number of spikes from 0 to 1.5 ms was divided by the maximum number of spikes in any bin between 5 and 25 ms. Any cluster with a refractory period ratio larger than 0.25 was discarded.

In experiments with the electrophysiological recordings, the position of the animal was estimated from the location of two infrared LEDs attached to one amplifier (RHD 32 channels or 54 channels). The infrared LEDs were attached to a costumed printed circuit board in the shape of a bracket. The PCB had one infrared LED (small) on the left side and two infrared LEDs (large) on the right side of the animal head. The distance between the small and large LEDs was 3 centimetres. Two cameras with an Infrared lens were installed on top of the arena and home base to record the position of the LEDs at 30 or 50 Hz during the task. The location of the mouse was extracted online from the position of the LEDs (https://github.com/kevin-allen/positrack or https://github.com/kevin-allen/positrack2).

Cable actuator: To ensure that the recording cable did not interfere with the mouse behaviour, a 2D motorised linear cable actuator was used. The cable actuator was

located 153 cm above the arena and had a movement range of 85 x 130 cm in the horizontal plane. The recording cable was attached to the cable actuator. The aim of the actuator was that its cable attachment remained directly above the animal to ensure that the animal could move with equal ease in any direction. The actuator used the online position tracking data to mirror the mouse's movements.

2.8 Analysis of electrophysiological data

Classification of putative pyramidal cells and interneurons: The presence of ripples (120-200 Hz) during rest trials was used to determine whether each shank of the silicon probe was located in the CA1 region. Only neurons recorded from shanks with clear ripples were considered in the analysis. Then the mean firing rate, spike-time autocorrelations and the mean waveforms of the neurons were used to classify the neurons as pyramidal cells or interneurons (Figure 22). Before the clustering, the principal component analysis was applied to the mean waveforms and spike-time autocorrelations. The first three respective components from each parameter were then selected. The resulting six features and the firing rate of the neurons (a total of 7 features) were then used as inputs for the K-mean clustering algorithm with k = 2. The neurons with the lower firing rate were considered pyramidal cells from the two output clusters.

Instantaneous firing rate: The instantaneous firing rate (IFR) of individual neurons was calculated for hippocampal remapping analysis and for correlating the firing rate of neurons to different behavioural variables. IFR of a cell was obtained by counting the number of spikes in equally sized time bins and applying a Gaussian smoothing kernel to the spike count vector. The spike counts were transformed into firing rates by dividing each spike count by the window size expressed in seconds. For remapping analysis, I used time bins of 100 ms (SD of smoothing kernel = 100 ms). For correlating IFR to behavioural variables, I used time bins of 20 ms (SD of smoothing kernel = 40). This shorter time bin size was chosen to match the sampling rate of the behavioural

variables (50 Hz). IFR association between two neurons was defined as the correlation coefficient between their respective IFR vectors.

Firing rate maps: Firing rate maps were generated by dividing the square platform into 3 × 3 cm bins. The time in seconds spent in each bin was calculated, and this occupancy map was smoothed with a Gaussian kernel (standard deviation of 5 cm). The number of spikes in each bin was divided by the smoothed occupancy map to obtain a firing rate map. A smoothing kernel (standard deviation of 5 cm) was applied to the firing rate map. Firing rate map stability was defined as the correlation coefficient between the firing rate maps of the same neuron in different conditions, whereas map similarity was the correlation coefficient between the firing rate maps of two neurons in the same condition.

Firing rate histograms: Firing rate histograms were calculated by merging the data from all search paths or all homing paths from the light or dark condition, leading to four task conditions: search-light, search-dark, homing-light, and homing-dark. Only paths from journeys, including a lever press, were considered. For each video sample within a path, I calculated the distance run within the path, time elapsed since the beginning of the path, y-axis coordinate of the animal position and the animal distance to the lever. For every neuron, I created a firing rate histogram for each of the four behavioural variables in each of the four task conditions (16 histograms per neuron).

All histograms contained 20 bins. The time in seconds spent in each bin was calculated, and this occupancy histogram was smoothed with a Gaussian kernel (standard deviation of 1 bin). The number of spikes in each bin was divided by the smoothed occupancy histogram to obtain a firing rate map. Later, a smoothing kernel (standard deviation of 1 bin) was applied to the firing rate histogram.

To have a direct comparison between the histograms of light and dark conditions, the minimum and maximum values of the histogram were set to be the same. In addition, I applied the following procedure to ensure the sufficient sampling in all bins of the histogram. The maximal value was obtained by calculating the 90th percentile for each behavioral variable for light and dark trial separately. To have a sufficeint binning the smallest 90th percentile of each light and dark trial were selected. The minimum possible value was selected as the minimum value for the firing rate histogram. Information scores of firing rate histograms was calculated as previously described, $\sum_{i=1}^{N} p_i \frac{\lambda_i}{\lambda} log_2 \frac{\lambda_i}{\lambda}$, where p_i is the probability to be in bin i, λ_i is the firing rate in bin i, and λ is the mean firing rate of the neuron (Skaggs et al., 1996). To calculate the information score no smoothing was applied.

Trial firing rate matrices: To quantify the reliability of the firing rate of neurons between trials, the correlation matrix for all pairs of single-trial firing rate histograms within one session was caclulated. Fo that, the firing rate matrices were created to perform analysis on single paths. Trial firing rate matrix were based on either search-light, search-dark, homing-light or homing-dark data. The neuron's firing rate was calculated for every path as a function of behavioural variables. The behavioural variables included distance run within the path, the time elapsed since the beginning of the path, the y-axis coordinate animal position or the animal distance to the lever. The bin size of the firing rate histogram was 2 cm, 0.15 sec, 2 cm, and 2 cm, respectively. The single-trial histogram was smoothed with a Gaussian kernel with a standard deviation of 2 bins. Later, a trial firing rate matrix was obtained by stacking the firing rate histograms of a neuron from all light or dark trials of one recording session. The mean of the correlation matrix, excluding the unit diagonal, was named trial firing rate matrix correlation and reflected how similar the firing rate histograms were across trials.

Analysis of cell activity around the lever box: To quantify the activity of the cells around the lever box, the animal distance from the lever was first calculated. The distance from the lever was defined as the distance between the centre of the animal's head and the lever box's closest wall. Histograms with the cell firing rate as a function of lever distance were calculated. The bin size for the histogram had a 1-cm bin size, and they were smoothed with a gaussian kernel (SD: 1 cm).

Three possible directional reference frames was considered in which the neuron could encode directional information (**Fig. 27b**). In the Cardinal reference frame, the direction of the animal around the lever box was measured from a vector pointing south. The original lever-centred data were in the Cardinal reference frame. In the Bridge reference frame, the direction of the mouse was measured from a vector pointing toward the centre of the bridge. To transform the data from the Cardinal to the Bridge reference frame, the vector's angle originating at the centre of the lever box (0,0) and pointing towards the bridge relative to a vector pointing south (0,-1) was first calculated. Then, the Cardinal lever-centred position data was rotated by this angle.

In the lever reference frame, the direction of the mouse was measured from a vector originating at the lever box centre and pointing towards the lever. To transform the lever-centred data from the cardinal to the Lever reference frame, the angle of the vector originating at the centre of the lever box (0,0) and pointing towards the lever relative to a vector pointing south was first calculated. Later, the Cardinal lever-centred mouse position data was rotated by this angle. In the lever-centred coordinate system, the coordinates of the lever box were subtracted from the animal position. Each position of the mouse can be seen as a 2D vector originating at 0,0 and pointing towards the direction of the mouse around the lever. Data from when the animal was more than 30 cm away from the lever were excluded from the analysis.

Next, 2D firing rate maps were generated for each cell using the lever-centred data of the three directional reference frames. These maps were calculated like the standard 2D firing rate maps, but the bin size was 1 cm, and the SD of the smoothing kernel was 2 cm. To quantify the degree of directional selectivity of the neurons around the lever, I calculated directional firing rate histograms. The directions around the lever were divided into 10-degree bins. The time in seconds spent in each bin was calculated, and this occupancy histogram was smoothed with a Gaussian kernel (standard deviation of 1 bin). The number of spikes in each bin was divided by the smoothed occupancy histogram to obtain a firing rate histogram. A smoothing kernel (standard deviation of 1 bin) was later applied to the firing rate histogram. The histogram's peak firing rate and mean vector length of the directional firing rate were used to measure directional selectivity.

Directional trial drift: To measure single-trial variability in the orientation of lever-anchored firing fields, I developed a measure called the trial drift (**Supplementary figure. 2**) calculated from the trial matrix. The x-axis of the trial matrix represented the direction of the mouse relative to the lever box. The trial matrix was first rolled in the x-axis until the maximal mean firing rate of the neuron was at direction 0 (**Supplementary figure. 2b)**. I then calculated an idealised tuning curve for the neurons by re-aligning all trials individually so that their peak firing rates were at direction 0 (**Supplementary figure. 2c**). I next performed a crosscorrelation between the idealised tuning curve and each row of the trial matrix with the maximal mean firing rate at direction 0 (**Supplementary figure. 2d)**. The trial drift was the location of the peak in each row of the convoluted trial matrix (**Supplementary figure. 2e**).

2.9 Statistical analysis

The statistical significance of differences between light and dark trials was tested with the Mann-Whitney rank test from the Scipy package. Furthermore, the linear SVM model was implemented with the Scikit-Learn package.

3. Results

Most of the results in this section of the thesis are part of the manuscript with the same title currently in progress. Most figures and figure legends are taken from the manuscript that is currently in progress and is co-written by myself.

3.1 Behavioral experiment:

Thirteen mice were trained in the AutoPI task. The training took between 6-8 weeks itself. As was discussed in the material and method section, the training started with the familiarisation step, followed by the lever training. The first six days of the lever training were performed with the lever placed inside the home base (**Figure 11. a**). The lever location changed between the training sessions to ensure that the mice learned to follow the lever. The number of lever presses, rewards and rewards ratio (the number of rewards per minute) are shown in **Figure 11. b,c,d.**

After each lever press, one pellet was delivered to the magazine. The animal needed to break the magazine and collect the reward before pressing the lever again. Otherwise, the lever presses would not lead to a pellet delivery inside the magazine. This procedure ensured that mice would return to the magazine on each trial. The number of lever presses and the rewards increased across different days (mice could get up to 100 rewards). Therefore, the data suggested that mice could learn to press the lever and collect the pellet inside the food magazine during the first six days of lever training.

The AutoPI apparatus contained a home base, a circular arena and an automated lever (**Figure 12. a.** see material method for more details). The trial started when the sliding door was opened. After mice could successfully press the lever inside the home base, the sliding door opened, and the lever was moved further to the arena.

The mouse needed to leave the home base, navigate to the lever on the arena, press it and later return to the home base to collect the reward from the magazine (**Figure 12. b**). To have a unique path on each trial, the lever orientation and position were changed on different trials. Besides, the arena was rotated between trials to ensure mice were not using the odour cues on the arena to navigate to the home base. After mice could reliably press the lever independent of the lever position and orientation, mice were tested in darkness. Each AutoPI trial (testing trial) started with seven light trials followed by alternating between the light and dark trials (**Figure 12. c**).

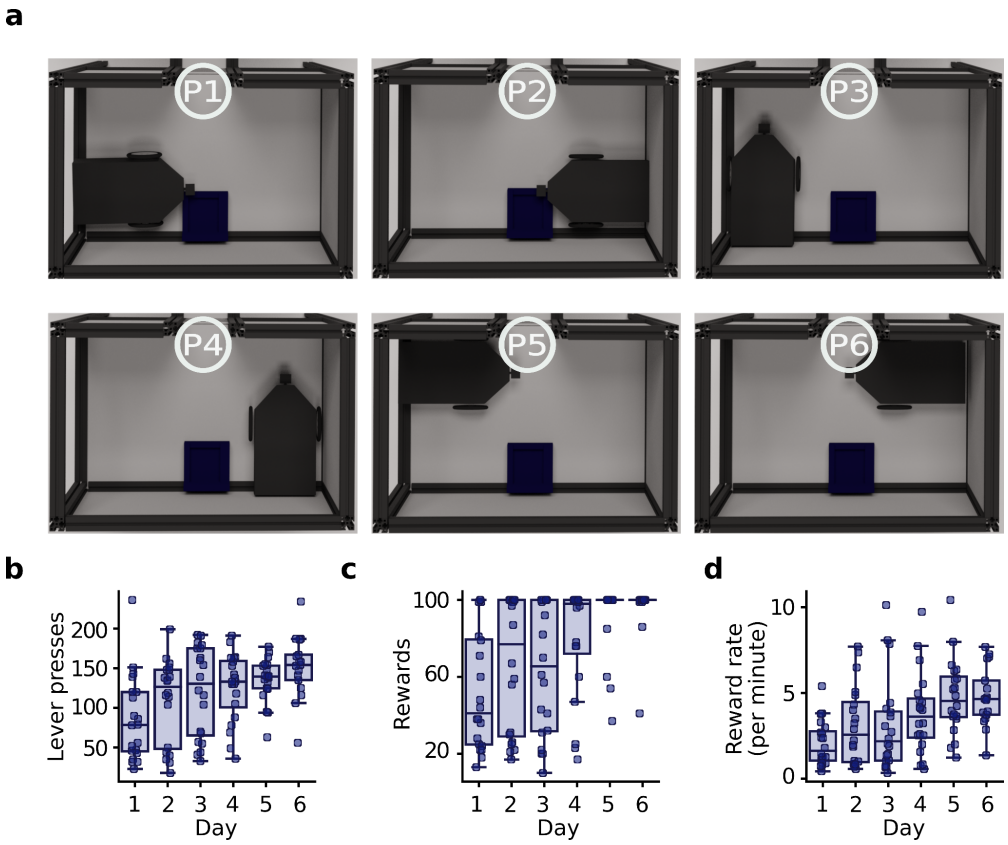

Figure 11. Lever Training in the AutoPI task. (**a**) Schematic showing the different positions of the lever within the home base when the mice learned to press the lever to trigger food delivery in the food magazine. The lever changed position between days (from P1 to P6). (**b, c and d**) Numbers of lever presses, number of rewards delivered and reward rate across six training days (P1 to P6) with the lever inside the home base.

All the light (46 trails) and dark trials (43 trials) in one session has been shown in **Figure 12. d, e.** From 67 test sessions recorded from 13 mice, on average, mice performed 71.45 trials during one hour. On each trial, the mouse had to search for the lever box, press the lever and return to the home base in a relatively straight line. Mice ran around the lever box to find and press the lever itself. A journey was defined as when the mouse entered the arena, searched for the lever and ended when the mouse returned to the bridge. Sometimes mice needed to perform more than one journey to complete the trial (**Figure 12. f, g**). The trial could have several journeys if 1) the mouse could not find the lever before returning to the home base and 2) the mouse failed to press the lever before returning to the bridge. Mice performed more journeys pre-trial during dark trials (**Figure 12. h**). As a result, the duration of the trials in dark conditions was more than the light conditions. (**Figure 12. i**). It was less likely that mice would find the lever in a given journey in dark trials than in light trials (**Figure 12. j**). However, the probability of pressing the lever was similar during the light and dark trials after finding the lever (**Figure 12. k**). The statistical unit that is used for figure 9 was trials. In total, 4453 trials were recorded during the AutoPI task, which contained 2429 light and 2024 dark trials. The same analysis was performed, considering mice as a statistical unit in **Figure 13**.

As discussed, the lever was automatically moved to different locations and orientations to have a unique search path on each trial. All the lever positions of the trials on the test sessions are presented in **Supplementary Fig. 1. a.** If the lever position was outside a circle with a radius of 25 cm, the trial was removed from the analysis (**Supplementary Fig. 1. b**). The lever position distribution and the lever's orientation were random during the test sessions (**Supplementary Fig. 1. c**).

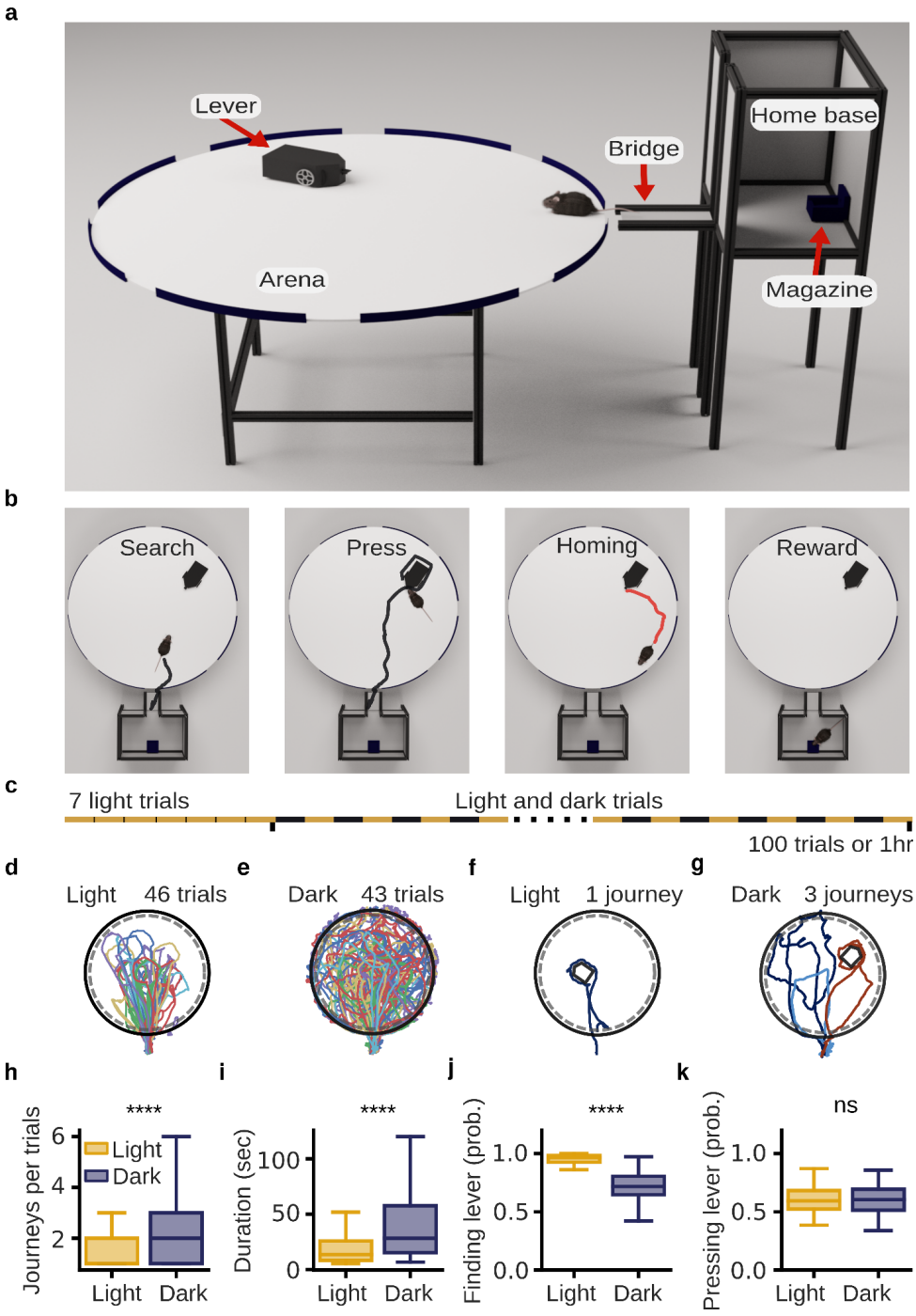

Figure 12. Automated path integration task (AutoPI). a, The main apparatus consisted of a home base, a circular arena, and a lever. The home base contained a food magazine on the wall opposite the arena. A motorised, inverted sliding door gave access to the bridge that led to the arena. The lever was built on a motorised platform, allowing the lever box to change its position and orientation between trials. **b**: Four main phases of a trial on the AutoPI task. The

animal leaves the home base to search for the lever on the arena (Search). The mouse then presses the lever (Press) and returns to the home base (Homing). A food reward is available in the magazine (Reward). **c**, Schematic of a testing session. A session started with seven light trials, followed by a series of trials alternating between light and dark trials. The session ended after 100 trials or when 60 minutes had elapsed, whichever came first. **d**, Running path for all light trials of a test session. The black and the dashed grey circle represent the arena's edge and periphery, respectively. **e**, Running path for all dark trials from the same testing session shown in **d**. **f**, Path of the mouse during a single journey of a light trial. **g**, Path of the mouse during three journeys of a dark trial. The three journeys are plotted in different colours. **h,** Number of journeys per trial for light and dark trials (n = 2429 light and 2024 dark trials, Mann-Whitney rank tests, $P = 6.28 \times 10^{-41}$). **i**, Trial duration for light and dark trials (n = 2429 light and 2024 dark trials, Mann-Whitney rank tests, $P = 2.40 \times 10^{-142}$). **j**, Probability of finding the lever on journeys associated with light and dark trials (n = 67 light and 67 dark trials, Mann-Whitney rank tests, $P = 6.04 \times 10^{-21}$). **k**, Probability of pressing the lever once the lever had been found during light and dark trials (n = 67 sessions, Mann-Whitney rank tests, $P = 8.64 \times 10^{-1}$). ****P < 0.0001, ns: non-significant.

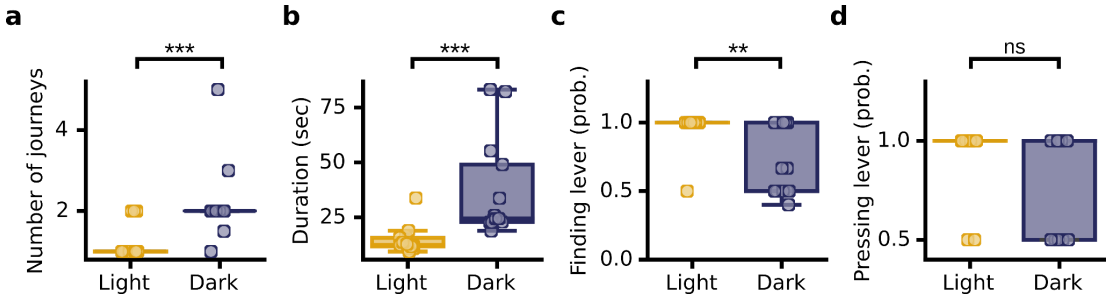

Figure 13. Behavioral characteristics of light and dark trials. The analysis is similar to that presented in **Fig. 12 h-k** but the statistical unit used here is the median of each mouse (n = 13). **a:** Number of journeys per trial for light and dark trials (Mann-Whitney rank tests, $P = 1.48 \times 10^{-4}$). **b**: The trial duration for light and dark trials per trial ($P = 7.93 \times 10^{-4}$). **c**, Probability of finding the lever on journeys associated with light and dark trials ($P = 2.49 \times 10^{-3}$). **d**, Probability of pressing the lever once the lever had been found during light and dark trials ($P = 2.05 \times 10^{-1}$). **P < 0.01, ***P < 0.001, ns: non-significant.

3.1.1 Characteristics of the search path predicting homing error

To compare the navigational behaviour of the mice during the light and dark trials, the search and homing paths of each trial (journeys) were separated and compared between the two light conditions. The analysis focused on the trial's journey in which the lever was pressed. First, the search and homing paths were extracted from each journey. The search path started when the mouse entered the arena and ended when the lever was found. The homing path started when the animal left the lever and ended when the animal reached the periphery of the arena. The path portion of the animal running around the lever was extracted for this analysis. Examples of search and homing paths during the light and dark trials are shown in **Figure 15. a.** As expected, the mice' search and homing trajectories were more direct during the light trials. During the light condition, the lever and home base were easily seen so the mice could directly go to the lever and return to the home base (**Figure 15. b-c**). However, during the dark trials, mice had to explore more parts of the arena to find the lever, which resulted in longer search paths that also lasted longer. Speed was the other parameter to compare the navigational behaviour during the light and dark trials. The running speed for both of the search and homing paths was lower during the dark trials compared to the light trials. During homing, the mean speed in light trials was higher (64.18 cm/sec.) than in dark (31.58 cm/sec) trials. The next parameter used was the degree of complexity in the search and homing paths. The mean vector length of the movement direction was first calculated for each path to calculate the complexity score. Since the scores were negatively skewed, the natural logarithmic was applied to the mean vector length. I referred to the transformed score as the complexity score. Six examples of the search paths with low to high complexity scores are shown in **Figure 14**.

Search and homing paths of dark trials were generally more complex than the light trials (**Figure 15. b-c**). During the dark trial, the homing path were less complex than the search paths (medians: dark-search = 2.2, dark-homing = 2.0; P = 5.3 x 10-16). This result suggested that mice returned to the arena periphery using a straighter

trajectory in light trials compared to the search paths in dark trials. The statistical unit that was used in this figure was trials.

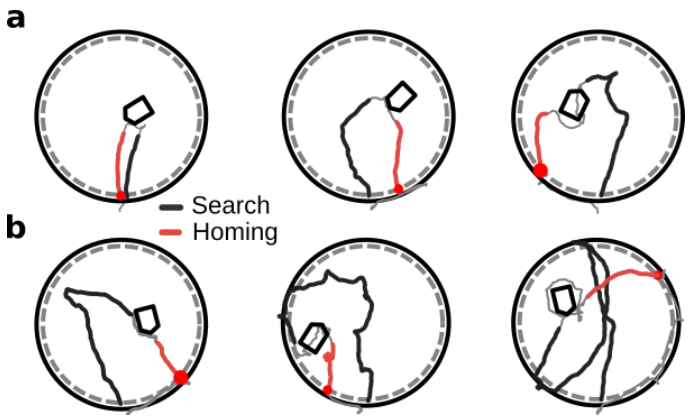

Figure 14. Examples of the complexity of the search paths. a. Examples of three trials with less complex search paths are shown here. Search paths are in black, and homing paths are in red. The complexity score increases from left to right **b.** Examples of three trials with more complex search paths.

The features explained so far (length, duration, mean running speed and complexity and light conditions, eight features) were used to predict whether a trial was performed in light or dark. I could predict the trial as light or dark with an accuracy of 0.91 using the eight features (SD: 0.012, linear support vector machine model, 10-fold cross-validation).

Next, calculated the error at the periphery was calculated to quantify how well the animal returned to the home base after pressing the lever on each trial. The error at the periphery was an angle between two vectors with the centre of the arena as the origin. The first vector pointed toward the bridge's centre, and the second vector pointed toward where the animal first hit the periphery of the arena (**Figure 16. c**). The error at the periphery was significantly larger for the dark trials than for the light trials (**Figure 16. d**). The median error at periphery was 4.26° and 18.15° for light and dark trials, respectively. Likewise, the error at periphery was significantly lower than the chance

level in dark trials (chance level: 90°, Wilcoxon signed-rank test, $P = 1.37 \times 10^{-289}$). This result suggested that mice were not heading toward the home base in a random direction. In contrast, mice returned to the home base roughly in a direct path but with more homing error than in the light trials. The same analysis was later performed with the mice as a statistical unit (**Figure 16. d**).

During a path integration task, the animal process self-motion cues to estimate the current position and orientation. However, without visual cues, the integration of information would accumulate errors in estimating the location and orientation (Hardcastle et al., 2015). It was expected that during dark trials, the error at the periphery increases when the distance run or more extended time pass from the start of the journey. The error can be corrected using known landmarks when the visual landmarks are available. Therefore, during dark trials in the AutoPI task, the error was expected to correlate with the length and duration of the search paths. I first divided dark trials into two halves based on the median length or duration of all dark trials. The trials with shorter lengths or duration of the search path were classified as short search paths. The trials with the length and duration above the median were classified as long search path trials. Larger errors at the periphery were associated with trials with larger search paths and duration during homing (**Figure 15. e and f**). The correlation analysis was then performed between the length and duration of the search path and the error at the periphery (**Figure 16. e**). During dark trials, the error at the periphery was positively correlated with the search path length and duration (**Figure 15. g**). The positive correlation between the search path and search length with the error at periphery supported the hypothesis that mice used path integration during dark trials in the AutoPI task. There was a non-significant correlation between the length and duration of the search paths and the error in light trials. During the light trials, mice could use the known landmarks to correct the accumulation of error during homing. Furthermore, the same analysis was performed later on the characteristic of the navigational behaviour of the mice during light and dark, but with mice as a statistical unit (**Figure 16 a-b**).

The AutoPI paradigm allowed us to collect enough trials in the dark conditions where mice had to use path integration. Therefore, the AutoPI paradigm provided a reliable task to study the neural basis of path integration.

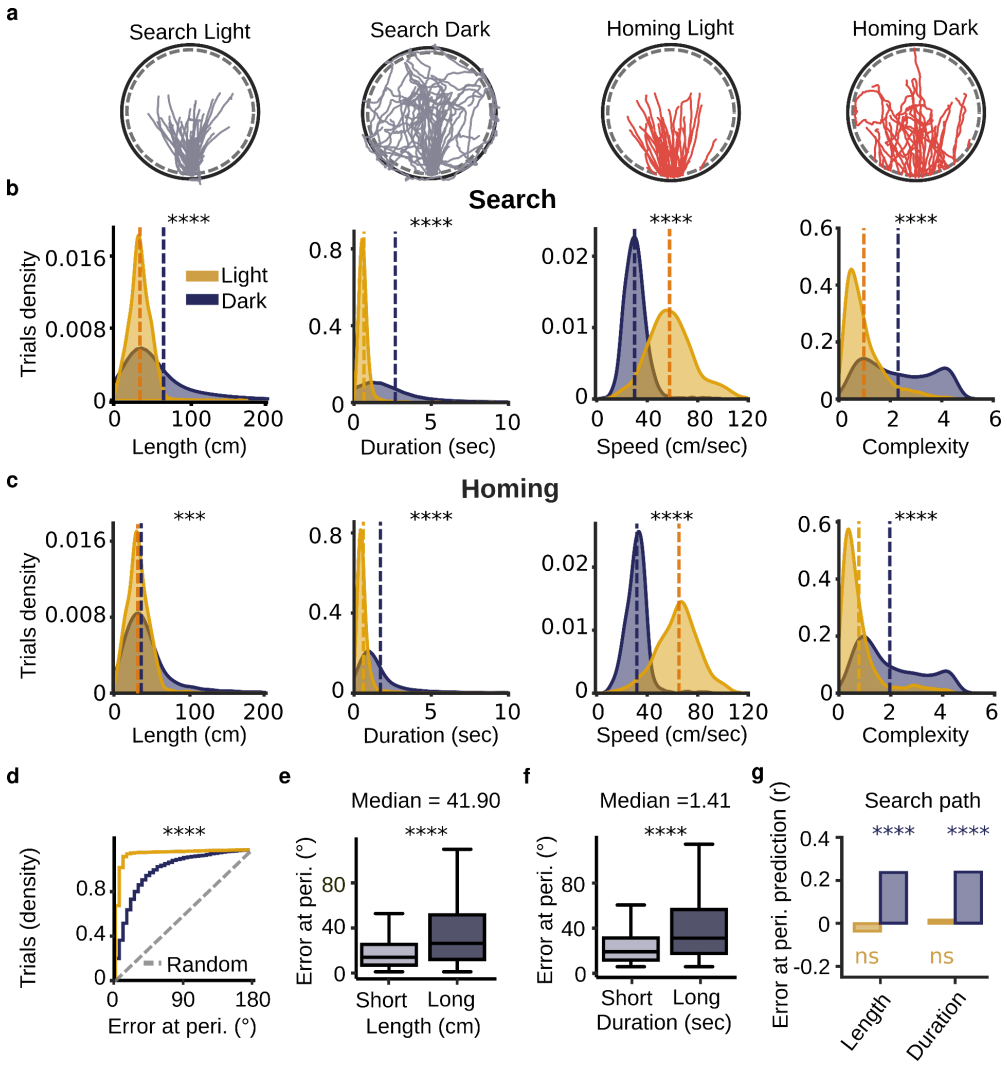

Figure 15. Characteristics of search and homing paths during light and dark trials. a: Examples of search and homing paths from one testing session during light and dark trials. The search and homing paths for light and dark trials are shown separately. **b**: Distribution of search path duration (Mann-Whitney rank tests, P = 1.2 x 10^{-142}), length (P < 1.0 x 10^{-310}), speed (P =

1.0 x 10^{-310}), and complexity (P = 2.34 x 10^{-273}) for light and dark trials. The vertical dashed lines indicate the medians of the distributions (blue: dark trials, orange: light trials). **c**: Distribution of homing path duration (P = 2.58 x 10^{-288}) , length (P = 3.66 x 10^{-23}), speed (P = 1.0 x 10^{-310}), and complexity (P = 2.97 x 10^{-309}) for light and dark trials. **d:** Cumulative distribution of homing error at periphery during light and dark trials (Mann-Whitney rank tests, P = 6.94 x 10^{-294}). The dashed line represents the distribution of error at the periphery expected by chance (homogeneous distribution). **e:** Homing error at the periphery for dark trials with short and long search paths (Mann-Whitney rank tests, P = 5.14 x 10^{-34}). Dark trials were classified based on whether the search path length was below or above the median of all dark trials. **f**: Same as in **e** but for search path duration (P = 1.1 x 10^{-26}). **g:** Correlation coefficients between homing error at the periphery and length (dark: P = 3.3 x 10^{-26}, light: P = 9.7 x 10^{-2}) and duration (dark: P = 1.1 x 10^{-26}, light: P = 5.2 x 10^{-1}) of the search paths. Correlation coefficients are shown separately for light and dark trials. The significance levels of the correlation coefficients for dark and light trials are displayed above and below the bars, respectively. ***P < 0.001, ****P < 0.0001, ns: non-significant.

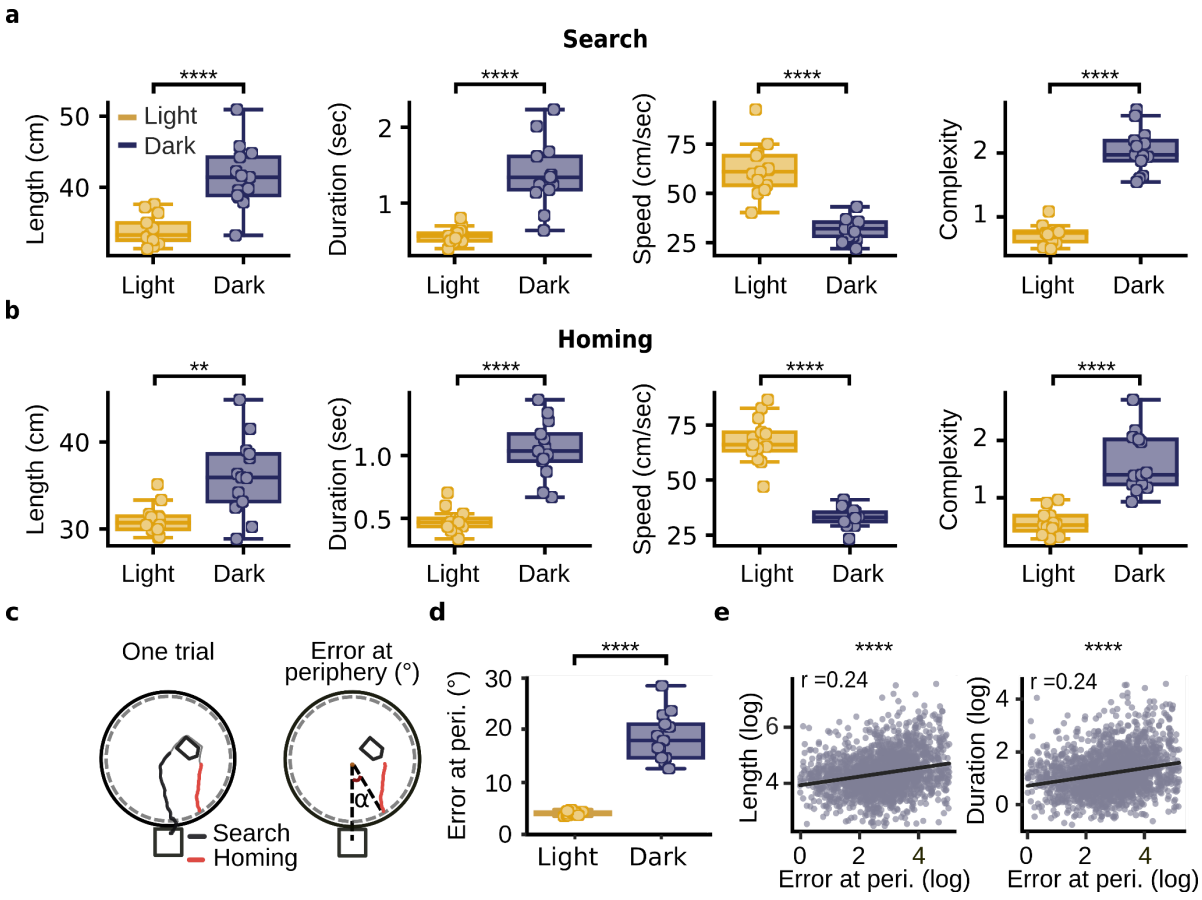

Figure 16. Characteristics of search and homing paths during light and dark trials. The analysis in **a** and **b** is similar to **Fig2. b-c** but the statistical unit used here is the median of each mouse (n = 13). **a**: Search path duration (P = 2.6 x 10^{-5}), length (P = 7.8 x 10^{-5}), speed (P = 2.08 x 10^{-5}), and complexity (P = 1.65 x 10^{-5}). The light and dark trials are shown separately. Each circle represents one animal. **b**: Homing path duration (P = 2.08 x 10^{-5}) , length (P = 3.47 x 10^{-3}), speed (P = 1.65 x 10^{-5}), and complexity (P = 2.08 x 10^{-5}). P-values are from Mann-Whitney rank tests. **c:** Left: Example of one trial in the AutoPI task. The search and homing paths are shown in black and red, respectively. Right: Schematic illustrating how error at the periphery was calculated. Error at the periphery is the angle between two vectors with the center of the arena as the origin. The first vector pointed towards the center of the bridge and the second vector pointed towards the position at which the mouse first reached the periphery of the arena. **d**: Median error at the periphery for each mouse during light and dark trials (P = 1.64 x 10^{-5}). **e**: Relationship between homing error at the periphery and the search path length (P = 3.3 x 10^{-26}) and search path duration (P = 1.1 x 10^{-26}). The values were log-transformed ($ln(x + 1)$) to reduce the skewness of the distributions. The P-values refer to the Pearson correlation coefficients. ** P < 0.01, **** P < 0.0001.

3.1.2 Above chance level performance after disruption of olfactory cues

To ensure that mice are not using the olfactory cues on the arena to return to the home base, the arena was rotated in between trials. However, it was still possible that mice use the odour that comes from the pellets behind the home base to return to the home base. To address this question, a fan with a 35 cm diameter was fixed above the arena (1.85 m) which directed the air flow toward the ceneter of the arena. The strong air flow would distribute the smells equally around the arena and should prevent the use of odour gradiant to navigate back to the home base. Two mice were tested in this experiment with 3 sessions each. Mice first performed 35 trials with no air flow that followed with 35 trials with air flow and up to 30 trials without the airflow again. The homing error at periphery was then calculated for the trials with and without the airflow. The result showed that the homing accuracy of mice decreased slightly during the dark trials with air flow (**Figure 17. a** lower part). Median error at periphery for the dark trials with the air flow on was 32.63°, and for the dark trials with airflow off was 23.42° (dark

trials with airflow on: n = 108, dark trials without airflow: n = 188, P = 3.25 x 10^{-2}). However, the performance of the mice was significantly above the chance level (90°, Error at periphery: P = 5.63 x 10^{-13}) (**Figure 18. a**.)

The result from the airflow experiment provides strong evidence that mice used self-motion cues to return to the home base. There was also a tendency for mice to run at a lower speed when the airflow was on, although the differences did not reach a significant level (**Figure 18. b-c**).

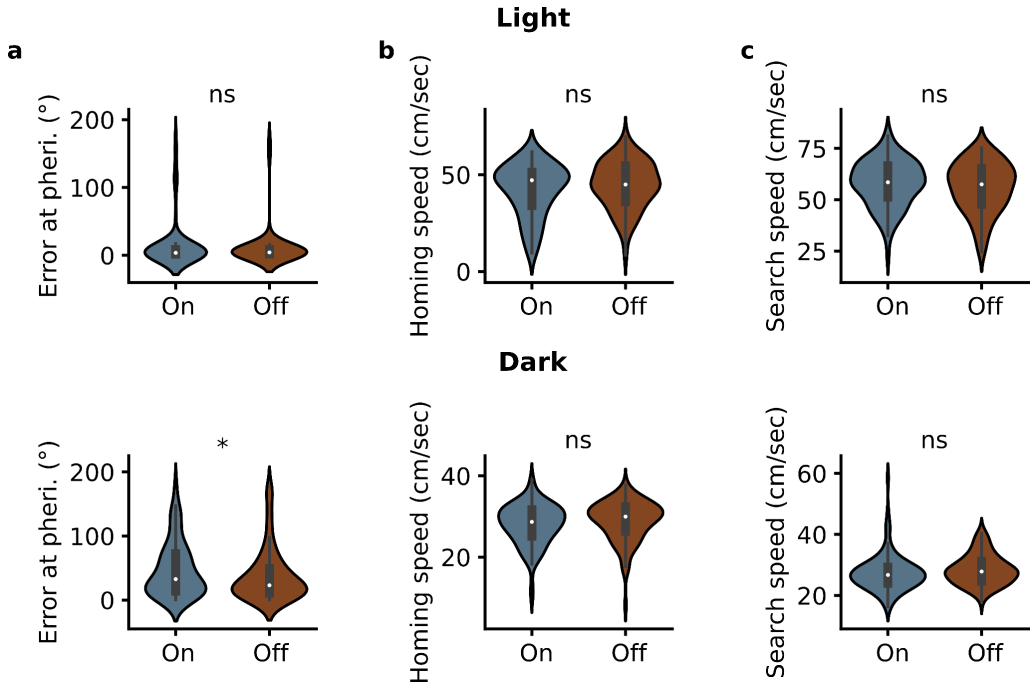

Figure 17. Homing accuracy and running speed with and without an artificial airflow above the arena. a: Error at periphery for the homing paths of light (top) and dark (bottom) trials for trials with (blue) and without (red) air flow (Mann-Whitney rank tests, light trials, P = 5.15 x 10^{-1}, dark trials: P = 4.3 x 10^{-2}). **b**: Homing speed for light (top) and dark (bottom) trials with and without airflow (Mann-Whitney rank tests, light trials, P = 1.07 x 10^{-1}, dark trials: P = 6.02 x 10^{-2}). **c:** Search speed for light (top) and dark (bottom) trials with and without airflow (Mann-Whitney rank tests, light trials, P = 3.02 x 10^{-1}, dark trials: P = 8.16 x 10^{-2}). *P < 0.05, ns: non significant.

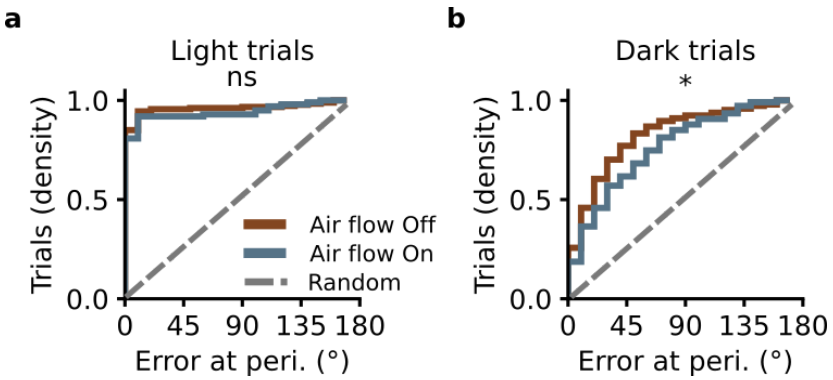

Figure 18. Cumulative error for error at the periphery in air flow experiment. a: The cumulative error for all the light trials with (blue, n= 100) and without (red, n= 182) airflow are shown here (Mann-Whitney rank tests, P = 5.17 x 10^{-1}) (number of mice =2, number of sessions= 6). The dashed line would represent the error at periphery if the mice were going in random directions. **b:** The cumulative error for all the dark trials with (blue, n= 108) and without (red, n= 147) airflow has been shown here (Mann-Whitney rank tests, P = 4.3 x 10^{-2}). The dashed line would represent the error at periphery if the mice were going in random directions. *P < 0.05,, ns: non significant.

3.2 Electrophysiological recording from the CA1 region of the hippocampus

3.2.1 Pyramidal cell classification

I trained another cohort of 9 mice in the AutoPI task to characterise the activity of the CA1 pyramidal cells during a path integration task. Mice were implanted with 1, 2 or 4 32-channel silicon probes (Neuronexus) in the CA1 region of the hippocampus. The coordinate used for the implantation were (ML: ±1.8 mm from the midline, AP: 2.0 mm posterior to bregma). Mice were trained one more week attached to the recording cable after the recovery from the surgery. The training was continued until mice could perform 100 trials while attached to the cable. The recording session started with 30 minutes in the open field. The arena used for the open field was similar to the AutoPI arena and was located precisely the same position. The home base was moved 30 cm away from

the arena to prevent the mice from going to the bridge. The random foraging trial was followed by a 20 minutes rest box where the mouse could sleep. After the rest period, the mouse performed the AutoPI task for 90-120 minutes. The second rest box was performed after the AutoPI task (**Figure 25. a**). The number of sessions recorded from each mouse is shown in **Figure 19. a.** The number of cells recorded per mouse and session is shown in **Figure 19. b-c**.

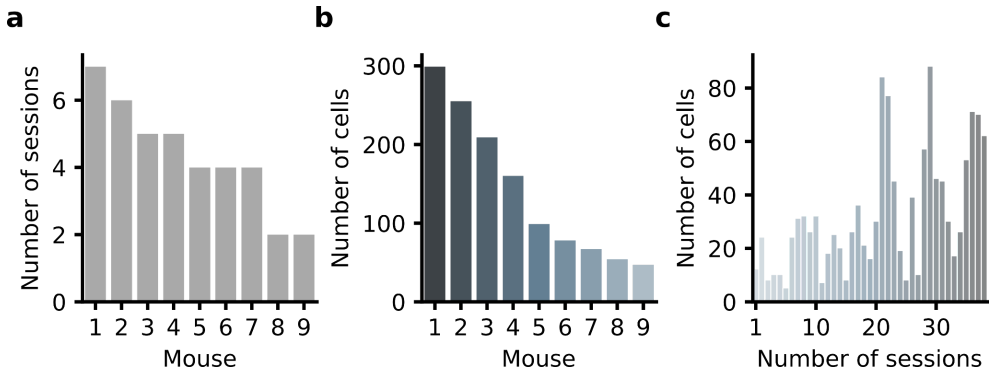

Figure 19. The number of mice and cells recorded in the CA1 region of the hippocampus. a: Number of sessions recorded with each mouse during the AutoPI task in the CA1 region. **b:** The number of cells recorded from each mouse. **c:** The number of cells recorded in each session.

I first detected the cells recorded on the shanks with sharp wave ripples to focus the analysis on CA1 pyramidal cells. The hippocampal sharp wave ripple (SWR) oscillations are the largest recorded brain signals with a frequency of 140-200 Hz. The spontaneus SWR happen as epochs of 50-100 ms. SWR occur during slow-sleep, awake immobility and some behaviours like eating, drinking and rearing. It is shown that around 10-20 precent of the pyramidal neurons in the hippocampus produce an action potential during the SWR (Patel, 2015). The presence of SWR on each shank was used to determine whether the shanks were located in the CA1. Only neurons recorded from the recording sites on the shanks with ripples were considered in the data analysis. One example of channel mapping on a 32-channel silicon probe is shown in **figure 20. a**.

The mean waveform of one neuron on the channels with the first eight highest amplitudes is shown in **Figure 20. b**.

Figure 20. Channels mapping for 1x32 channel Neuronexus probes is shown here. a. The mean waveform of one neuron in all channels is presented in blue. **b.** The mean waveform of the neuron on the eight channels with the largest amplitude.

To extract the SWR, I first band-passed the raw data with frequencies between 150-200 Hz. Then, the data's power (root mean square) was calculated for each channel and summed across channels to reduce the variability. I then used the power of the filtered data to determine the beginning, peak and end of each ripple episode (**Figure 21. b**). The threshold of 5 standard deviations above the background mean power (the reference channel, channel without the ripple) was used to detect the channels with SWR on each shank (**Figure 22**). The channels with the SWR were labelled as channels in the pyramidal cells layer.

Three criteria was set to determine the cells that are outliers. 1) the number of the spike in the autocorrelation was less than 100 spikes, 2) the refractory ratio was less than 0.25 ms, 3) the cells were recorded outside the CA1 pyramidal cells layer of the hippocampus (**Figure 23 a-d**).

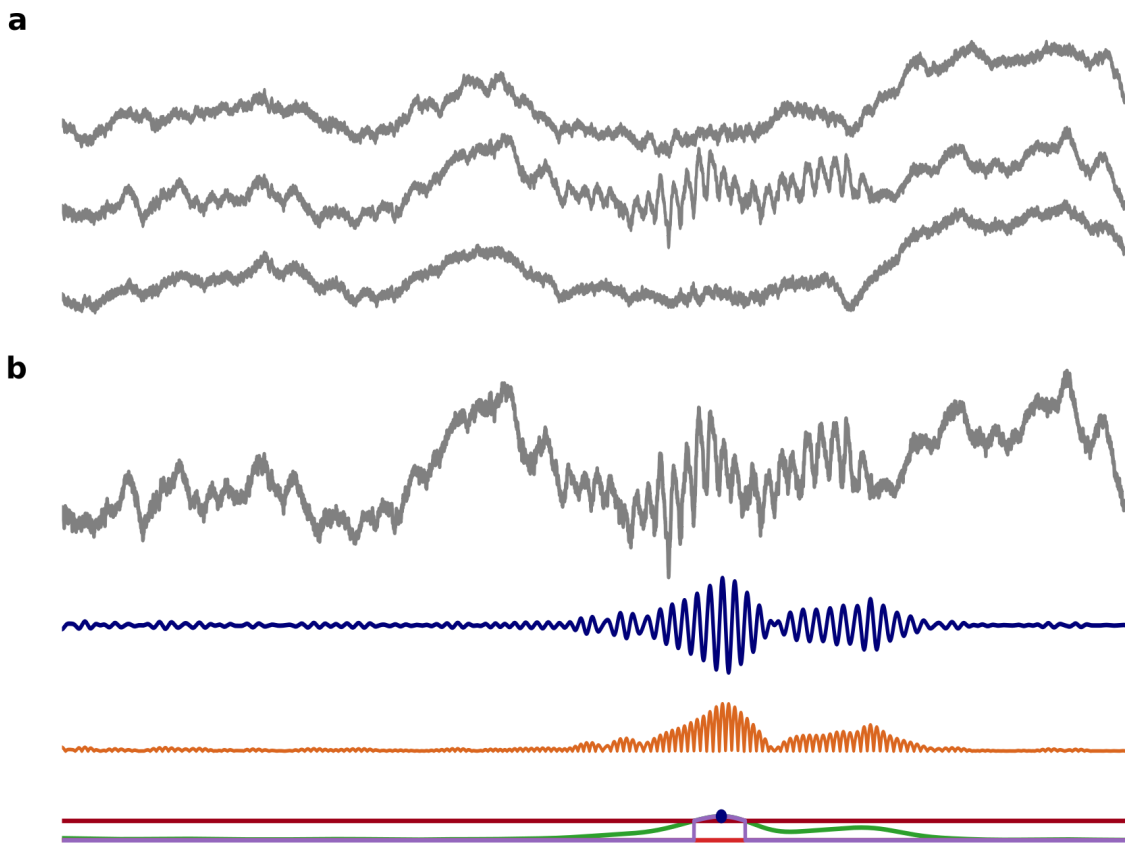

Figure 21. Detection of channels with sharp wave ripples. a: Raw signal recorded from the CA1 region of the hippocampus. Only one of the channels contained sharp wave ripples. **b:** The procedure in which the SWR was detected. The grey signal represents the channel containing SWR. For each session, one channel with SWR and one without (reference channel) were first detected manually. Later the data was band-pass filtered between the frequencies of 150-200 Hz (blue signal). Then, the square root of the differences (orange signal) between the band-pass filtered of the raw data and the reference channel was calculated. Finally, a convolution between the signal (root mean square) and a gaussian filter with the standard deviation of 10 as a kernel was calculated**.** I defined the threshold as the five-time standard deviation of the mean of the convoluted signal presented in red. The convoluted signal itself is presented as green. I defined the peak as the convoluted signal that is more than the threshold value. (Csicsvari et al., 1999).

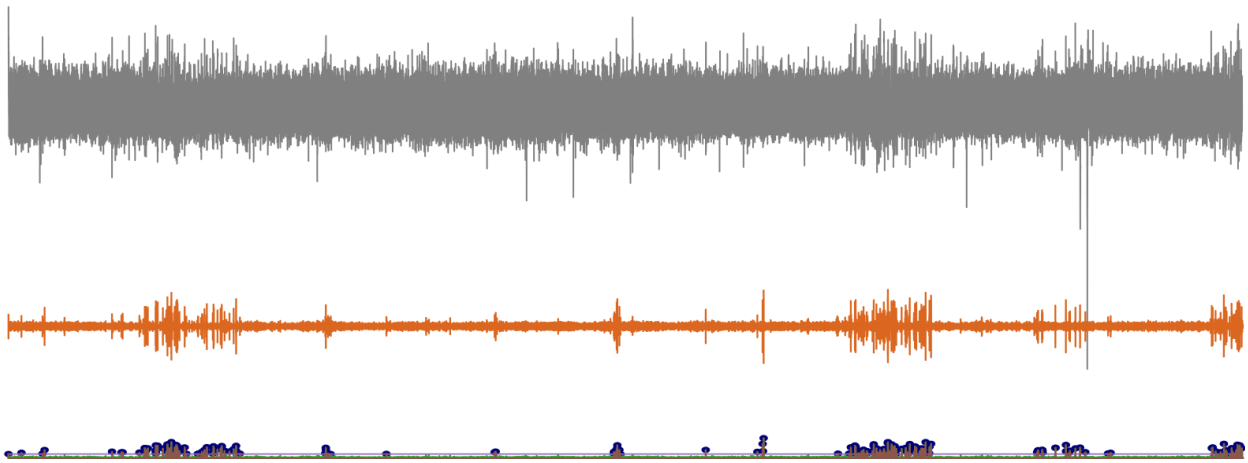

Figure 22. SWR detection using the power of the filtered data. Raw data is shown in grey. The orange signal represents the filter banned data. The last row shows the episode of the signal with a power higher than 5 SDV above the mean power of the background.

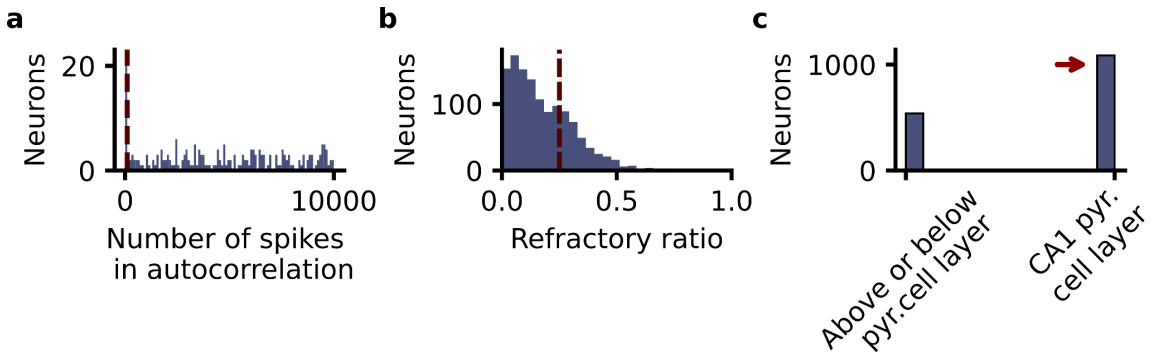

Figure 23. Removing spike clusters of poor quality. a: The cells with less than 100 spikes in the autocorrelation were excluded from the analysis. **b:** Cells that had a refractory ratio smaller than 0.25 were excluded. I first calculated the number of spikes within and outside the refractory period. I calculated the spike time autocorrelation and the mean number of spikes within the refractory period and divided them by the mean number of spikes outside the refractory period. Neurons that had a ratio of larger than 0.25 were considered excluded. **c:** The number of cells recorded from the pyramidal cell layers vs those recorded from above or below the pyramidal cell layers.

Out of 1265 cells recorded during the AutoPI task, 758 cells were valid. I used mean firing rate, spike time autocorrelation and mean waveform to classify the cells as

pyramidal or interneurons. A principle components analysis (PCA) was applied to the cell's mean waveform and spike time autocorrelation before the classification. The first three components of each of the two features were then selected (in total, six features) (**Figure 24. ci-iii**). The trajectory of the cells based on the first two components of mean waveform and spike time autocorrelations is shown in **Figure 24. c iiii**. As evident in **Figure. 24 c iiii**, it was difficult to separate the cell types based on the first two components of the PCA. Furthermore, to better separate the interneurons and pyramidal cells, the mean firing rate was added as another feature for the classification (7 features in total) as input for the k-mean clustering with the k=2. The data transformation based on the PCA1 of the autocorrelation vs PCA1 of other features are plotted in **Figure 24. d**. Neurons with higher firing rates were identified as interneurons. The distribution of the mean firing rate, spike time autocorrelation, and mean waveform of the pyramidal cells vs the interneurons are shown in **Figure 24. e-g**.

The linear discrimination analysis was applied to identify whether the two cell types overlap (**Figure 24. h**). The results demonstrated that the two populations are largely non-overlapping. Out of 758 valid cells, 441 cells were classified as pyramidal neurons. The rest of the data analysis focused on the pyramidal cells.

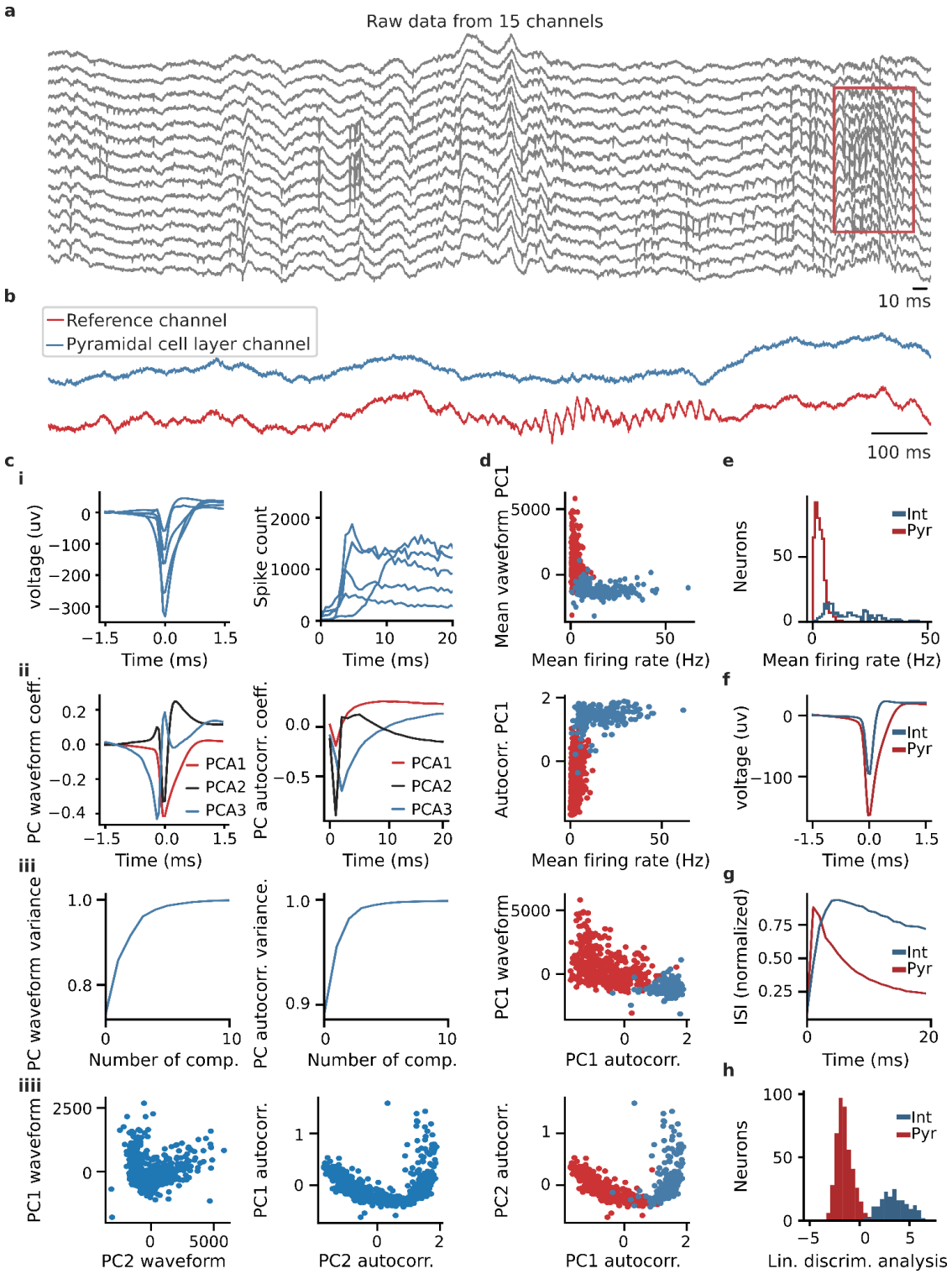
a
Raw data from 15 channels
10 ms
b
Reference channel
Pyramidal cell layer channel
100 ms
c
i
voltage (uv)
Time (ms)
Spike count
Time (ms)
ii
PC waveform coeff.
PCA1
PCA2
PCA3
Time (ms)
PC autocorr. coeff.
PCA1
PCA2
PCA3
Time (ms)
iii
PC waveform variance
Number of comp.
PC autocorr. variance.
Number of comp.
iiii
PC1 waveform
PC2 waveform
PC1 autocorr.
PC2 autocorr.
d
Mean vaweform PC1
Mean firing rate (Hz)
Autocorr. PC1
Mean firing rate (Hz)
PC1 waveform
PC1 autocorr.
PC2 autocorr.
PC1 autocorr.
e
Neurons
Int
Pyr
Mean firing rate (Hz)
f
voltage (uv)
Int
Pyr
Time (ms)
g
ISI (normalized)
Int
Pyr
Time (ms)
h
Neurons
Int
Pyr
Lin. discrim. analysis

Figure 24. Classification of recorded neurons into pyramidal cells and interneurons. a: Example of raw signals recorded from the CA1 region. The red rectangle highlights ripples recorded from the pyramidal cell layer. Only neurons recorded from shanks with ripples were included in the analysis. **b:** Examples of signals recorded near the pyramidal cell layer and further away (reference channel). **c:** Transformation of spike waveforms (left) and spike-time autocorrelations (right) using principal component analysis. **i:** Examples of spike waveforms and spike-time autocorrelations of neurons recorded in the pyramidal cell layer. **ii**: Coefficients of the first three principal components. **iii**: Proportion of the variance explained by the first ten components. **iiii:** Mean waveforms and spike-time autocorrelations plotted in the first and second dimensions of the PCA. **d:** Results of a k-means clustering algorithm applied on the first three principal components of the waveforms, the first three principal components of the spike time autocorrelations, and the normalised firing rates. Neurons are plotted using different combinations of principal components and mean firing rate. **e:** Distribution of mean firing rate for putative pyramidal cells (Pyr) and interneurons (Int). **f:** Mean waveforms of pyramidal cells and interneurons. **g:** Mean spike-time autocorrelations of pyramidal cells and interneurons. **h:** The linear discriminant analysis (LDA) showed that the pyramidal cells and interneurons were largely non-overlapping populations.

3.2.2 Task-dependent hippocampal remapping

Each recording session starts with a trial in the open field before the AutoPI trial (**Figure 25. a-c**). It was shown that the spatial and directional properties of the hippocampal place cells change depending on the behavioural task that the animal is performing (Markus et al., 1995). Therefore, I hypothesised that the activity of the cell assemblies in the AutoPI task is task-dependent. To test this idea, the activity of the cell assemblies during the random foraging trials was compared to the activity of the same assemblies during the AutoPI task. The arena used for the random foraging was in the same colour, shape, size and location as the arena in the AutoPI task. I had two differences between the two arenas: 1) the small walls (1.6 cm in height) around the arena in the open field had no opening to avoid food pellets falling from the arena. 2) the home base was moved 30 cm away from the arena to prevent the animal from jumping onto the bridge. Examples of three pyramidal cells during the random foraging and the AutoPI task are shown in **Figure 25. c**. Pyramidal cells showed a different firing rate map in the AutoPI task compared to the random foraging trials, suggesting a remapping between tasks.

To test the activity of the cell assemblies, the instantaneous firing rate (IFR) of all simultaneously recorded pairs of cells (n= 5168 pairs) was first calculated in both random foraging and the AutoPI (all paths were combined). The analysis was limited to the pairs of cells that were recorded when the animal was in the circular arena. The IFR activity of the cells between the first and second halves of the random foraging was highly correlated (**Figure 25. d,** RF1-RF2, r = 0.738, $P < 1.0 \times 10^{-200}$). The IFR of the cells were also correlated when comparing the trials from the first and second halves of the AutoPI task (T1-T2, r = 0.821, $P < 1.0 \times 10^{-200}$). However, the IFR of the cells between the random foraging and the AutoPI task were weakly correlated (RF1-T1, r = 0.100, $P = 9.2 \times 10^{-13}$). The comparison between the IFR of the cells in random foraging and the task showed the near-complete reorganisation (remapping) of the cell assemblies during the AutoPI task (all paths included). The same comparison was conducted between the map similarity of the trials in the random foraging vs the AutoPI trial. The firing rate maps of the cells between the random foraging and the AutoPI task were not significantly correlated (RF1-T1, r = 0.007, P = 0.625).

The navigational strategies during the light and dark trials differ in the AutoPI task and during the search and homing behaviors. The search and homing paths of one session during the light and dark trials are shown in **Figure 25. e**. The firing rate map of the cells in different conditions was not similar during the task (**Figure 25. f**). Different firing patterns suggested hippocampal reorganisation should have occurred between different conditions. To test whether different hippocampal assemblies were active during the light, dark or search and homing behaviour, the IFR of pairs of cells during these conditions (light versus dark) and different behaviours (search versus homing) were first calculated (**Figure 25. g**). The IFR association stability decreased between the different light conditions and behaviours. For example, the IFR association stability of the cells between the search and homing behaviour in the light was significantly lower

than the IFR activity of two sets of trials during the search behaviour in the light condition (r = 0.161 and 0.537, z = 21.167, $P = 2.0 \times 10^{-98}$).

The IFR association stability and the firing rate map similarity for different conditions are shown in **Figure 26. a-b**. The map similarity of the cells between different conditions also decreases, similar to the IFR association stability. The comparison between the IFR association stability and the map similarity between the different conditions versus within the conditions suggested that the hippocampal cells change their firing pattern between conditions but not within the conditions (**Figure 25. c**). These results demonstrated that the cell ensembles change their firing pattern between light conditions and behaviours in the AutoPI task. Therefore, the firing activity of the cells in the four different conditions was considered separately for further analysis.

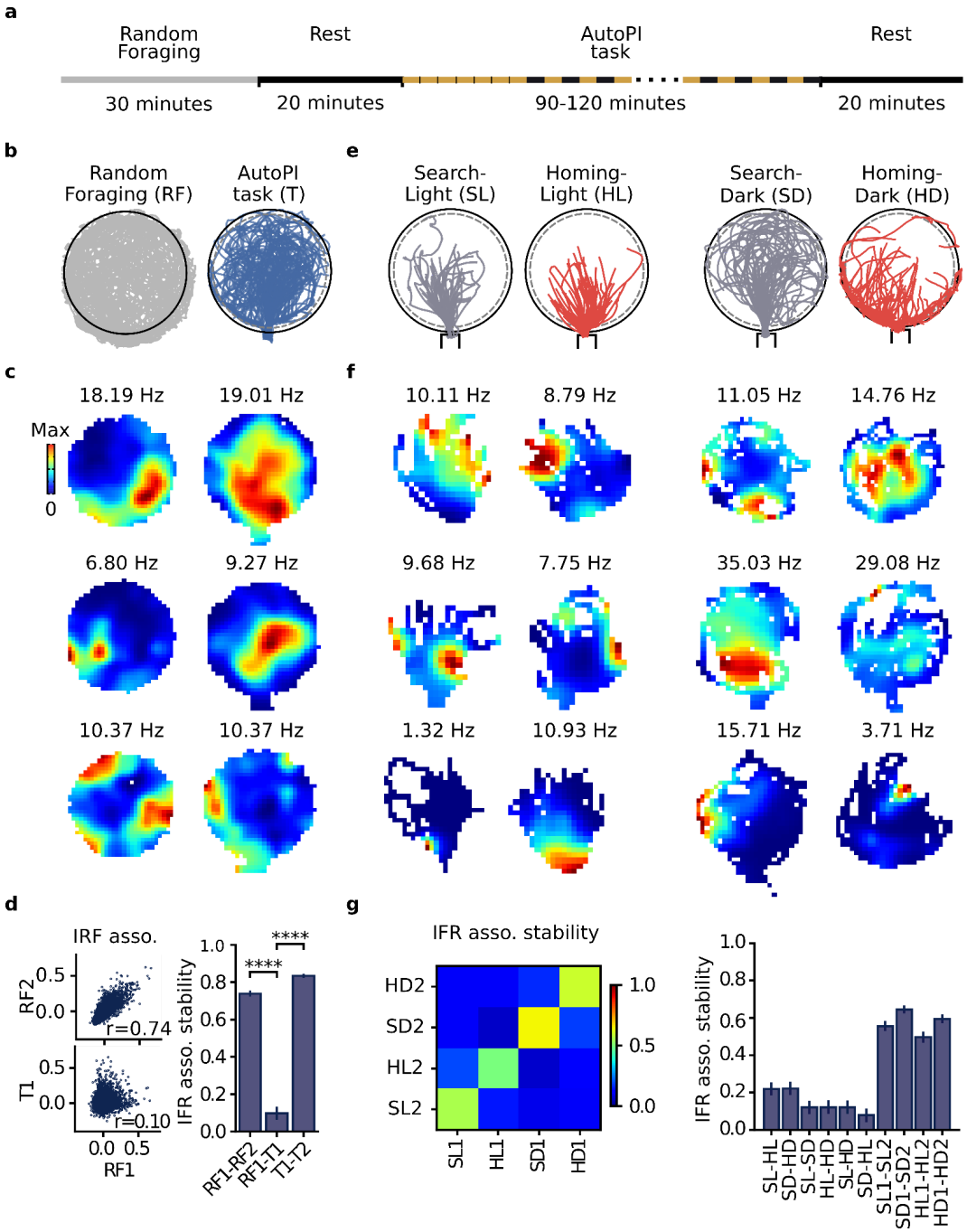

Figure. 25: **Task-induced hippocampal remapping. a**: Schematic of a recording session. The session started with a random foraging trial and a rest trial. The mouse then performed the AutoPI task for approximately 90-120 minutes, followed by an additional rest trial. **b**: Path of a mouse on the circular arena during random foraging (left) and the AutoPI task (right). **c**: Example of firing rate maps of three neurons during random foraging (left) and the AutoPI task

(right). The numbers above the maps indicate the peak firing rates of the neurons. **d**: Top left: Instantaneous firing rate (IFR) associations of pairs of neurons (n = 5168) during the first and second half of the random foraging trial (RF1 and RF2). Bottom left: IFR associations of neuronal pairs during the first half of the random foraging trial (RF1) and half of the trials on the AutoPI task (T1) trials. The stability of IFR associations is defined as the correlation coefficient between the IFR associations across two conditions. Right: IFR association stability across the different conditions (RF1-RF2, RF1-T1, and T1-T2). T1 and T2 were two independent sets of trials on the AutoPI task. **e**: Mouse path during light and dark trials and search and homing behaviour. **f**: Example of firing rate maps of three neurons during light and dark trials and search and homing behaviour. From left to right: search-light, homing-light, search-dark, homing-dark. **g**: Left: Matrix containing the stability of IFR associations for pairs of simultaneously recorded neurons across four different conditions (n = 5168, SL: Search-Light, HL: Homing-Light, SD: Search-Dark, HD: Homing-Dark). The trials of each condition were divided into two independent sets of trials (e.g., SL1 and SL2) to allow within-condition comparisons. Right: IFR association stability with confidence intervals (99%). ****$P < 0.0001$.

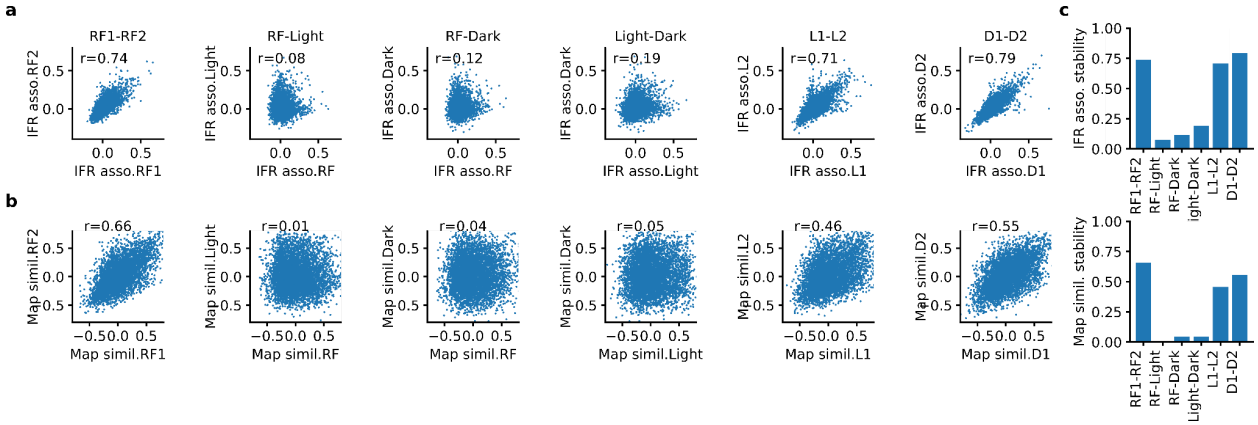

Figure 26. Hippocampal cell assemblies remapped between different conditions in the AutoPI task. a. The correlation between the random foraging and light conditions of the AutoPI task. The IFR stability decreases in between conditions. **b.** The correlation between the map similarity for the same condition is shown here. **c.** The correlation coefficient for the IFR association stability and map similarity within and between different conditions are shown here. The result suggested that the hippocampal place cells remap in between different light conditions and different behaviours.

3.2.3 Lever-box location modulates hippocampal activity during search and homing behaviour

As mentioned before, the behavioural demand is different in light conditions as well as in search and homing behaviours. The search and homing paths for each trial was then identified to characterise the firing activity of the hippocampal pyramidal cells during search and homing paths. The paths of the animal around the lever were excluded for this analysis. The firing rate maps of three different cells for each condition are shown in **Figure 27 a**. The trial matrix for the search and homing paths of each neuron was calculated to quantify the reliability of the firing pattern of the cells across various trials. Each row in the trial matrix shows the cell's firing rate on each trial. The firing rate of cells in trial matrixes was plotted based on either 1) the position of the mouse along the y-axis coordinate (the axis parallel to the centre of the bridge and centre of the arena) or 2) the distance between the mouse and the lever box (**Figure 27. a**). Two groups of cells were found: 1) Some cells fired in a stable position on the arena. In the trial matrix of these cells, the cell consistently fired at the same y-coordinate on the arena on each trial. 2) Another subset of neurons fired close to the lever box independent of the position of the lever on the arena. In the trial matrix, the second group of the cells mainly fired at a fixed distance to the lever box.

To estimate the reliability of the firing pattern of the cells based on the two variable (y-coordinate or the distance of the animal to the lever box), the trial matrix correlation was then calculated for each variable separately (**Figure 27. b, Supplementary Fig. 2**). The trial matrix correlation was calculated for the light conditions (light and dark) and different behaviours (search and homing). Next, I compared the proportion of active neurons across different conditions. Only cells with a firing rate of more than 2.0 Hz were included in this analysis. The proportion of the active cells in different conditions ranged from 0.436 to 0.516 and was not significantly changed (chi-squre test, P = 0.309). The factorial ANOVA with the factors of light conditions and path types was used to assess the differences in the trial matrix

correlation. The trial matrix correlation with the y-axis coordinates was lower for the homing behaviour in the dark trials compared to the homing in light trials (P = 0.0015) (**Figure 27. b left**). The trial matrix correlation for the distance from the lever box was lower during the dark compared to the light trials both during the search and homing behaviour (search P = 1.55-10, homing P = 0.044). Besides, the trial matrix correlation was lower during search behaviour in the dark trials than during the homing behaviour in the dark (P = 1.5 x 10-5). The data presented so far suggested that the influence of the animal's distance to the lever box was more on the firing activity of the hippocampal place cells during homing behaviour in dark trials. Therefore, the data suggested that estimating the distance to the lever box requires visual information during search behaviour.

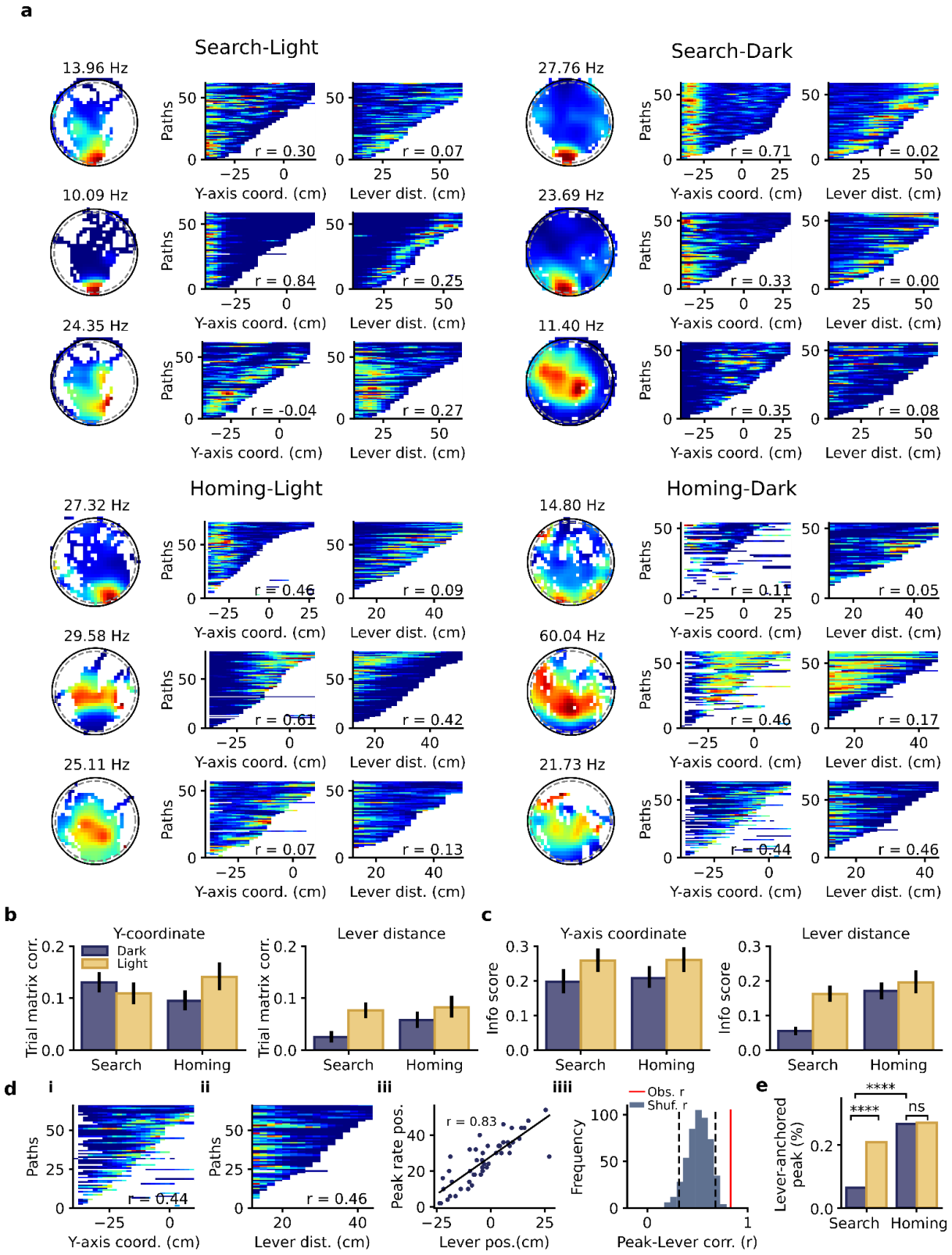
a
Search-Light
Search-Dark
Homing-Light
Homing-Dark
13.96 Hz
10.09 Hz
24.35 Hz
27.76 Hz
23.69 Hz
11.40 Hz
27.32 Hz
29.58 Hz
25.11 Hz
14.80 Hz
60.04 Hz
21.73 Hz
Paths
Y-axis coord. (cm)
Lever dist. (cm)
b
Y-coordinate
Lever distance
Dark
Light
Trial matrix corr.
Search
Homing
c
Y-axis coordinate
Lever distance
Info score
d
i
ii
iii
iiii
Peak rate pos.
Lever pos.(cm)
Frequency
Obs. r
Shuf. r
Peak-Lever corr. (r)
e
Lever-anchored peak (%)
****
ns

Figure. 27: **Lever-box location modulates hippocampal activity during search and homing behaviour**. **a**: Example of pyramidal cells active during the search-light, search-dark, homing-light, and homing-dark conditions. Three neurons are shown per condition, one per row. The 2D firing rate map and two trial matrices are shown for each neuron. The number above the 2D firing rate map is the peak firing rate. The first trial matrix shows the firing rate as a function of the mouse's position on the y-axis (y-axis in the 2D firing map, 0 being the centre of the arena and -40 the arena's edge near the bridge). The second trial matrix shows the neuron's firing rate as a function of the distance between the mouse and the lever box. The r value on each matrix is the trial matrix correlation. **b**, Mean trial matrix correlation for active pyramidal cells obtained from trial matrices with y-axis coordinate (left) or distance to the lever box (right). The data are shown separately for light and dark trials and search and homing behaviour. **c**, Information score of 1D firing rate histograms with the firing rate as a function of y-axis coordinate (left) or distance to the lever box (right). **d**, Example of a neuron with a firing field anchored to the lever position during the homing paths of dark trials. **i** and **ii**: Trial matrix of the neuron as a function of the y-axis coordinate and the distance to the lever box, respectively. **iii**: Y-axis location of the peak firing rate of the neuron and the y-axis location of the lever for single homing paths in darkness. The lever box location can predict the location of the peak firing rate of the neuron. **iiii**: Distribution of r values between firing rate peak location and lever location obtained after shuffling the firing rate values within each trial. The observed r value felt outside the random distribution, indicating a significant correlation between peak rate location and lever location. **e**, Percentage of active pyramidal cells for which the location of their peak firing rate was significantly correlated with the lever position (Search-Light vs Search-Dark: P = 1.7 x 10-7; Homig-Light vs Homig-Dark: P = 0.48; Search-Dark vs Homing-Dark : P = 3.25 x 10-11). ****P < 0.0001.

The information score was the second measure used to quantify the influence of the y-axis coordinate and the distance from the lever (**Figure 27. c left**). All of the trials from one condition (search-light, search-dark, homing-light and homing-dark) were merged to calculate the information score in each condition. The firing rate histogram for each condition was then calculated separately. The information score was calculated based on the Skaggs et al., 1996 (see material and method). The information score for the y-axis coordinate was higher during the light than in dark trials (P = 1.7 x 10-4) (**Figure 27. c left**). The information score was lower for the search paths in the dark trials compared to the light trials (P = 1.03 x 10-20). The information scores during the homing behaviour were not significantly different in light compared to dark trials. This data suggested that hippocampal neurons can encode the distance from the lever once

the animal encounters the lever in darkness using path integration. An example of a hippocampal pyramidal cell that fired at a fixed distance from the lever box is shown in **Figure 27. d i-ii.**

Later, the proportion of the cells fired from the lever in a fixed location was estimated. For this analysis, the trial matrix of the individual neuron was calculated for each light condition (light and dark) and the behaviours (search and homing) separately. Moreover, it was tested whether the location of the peak of the firing in the y-axis correlated with the coordinates of the lever- box. Neurons considered in this analysis had two criteria: 1) The average peak of the firing rate above 7.5 Hz in the y-axis coordinate or the lever distance trial matrix. 2) Significant correlation for the trial matrix correlation of the cells in the y-axis coordinate or the distance from the lever box. The number of neurons for each condition were as following: search-light = 105, search-dark = 108, homing-light= 81, homing-dark= 75 (chi-square test P = 0.02). The peak firing rate location of the cells against the lever box location in the y-axis coordinate is shown in figure 25. d iii. It was hypothesised that neurons that fire at a fixed distance from the lever box should have a positive correlation between the position of the peak of the firing rate and the lever box's position (**Figure 27. d iii**). The correlation coefficient of the cells between the firing peak's location and the lever box's position was then calculated. Neurons with the significant r value were classified as cells encoding the lever distance from the animal.

During the search-light and search-dark, 20.95% and 7.41% of the cells were influenced by the animal's distance from the lever box (**Figure 27. e**). The percentage of the cells that encoded the lever distance was higher for search behaviour during light trials than in dark trials (chi-square test, P = 1.7 x 10-7). However, The percentage of the cells encoding the lever distance was not significantly higher than chance during the search behaviour in dark trials (chance level of 5%, chi-square, P = 0.18). In addition, 25.93 % and 26.67% of the cells encoded the lever distance during the homing-light and homing-dark, respectively. The differences between the percentages of the cells during

the homing behaviour in light vs dark were insignificant (P = 0.48). The percentage of the cells encoding the lever distance during the dark trial was higher for homing behaviour than in the search behaviour (P = 3.25 x 10-11). The result showed that the lever distance from the animal influenced approximately 25% of the cells during homing.

3.3.3 Hippocampal firing fields anchored to the lever box

I found that some hippocampal pyramidal cells are firing at a fixed distance to the lever box during the search and homing behaviour. Here I am focusing on the firing pattern of the cells when the mouse was at the lever box. On each trial, the mouse typically circled around the lever before finding and pressing the lever. It was hypothesized that some hippocampal place cells are firing consistently close to the lever but independent of the lever position on the arena. To quantify that, I first overly the spikes of each neuron on the single path of the mouse during single trials. It was found that several neurons fired when the mouse was around the lever. These cells were later called lever-box-anchored cells (**Figure 28. a**). The firing rate of the cells as a function of the animal's distance to the lever was then calculated. Some neurons showed a clear peak within 10 cm from the lever box. The peaks of the spikes occurred when the mouse was around the lever, where the animal spent more time than at the other distances. The result from this analysis suggested that many neurons fire at a given distance from the lever on most trials and independent of the lever box position in the arena (**Figure 28. a**). The data also suggested that the cells fired when the animal was in a specific direction around the lever box (**Figure 28. a**).

I then transformed the position data so that the centre of the lever box was located at (0,0). This data transformation allowed us to generate the firing rate map with the lever box always at the centre of the map. To calculate the directional selectivity of the cells, I needed to compute the direction relative to a reference vector. The origin of the reference vector was set to the centre of the lever box, and set the directional

reference frame for the analysis. Three directional reference frames were considered as illustrated in figure 26. b. In the cardinal reference frame, the reference frame is pointing toward the south. Nevertheless, in the bridge reference frame, the reference vector pointed toward the Bridge's centre. The reference vector pointed toward the lever direction in the lever reference frame. Then I calculated the firing rate map and the polar firing histogram for each neuron in all three reference frames (**Figure 28. b**). The animal's position was limited to 12 cm from the lever box for this analysis. Most neurons had higher firing rates and directional selectivity in the Bridge and Cardinal reference frame than in the lever reference frame (**Figure 28. c**).

Using three reference frames, I could identify the cells with stable firing fields when the animal was around the lever. Three criteria was defiend for the cell as the lever-box-anchored cell. 1) The peak of the firing rate as a function of the lever distance occurs within a 10 cm distance from the lever box. 2) Peak of the firing rate larger than 7.5 Hz 3) The map similarity of larger than 0.4 between the 2D firing rate maps of the same cell as a function of the lever distance when considering two different sets of trials in one condition. Using these three criteria, I could identify 23-25% of the hippocampal pyramidal cells within the Cardinal and Bridge reference frame (**Figure 28. e**). The percentage of the lever-box-anchored cells was significantly higher in the Cardinal and Bridge reference frame compared to the lever reference frame (chi-square tests, all $P < 0.05$). However, the differences between the number of cells in the Cardinal and Bridge reference frames were insignificant (all P values > 0.05). In addition, there were no significant differences between the percentage of the lever-box-anchored cells in the light vs dark trials in any of the reference frames (chi-square tests, all $P > 0.05$). Then, I calculated the preferred direction of the lever-box-anchored cells from the polar firing histogram rate. The firing fields were distributed homogenously around the lever box in all three reference frames. (Rayleigh tests, all $P > 0.05$) (**Figure 28. e**).

Next, I compared the cells' spatial coding in all three reference frames. To do that, I first calculated the mean vector length of the cells from the polar rate histogram around the lever box. Then, an ANOVA test was ran on the mean vector length of the cells from the polar firing rate histograms. All the pyramidal cells showed the significant effect of lightening (F = 12.10, *P* = 5.1 x 10-4) and reference frame (F = 98.10, *P* = 9.0 x 10-42). There were significant differences between the mean vector length of the cells in Cardinal and Bridge reference frames compared to the lever reference frame (*P* = 8.1 x 10-15 and *P* = 1.4 x 10-13, correspondingly). The differences between the reference frames remained when limited the analysis was limited to the lever-box-anchored cells.

When the lever was close to the x-axis centre of the arena, the Cardinal and Bridge reference frames were nearly aligned. Therefore, It was expected a slight change in the mean vector length of the cells when comparing the Bridge and Cardinal reference frames. To contrast the Bridge and the Cardinal reference frame more directly, I focused the analysis on the cells classified as lever-box-anchored cells in the Bridge and/or the Cardinal reference frame. Then, the within-neuron comparison was performed on the mean vector length of the cells in the two reference frames (**Figure 28. g-h**). The mean vector length in the Cardinal reference frame was larger than in the Bridge reference frame (Wilcoxon signed-rank tests, dark: *P* = 9.7 x 10-6, light: *P* = 0.0038). This result suggested that most of the firing fields around the lever were best encoded in the Cardinal reference frame.

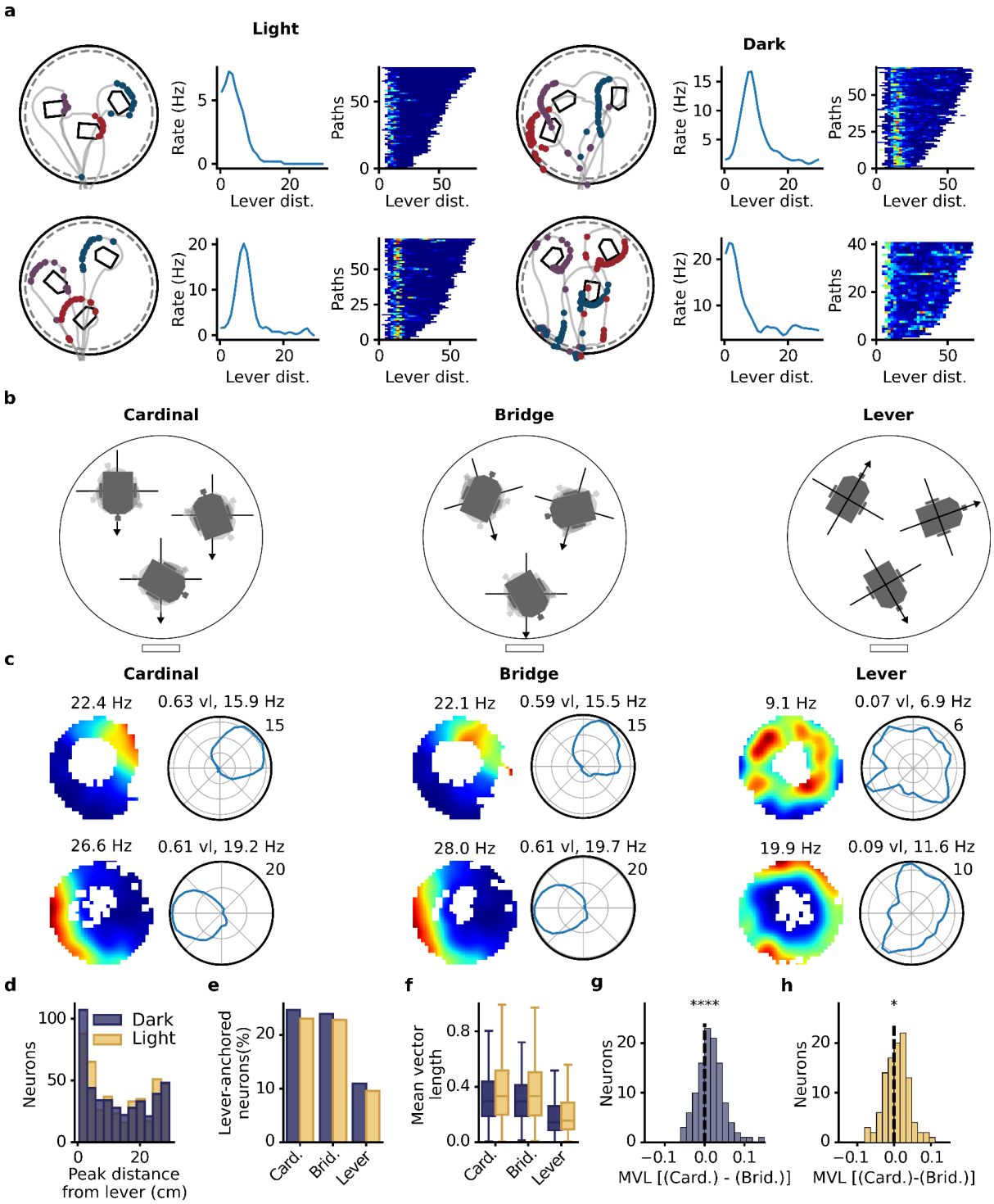

Figure. 28. **Hippocampal firing fields anchored to the position of the lever box. a**: Examples of four neurons (two in light trials, two in dark trials, one per row) with firing fields near the lever box. Left: Spikes (dots) on the mouse paths (grey lines) during three trials. The spikes of the different trials are plotted using different colours. Middle: Firing rate as a function of

distance from the lever box. Right: Trial matrix containing the neuron's firing rate as a function of distance from the lever box. Each row of the matrix represents a single journey on the arena where the animal pressed the lever. **b**: Schematic depicting three possible directional reference frames when calculating the firing rate of a neuron around the lever box. Cardinal: Direction is calculated relative to a vector pointing south. Bridge: Direction is relative to a vector pointing towards the bridge's centre. Lever: Direction is relative to a vector starting at the centre of the lever box and pointing towards the lever itself. **c**: Lever-box-centered firing rate maps and polar firing rate histograms in three different lever-box-centred reference frames (Cardinal, Bridge, and Lever). The maps and polar firing rate histogram include the data from all journeys in which the mouse pressed the lever. The polar plot shows the firing rate of the neuron as a function of the direction of a vector originating at the lever box centre and pointing towards the head of the mouse. The data in the first and second rows are from two different neurons and light and dark trials, respectively. **d**: Distribution of peak-firing-rate distance from the lever box. Many neurons had firing rate peaks close to the lever box. **e**: Percentage of neurons with a firing field anchored to the lever box position. **f**: Mean vector length of the lever-centred circular firing rate histogram in different reference frames. **g**: Change in mean vector length of the lever-centred circular firing rate histogram between the Cardinal and Bridge reference frames for dark trials (Wilcoxon signed-rank test, P = 3.48 x 10-5). **h**: Same as **g** but for light trials (P = 0.013). *P < 0.05, ****P < 0.0001.

3.3.4 Long search paths associated with reduced directional selectivity of lever-box-anchored firing fields

During the dark trials in the AutoPI task, mice were updating their position and orientation estimation using path integration. So far, It was found that a subpopulation of hippocampal place cells are anchored to the lever box. It was also found that the lever-box-anchored cells have directional selectivity and fire in a specific direction from the lever-box itself. Therefore, there should be an accumulation of errors that would affect the directional selectivity of the lever-box-anchored cells (Hardcastle et al., 2015, Pérez-Escobar et al., 2016). To test this hypothesis, I first divided the trials into two equally sized groups based on the length of the search paths. The trials with the search paths shorter than the median of the search path length were categorized as short search path trials. The trials with the length of the search paths larger than the median were long search path trials (**Figure 29. a**). The mean vector length (MVL) and the peak

of the firing rate were used for short and long search paths separately to quantify the directional selectivity of the cells around the lever.

The data showed that the mean vector length and the peak of the firing rate were higher for shorter search path trials (**Figure 29. b-c**). To assess the stability of the cell's firing rate around the lever, I calculated the trial matrix for each short and long trial separately. Each line of the trial matrix contained the cell's firing rate as a function of the direction of the mouse around the lever box. To quantify the stability of the firing rate, I then calculated the trial matrix correlation across different trials of the same type. The data showed a higher trial matrix correlation for the trials with shorter search paths than those with longer search paths (**Figure 29. d**). To assess the similarity of the directional selectivity of the cells during search paths, another parameter called average directional trial drift was defiened, which was calculated from the trial matrices (**Supplementary Fig. 2**, see material method). The trial with shorter search paths showed a smaller trial drift (**Figure 29. e**). The same analysis was performed for the search duration instead of the length of the search path, and the same result was observed (**Supplementary Fig. 3**). Together, these results demonstrated that during the longer search paths, the directional selectivity of the lever-box anchored cells dropped. Therefore, It could be suggested that during dark trials that the animal had to use path integration, the activity of the lever-box-anchored cells was affected by the search path’s length and duration.

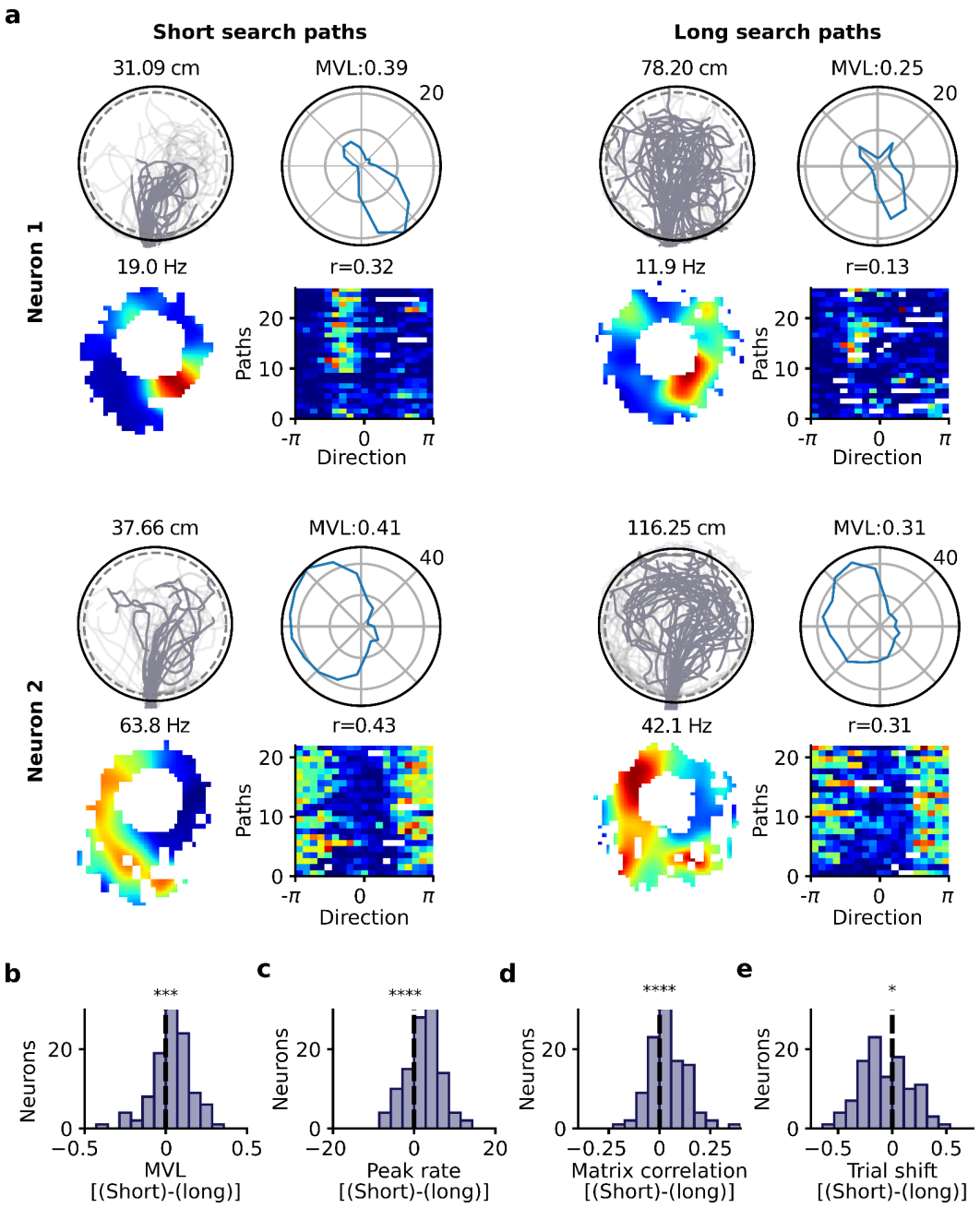

Figure. 29. Search path length influences the directional selectivity of lever-anchored firing fields during dark trials. a: Examples of two neurons with a lever-box-anchored firing field during dark trials. Their firing activity around the lever box is shown separately for trials with short (left) and long (right) search paths. For each neuron, four plots are shown for dark trials with short and long search paths. Top-left: Search paths (dark grey) of the animal during dark trials. The number indicates the median length of the search path. Bottom-left: 2D lever-box-centered firing rate map. The number indicates the peak firing rate. Top-right:

Directional firing rate histogram showing the firing rate of the neuron as a function of the direction of the mouse from the lever-box centre. The number indicates the polar plot's mean vector length (MVL). Bottom-right: Trial matrix of the neuron. Each row of the matrix is the firing rate as a function of the direction of the mouse from the lever-box centre for a single trial. The number above the matrix refers to the trial matrix correlation. **b,c,d,e**: Quantification of the differences in directional selectivity around the lever box between trials with short and long search paths. Only neurons with a lever-box-anchored field in the Cardinal reference frame were considered (n = 108). Directional selectivity was measured using the MVL (**b**) and peak rate of the directional polar histogram (**c**), the trial matrix correlation (**d**), and the directional trial drift (**e**). The plots show the differences between scores for trials with short and long search paths [(Short) - (Long)]. A value above 0 means the score was higher for trials with short search paths. *P*-values are from Wilcoxon signed-rank tests. **P* < 0.05, ****P* < 0.001, *****P* < 0.0001.

3.3.5 Lever-box-anchored fields get unstable during inaccurate trials

As mentioned, the mean vector length and the peak of the firing rate directional histogram of the lever-box-anchored cells decreases during the long search paths. Based on this observation, it was asked whether the firing pattern of the lever-box-anchored cells correlated with the homing accuracy of the animal during the homing behaviour. It was hypothesised that the directional selectivity of the lever-box-anchored cells was reduced during the inaccurate trials. To test this hypothesis, the dark trials were first divided into two sets of equally size datasets based on the median of the homing error at the periphery of each session (**Figure 30 a.**). The trials with a lower error at the periphery than the session median were classified as accurate. In contrast, the trials with the error at the periphery higher than the median of the error at periphery were classified as inaccurate trials. In addition, the directional selectivity of the cells was estimated using the mean vector length of the directional firing rate histogram and the trial matrix correlation of the cells (**Figure 30. a-b**). The mean vector length and the trial matrix correlation were larger for dark trials with accurate homing compared to the trials with inaccurate homing. To assess the directional selectivity of the cells during homing in dark trials, another parameter called trial drift was defined (see Material and Method). The average preferred direction of the

cell in all trials was first caculated and compared that to the directional tuning of the cell inaccurate and inaccurate trials (P = 0.0091). Investigation of the mean firing rate of the cells in accurate versus inaccurate trials also showed a decrease in the mean firing rate of the cells in inaccurate trials (P = 0.014). Together this data suggested that the lever-box-anchored firing fields were more stable during accurate homing in dark trials.

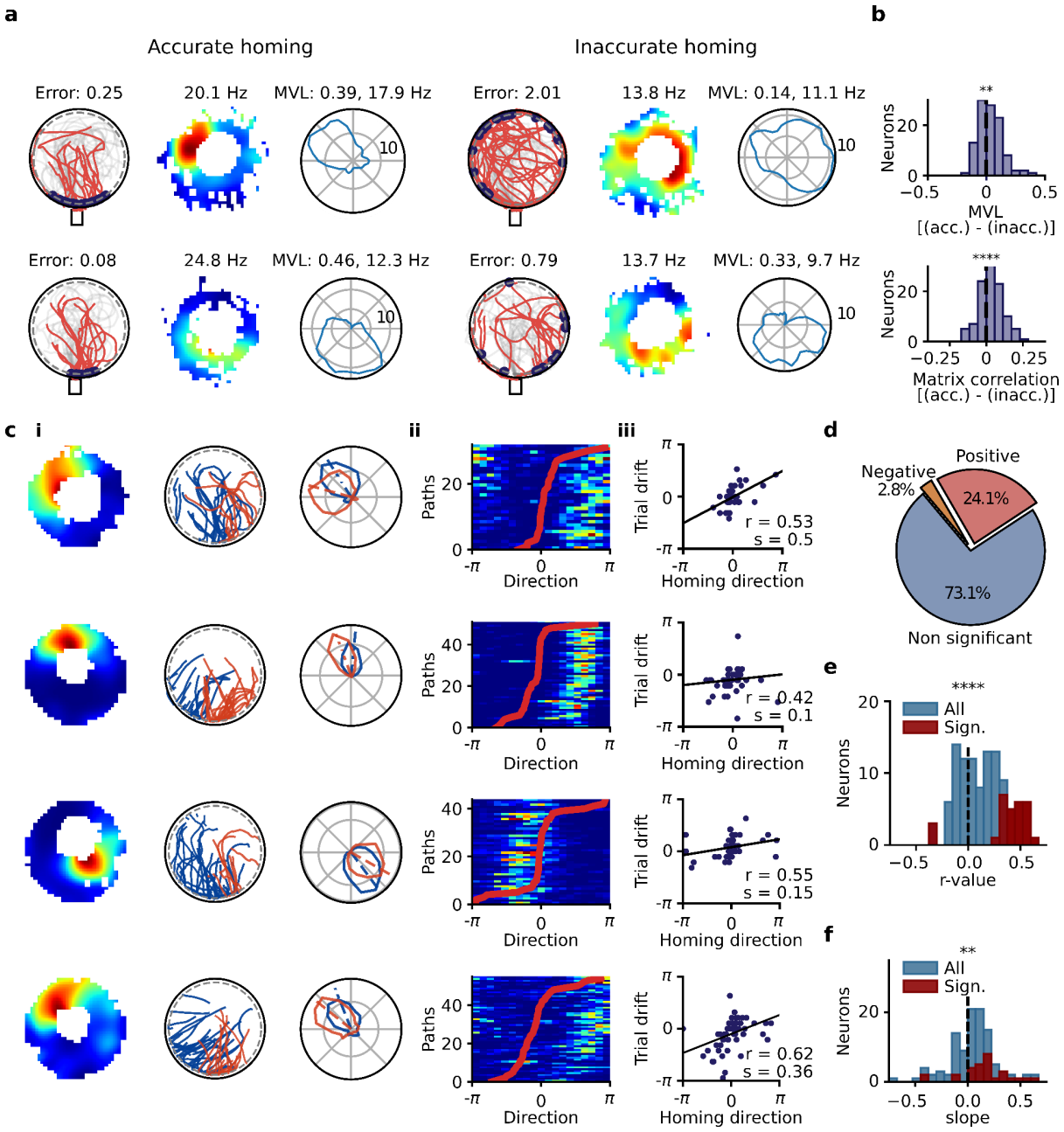

Figure 30: Direction of lever-box-anchored fields predicts homing direction during dark trials: a, Example of two neurons (one per row) with a lever-anchored firing field during dark trials. The activity at the lever box is shown separately for trials with accurate (left) and inaccurate (right) homing. Left: Homing paths of the mouse. The blue dots indicate the locations at which the mouse reached the arena periphery. The number indicates the median homing error in radian at the periphery of the arena. Middle: 2D lever-box-centred firing rate map. The number indicates the peak firing rate. Right: Directional firing rate histograms in the Cardinal

reference frame. The mean vector length (MVL) and peak rate are shown above the plot. **b**, Differences between the mean vector length and trial matrix correlation obtained from dark trials with accurate and inaccurate homing. A positive difference indicates a higher score during accurate trials than inaccurate trials. **c**, Example of four neurons with a significant correlation between the direction of its firing field around the lever and the homing direction of the mouse during dark trials. **i**, Left: 2D lever-box-centred firing rate map. Middle: Homing paths of the mouse. The colour of the homing path indicates whether the mouse reached the periphery of the arena on the left (blue) or right (red) side of the mean homing direction of the recording session. Right: Directional firing rate histogram for trials in which the mouse reached the periphery of the arena on the left (blue) or right (red) side of the mean homing direction. The dashed lines indicate the mean firing direction of the directional firing rate histograms. **ii**, Trial matrix and homing direction of the mouse. The trial matrix shows the firing rate of the neuron on each dark trial as a function of the direction around the lever box. The trials were sorted according to the homing direction of the mouse, which is displayed as a red line. **iii**, Trial drift of the neuron on each dark trial plotted against the homing direction of the mouse. The peak firing rate direction was rotated so that its preferred direction was 0. The regression line, together with the correlation coefficient (r) and slope of the regression line (s), are shown. **d**, Percentage of the lever-anchored neurons with a significant positive, negative, or non-significant correlation between the trial drift of the neuron and the homing direction of the mouse. **e**, Distribution of correlation coefficients between the trial drift of the neuron and the homing direction of the mouse for all neurons with a lever anchored firing field. **f**, Distribution of regression slopes between the trial drift of the neuron and the homing direction of the mouse for all neurons with a lever-box-anchored firing field. $^{**}P < 0.01$, $^{****}P < 0.0001$.

3.3.6 The trial drift of the lever-box-anchored cells correlates with homing direction during dark trials

It was next hypothesised whether the homing direction of the mouse could be predicted from the directional selectivity of the lever-box-anchored cells on each trial. To do that, the homing direction of the cells was first calculated as an angle between the two vectors originating at the centre of the lever box. One of the vectors points towards the centre of the bridge, and the other one towards the point where the mouse first hits the periphery of the arena. For each session, I classified the trials into two groups based on whether the homing direction of the trial was below or above the median homing direction of the session (**Figure 30. ci, middle row**). Then I calculated the polar firing

rate histogram for dark trials for both sets separately. Some cells changed their preferred directional selectivity associated with the homing direction of the cells. To check whether the changes were significant, I compared the changes with the homing direction vectors after shuffling the homing vector 500 times. The preferred direction of the cells significantly changed in association with the homing direction ($P < 0.05$) in 25 % of the neurons (27/108 neurons). The changes were also statistically significant when considering all the lever box-anchored cells for this analysis (n = 108 neurons, **supplementary fig . 4 a,b,c,d**). Then, it was tested whether different lever positions caused the changes that was observed. First, the analysis was limitedto the trials where the lever was located near the centre of the arena (**supplementary fig . 4 a,b,c,d)**.

Finally, it was tested whether there is a linear relationship between the trial drift in the firing direction of a neuron and the homing direction (**Figure 30. c ii, iii**). First, I sort trials based on the amount of homing error and plot the trial drift based on homing error. (**Figure 30. c ii**). Later, a circular-circular correlation was performed between the trial drift and the homing direction of the mouse (**Figure 30. c iii**). It was observed a significant correlation in 26.9 % of the lever-box-anchored neurons. 24.1 % of the cells had a positive r value with a significant correlation (vs 2.8 % with a negative r value) (**Figure 30. d**). At the population level, a significantly more positive correlation coefficient was observed (**Figure 30. e**). Our result indicated that the clockwise trial drift in the neuron's activity caused a clockwise rotation of the homing direction. In addition, the slope of the regression line was generally smaller than one indicating that trial drift in the homing direction of the neuron was usually smaller than the change in the homing direction of the animal (**Figure 30. f**). Together, the data suggested that the directional firing of the hippocampal pyramidal cells around the lever box was linked to the homing direction of the animal.

4. Discussion

Animals with lesions in the hippocampus showed a deficit in the tasks requiring PI (Whishaw, I. Q. & Tomie, 1997; Maaswinkel et al., 1999; McNaughton et al., 2006). Previous theoretical and experimental work also emphasised the role of pyramidal hippocampal cells in integrating self-motion cues during homing behaviour based on PI (Gothard et al., 1996a; Gothard et al., 1996b). Moreover, self-motion cues determine the place fields in premature rats when the input from the grid cells is still unavailable (Bjerknes et al., 2018). However, only a few studies investigated the activity of spatially selective neurons during PI tasks in freely moving rodents (Valerio & Taube, 2012b).

In this thesis, it was asked 1) whether the activity of place cells during the PI task is the same as random foraging trial and 2) whether successful navigation in a PI task would also affect the firing activity of place cells. A new PI task was developed that enabled us to record the cell's spatial properties when the animal engaged in a PI task. During the AutoPI task, the animal needed to search for a movable lever on a circular arena, press it and return to the home base for a reward. I compared the activity of place cell ensembles during the random foraging and AutoPI task. Near global remapping occurred between the random foraging versus the AutoPI task. During the AutoPI task itself, different cell ensembles were active in search and homing behaviours and under different light conditions. Place cells were either firing in a fixed place in the environment, encoded the distance between the animal and the lever box, or had a firing field close to the lever box (lever-box-anchored cells) independent of the lever location. The lever-box anchored cells had directional selectivity and were only active if the animal was in a specific direction from the lever in the Cardinal reference frame. In the darkness, when the animal had to use PI, the directional tuning of the lever-box-anchored cells was reduced in long search paths or during inaccurate homing. A significant correlation between the peak of the firing direction of

lever-box-anchored neurons and homing direction of the animal in single trials was also observed.

4.1 Why do we need another behavioural PI paradigm?

Food carrying task is one of the common paradigms to study PI. However, it is not possible to record the cell's spatially selective properties in a large environment using this paradigm (Maaswinkel et al., 1999; Hines & Whishaw, 2005; Valerio & Taube, 2012b). The neural basis of PI can also be studied in head-fixed rodents running on a floating ball. Linear track experiments, rotating balls together with adaptable visual stimuli, and floating arenas are some of the VR platforms that have been used so far to assess distance estimation using PI in 1D environments (Ravassard et al., 2015; Kislin et al., 2014; Nashaat et al., 2016; Go et al., 2021). One of the major limitation of VR tasks with the head-fixed or body-fixed paradigm is that it creates conflict between the vestibular cues and motor feedbacks which is rarely seen during navigation in the real world. AutoPI paradigm enabled us to 1) record more than 100 trials per session in an automated platform. 2) provided a paradigm for freely moving mice in 2D with more resemblance to the natural environment. 3) ensure having unique search paths on each trial on the AutoPI task enforcing the animal to use the within-trial information for homing, unlike most PI tasks in using a VR platform. 4) The automated setup allowed scaling up the training procedure in which large number of mice could be trained. Altogether, the AutoPI paradigm provides a new platform to assess the neural basis of PI in a 2D environment in freely moving mice.

4.2 Task-dependent activity of place cells

The activity of place cells in the random foraging trial was compared to the AutoPI trials. A complete reorganisation of neural ensembles was observed between the two tasks. This result is similar to the previous observation by Markus and his

colleagues in 1995. In this experiment, the activity of place cells was compared in the random foraging task with the radial arm maze. The directional selectivity of the cells was higher in the radial arm maze in comparison to the random foraging task. The activity of the place cells was also investigated when the animal had to search for the food in a fixed location on the arena versus when the food was scattered randomly during the foraging task. The navigational tasks performed here were different in some aspects, such as visual environment, motor behaviours (such as linear and angular velocities) and behavioural context (presence or absence of a goal). The results showed that the place fields were changing to a different location or went utterly silent when comparing the place cell's activity between the random foraging and radial arm maze (Markus et al., 1995). Reorganisation of the CA1 place cells between the random foraging and AutoPI task can be explained by the change of navigational strategies needed in these two tasks, resulting in the use of different sensory modalities (Geva-Sagiv et al., 2016; Radvansky et al., 2021).

Moreover, In the AutoPI task, the various light conditions might result in the different behavioural demands that remapped the CA1 place activity in between conditions. It was shown before that most place cells preserved their firing pattern without visual landmarks in the random foraging experiment (Quirk et al., 2008; Zhang et al., 2014). During random foraging, the animal does not need to plan a defined destination for its path. Therefore, the behavioural demand would remain the same in light and dark conditions. However, in the AutoPI task, removing the visual landmark would force the animal to plan its path based on PI instead of directly running to the lever or the home base. As a result, the running speed, length of the path, and complexity changed in light versus dark conditions in the AutoPI task.

4.3 Cells with task-relevant reference frames

Some hippocampal place cells encoded the animal's distance to or from the lever during the search and homing paths in the AutoPI task. I also recorded place cells with fixed place fields on the arena relative to the room. Interestingly, place cells only encode the animal's distance to the lever during the search paths in light trials when the lever was visible. In contrast, during homing, the cells encoded the animal's distance to the lever in both light and dark trials. Our data suggest that the animal's distance to the lever was encoded in dark trials using PI. This conclusion is in line with previous work showing a contribution of self-motion cues in determining the location of place fields. (Gothard et al., 1996b; Rivard et al., 2004; Bjerknes et al., 2018). For example, Gothard and her colleagues (1996) reported that place cells were more encoding the animal's distance relative to their starting point in a linear track with different lengths using PI. Also, place cells in premature rats encode the animal's distance to the starting point in a linear track with changeable length even when the grid cells are not entirely developed (Bjerknes et al., 2018).

In addition to the classical place cells with a fixed place field on the arena and the cells that encode the animal's distance from the lever, I found some cells that were active when the mouse was at the lever (distance of less than 10 cm from the lever) called lever-box-anchored cells. Lever-box-anchored cells were active close to the lever box independent of the lever's location on the arena in a lever-box reference frame (task-relevant object reference frame). Lever-box-anchored cells are similar to the goal/landmark-centre reference frame that Gothard and colleagues reported in 1996. In their experiments, rats were released from a box with a random location on an arena to find a reward before returning to the box for another reward. The position of the reward was near two objects on the arena. The location of the objects, together with the reward location, changed between trials, forcing the animal to rely mostly on visual landmarks for navigation. They found cells with a 1) fixed place field on the arena, 2) goal/landmark

cells that fired close to the goal or landmark independent of the location of the goal or landmark on the arena. 3) box-related cells that only fired when the rat was entering or closing the box (Gothard et al., 1996b). The goal/landmark cells are very similar to our lever-box-anchored cells described in my thesis.

In yet another study, Rivard and his colleagues recorded a subpopulation of the hippocampus cells that fire the animal's position relative to the environment's barrier regardless of the barrier location in the environment (Rivard et al., 2004). In this experiment, the position of the barrier was either fixed on the arena or it was moved to another location. When the barrier was fixed on the arena the cells behaved like classical place cells with a fixed place field on the arena. However, when the barrier was moved to a new location providing information about the barrier's locatoin on the arena. Together our results are inconsistent with the previous ones suggesting that a subpopulation of hippocampal cells encodes the animal's location in a fixed spatial frame (room frame), and other subpopulations encode the animal's location in task-dependent or object-dependent reference frames.

Furthermore, it was shown that the cells with the object-related firing fields were encoding the animal's location relative to the object in the darkness. The lever-box-anchored cells also fired the direction of the animal relative to the lever in the Cardinal reference frame in the AutoPI task. The directional selectivity of the lever-box-anchored cells in darkness, therefore might provide information about the position of the animal relative the lever using PI. The directional selectivity of these cells is similar to what was observed in the landmark-vector cells before in the hippocampus and MEC (Høydal et al., 2019; Dannenberg et al., 2020). Therefore, our data suggest that the activity of the lever-box-anchored cells and their directional selectivity can be related to the HD cells. The HD system can integrate the angular self-motion cues to estimate the direction of the animal related to the lever. Moreover, the homing direction of the animal on each trial also correlates to the homing direction. These data are

consistent with what Valerio and Taube (2012) observed in HD cells during a PI task. In addition, the MEC contains cells like HD, border and object-vector cells that make it a good candidate for translation of the HD signal to the position-direction codes reflected in lever-box-anchored cells. Border cells demonstrated directional selectivity coherent with the preferred direction of HD cells (Solstad et al., 2008). I assumed that the input from the border cells and object-vector cells in MEC to the hippocampus could contribute to the lever-box-anchored firing field in the AutoPI task. However, the characterisation of spatially selective cells in MEC in the AutoPI task is needed to understand the mechanism behind the formation of lever-box-anchored fields.

4.4 PI contributes to the directional selectivity of lever-anchored cells in the dark

The animal needed to integrate the linear and angular cues during the search paths to return to the home base in dark trials in the AutoPI task. To ensure that the animal uses PI in the dark, it was masked the potential auditory and olfactory cues using white noise and arena rotation. Using PI and in the absence of external landmarks, the accumulation of error increased with the length and duration of the search paths in the AutoPI task as it was previously reported (Allen et al., 2014; Valerio & Taube, 2012; Gil et al., 2018; Müller & Wehner, 1988; Stangl et al., 2020). The positive correlation between the search path's length and duration and the homing error in dark trials suggested that mice used PI in the AutoPI task.

It was also observed that the directional representation of the place cells around the lever box is getting updated in dark trials. When the length of the search paths increased in the dark trials, the variability in the direction selectivity of the lever-box-anchored cells also increased. The lever-box-anchored fields were located relative to the lever box (task/object-related reference frame) but not the global reference frame in the room (Cardinal reference frame). Therefore, the error in

estimating the movement during the search path should not affect the firing field stability since the field's location was set when the animal encountered the lever. Furthermore, the directionality of the firing fields for the lever-box-anchored cells correlated to the homing direction of the animal. Our data suggested that although the linear PI was not critical to set the directional selectivity of the lever-box-anchored cells, it was still required for accurate homing in the AutoPI task.

4.5 Lever-box-anchored fields predict the homing direction

Approximately 25% of the hippocampal pyramidal cells recorded in the AutoPI task had directional firing fields around the lever box. The preferred direction of the lever-box-anchored cells around the lever could also predict the homing direction of the animal. For instance, when the preferred direction of the lever-box-anchored cells rotated clockwise relative to the average preferred direction of the cell, the homing direction of the mouse on a given trial also rotated clockwise, respectively. Although, object-related firing fields have been reported in the hippocampus and MEC (Høydal et al., 2019; Deshmukh & Knierim, 2013). However, our results suggested that the object-task-related firing fields would also encode the information relevant to the homing direction of the animal during PI. It was hypothesised that 1) lever-box-anchored firing fields contribute to the homing behaviour by providing information in a Cardinal reference frame contributing to planning the homing direction. 2) A subpopulation of CA1 pyramidal cells that are active at the lever encode the time of the path on each trial when the animal reaches the lever and needs to plan for homing direction (Dragoi & Buzsáki, 2006). 3) The hippocampal cells contribute to the homing behaviour by providing spatial information, a series of meaningful events and the time points where the animal needs to decide in which direction it needs to go (Eichenbaum et al., 1999; Dragoi & Buzsáki, 2006; Buzsáki & Moser, 2013). I propose that hippocampal CA1 cells provide a cognitive plan to organise a homing direction in a homing based on the PI task.

5. Limitations and future work

A new behavioural paradigm to study homing based on path integration was developed in this thesis. The role of the hippocampal pyramidal cells was then investigated during the dark trials where the animal used PI. To confirm that the hippocampus is essential for homing behavirour in the AutoPI task, we would need to assess homing ability after manipulating the activity of hippocampal neurons during the task. One strategy could be to excite interneurons using channelrhodopsin to reduce the activity of principal cells. Light stimulation could be delivered during the search path up until the time at which the animal presses the lever. Based on previous lesion studies that showed a role of the hippocampus in homing based on path integration, I would hypothesize that the optogenetic manipulation of interneuron populations in the hippocampus would impair homing accuracy selectively during dark trials.

Another potential improvement on the experiments presented in this thesis would be to add controls for the potential use of odours. For instance, the pellets that are located behind the home base might provide an olfactory cue for the mice to return to the home base. For instance, one could move the home base to a new location while the mouse was in the arena during the dark trial, which would be difficult to implement. Another possible manipulation could be to train the mice in a paradigm with two or more home bases. Only returning to one of them would lead to the reward on each trial. Multiple pellet sources around the arena would reduce the chance of using odour cues to navigate back to the home base. However, adding multiple home bases to the paradigm would have expanded the training period, which is already long (6-8 weeks). It should also be noted that mice performed way above chance level during dark trials in which a strong airflow made the use of olfactory cues unlikely, suggesting that the performance of mice during dark trials likely depended on path integration.

It was argued in the discussion that the lever-box-anchored cells are task-relevant, and the directional selectivity of these cells predicts the homing direction

of the mouse during homing. The observation of lever-box-anchored cells also raised the question of whether the cells observed around the lever are the same as the object-vector-anchored cells in MEC or other brain areas. To have a better control experiment for this question, one would need to compare the spatial properties of the cells during the random foraging task but with the lever located on the arena. I would hypothesise that the pyramidal cells would not fire around the lever during the random foraging trial.

6. Conclusion

I extended a classical operant conditioning protocol to study PI in mice. A population of hippocampal cells (lever-box-anchored) fired when the animal was running around the lever before starting its homing path. The lever-box-anchored cells were firing in a lever reference frame with the lever at its centre. The directional selectivity of these neurons was relative to the room reference frame. Our finding rules out the hypothesis that during a homing task all hippocampal neurons fire in a global and stable reference frame that includes the start and end of a journey. A next step could be to investigate the firing patterns of grid cells located in the MEC, one of the main inputs to the hippocampus. The implicit assumption in the grid cell literature is that grid cells should fire in a global reference frame during a PI task. This assumption will soon be addressed using the behavioral paradigm I developed in my thesis.

6. References

Agster, K. L., & Burwell, R. D. (2009). Cortical efferents of the perirhinal, postrhinal, and entorhinal cortices of the rat. *Hippocampus*, *19*(12), 1159–1186. https://doi.org/10.1002/hipo.20578

Allen, K., Gil, M., Resnik, E., Toader, O., Seeburg, P., & Monyer, H. (2014). Impaired path integration and grid cell spatial periodicity in mice lacking GluA1-containing AMPA receptors. *Journal of Neuroscience*, *34*(18), 6245–6259. https://doi.org/10.1523/JNEUROSCI.4330-13.2014

Bassett, J. P., & Taube, J. S. (2001). Neural correlates for angular head velocity in the rat dorsal tegmental nucleus. *Journal of Neuroscience*, *21*(15), 5740–5751. https://doi.org/10.1523/jneurosci.21-15-05740.2001

Bassett, J. P., Wills, T. J., & Cacucci, F. (2018). Self-Organized Attractor Dynamics in the Developing Head Direction Circuit. *Current Biology*, *28*(4), 609-615.e3. https://doi.org/10.1016/j.cub.2018.01.010

Bjerknes, T. L., Dagslott, N. C., Moser, E. I., & Moser, M. (2018). *Path integration in place cells of developing rats*. *7489*, 1637–1646. https://doi.org/10.1073/pnas.1719054115

Britten, K. H. (2008). Mechanisms of self-motion perception. *Annual Review of Neuroscience*, *31*, 389–410. https://doi.org/10.1146/annurev.neuro.29.051605.112953

Brun, V. H., Otnæss, M. K., Molden, S., Steffenach, H. A., Witter, M. P., Moser, M. B., & Moser, E. I. (2002). Place cells and place recognition maintained by direct entorhinal-hippocampal circuitry. *Science*, *296*(5576), 2243–2246. https://doi.org/10.1126/science.1071089

Buzsáki, G., & Moser, E. I. (2013). Memory, navigation and theta rhythm in the hippocampal-entorhinal system. *Nature Neuroscience*, *16*(2), 130–138. https://doi.org/10.1038/NN.3304

Chiba, A. A., Kesner, R. P., & Reynolds, A. M. (1994). Memory for spatial location as a function of temporal lag in rats: Role of hippocampus and medial prefrontal cortex. *Behavioral and Neural Biology*, *61*(2), 123–131. https://doi.org/10.1016/S0163-1047(05)80065-2

Clark, B. J., & Taube, J. S. (2012). Vestibular and attractor network basis of the head direction cell signal in subcortical circuits. *Frontiers in Neural Circuits*, *6*(March), 1–12. https://doi.org/10.3389/fncir.2012.00007

Collett, T. S., Cartwright, B. A., & Smith, B. A. (1986). Landmark learning and visuo-spatial memories in gerbils. *Journal of Comparative Physiology A Sensory, Neural, and Behavioral Physiology*, *158*(6), 835–851. https://doi.org/10.1007/BF01324825

Cooper, B. G., Miya, D. Y., & Mizumori, S. J. Y. (1998). Superior colliculus and active navigation: Role of visual and non-visual cues in controlling cellular representations of space. *Hippocampus*, *8*(4), 340–372. https://doi.org/10.1002/(SICI)1098-1063(1998)8:4<340::AID-HIPO4>3.0.CO;2-L

Corkin, S., Amaral, D. G., Gilberto González, R., Johnson, K. A., & Hyman, B. T. (1997). H. M.'s Medial temporal lobe lesion: Findings from magnetic resonance imaging. *Journal of Neuroscience*, *17*(10), 3964–3979. https://doi.org/10.1523/jneurosci.17-10-03964.1997

Csicsvari, J., Hirase, H., Czurkó, A., Mamiya, A., & Buzsáki, G. (1999). Oscillatory coupling of hippocampal pyramidal cells and interneurons in the behaving rat. *Journal of Neuroscience*, *19*(1), 274–287. https://doi.org/10.1523/jneurosci.19-01-00274.1999

Cullen, K. E., & Taube, J. S. (2017). Our sense of direction: Progress, controversies and challenges. *Nature Neuroscience*, *20*(11), 1465–1473. https://doi.org/10.1038/nn.4658

Dannenberg, H., Lazaro, H., Nambiar, P., Hoyland, A., & Hasselmo, M. E. (2020). Effects of visual inputs on neural dynamics for coding of location and running speed in medial entorhinal cortex. *ELife*, *9*, 1–34. https://doi.org/10.7554/ELIFE.62500

Deacon, R. M. J., & Rawlins, J. N. P. (2006). *T-maze alternation in the rodent*. *1*(1), 7–12. https://doi.org/10.1038/nprot.2006.2

Deshmukh, S. S., Johnson, J. L., & Knierim, J. J. (2012). Perirhinal cortex represents nonspatial, but not spatial, information in rats foraging in the presence of objects: Comparison with lateral entorhinal cortex. *Hippocampus*, *22*(10), 2045–2058. https://doi.org/10.1002/hipo.22046

Deshmukh, S. S., & Knierim, J. J. (2013). Influence of local objects on hippocampal representations: Landmark vectors and memory. *Hippocampus*, *23*(4), 253–267. https://doi.org/10.1002/HIPO.22101

Dragoi, G., & Buzsáki, G. (2006). Temporal Encoding of Place Sequences by Hippocampal Cell Assemblies. *Neuron*, *50*(1), 145–157. https://doi.org/10.1016/j.neuron.2006.02.023

Eichenbaum, H., Amaral, D. G., Buffalo, E. A., Cohen, N., Davachi, L., Frank, L., Heckers, S., Morris, R. G. M., Moser, E. I., Nadel, L., Keefe, J. O., Preston, A., & Ranganath, C. (2016). *Hippocampus at 25*. *1249*, 1238–1249. https://doi.org/10.1002/hipo.22616

Eichenbaum, H., Dudchenko, P., Wood, E., Shapiro, M., & Tanila, H. (1999). The Hippocampus, Memory, Review and Place Cells: Is It Spatial Memory or a Memory Space? might occur at different locations. Olton and colleagues Neuron 210 Figure 1. Schematic Overhead Views of Four Different Types of Apparatus and Examples of Location-S. *Neuron*, *23*, 209–226. http://cogs200.pbworks.com/f/Eichenbaum 99 Hippocampus.pdf

Eichenbaum, H., Otto, T., & Cohen, N. J. (1992). The hippocampus-what does it do? *Behavioral and Neural Biology*, *57*(1), 2–36. https://doi.org/10.1016/0163-1047(92)90724-I

Elduayen, C., & Save, E. (2014). The retrosplenial cortex is necessary for path integration in the dark. *Behavioural Brain Research*, *272*, 303–307. https://doi.org/10.1016/j.bbr.2014.07.009

Ergorul, C., & Eichenbaum, H. (2004). The hippocampus and memory for "what," "where," and "when." *Learning and Memory*, *11*(4), 397–405. https://doi.org/10.1101/lm.73304

Etienne, A. S., Teroni, E., Maurer, R., Portenier, V., & Saucy, F. (1985). Short-distance homing in a small mammal: the role of exteroceptive cues and path integration. *Experientia*, *41*(1), 122–125. https://doi.org/10.1007/BF02005909

Etienne, Ariane S. (1980). The orientation of the golden hamster to its nest-site after the elimination of various sensory cues. *Experientia*, *36*(9), 1048–1050. https://doi.org/10.1007/BF01965961

Etienne, Ariane S., Maurer, R., & Séguinot, V. (1996). Path integration in mammals and its interaction with visual landmarks. *Journal of Experimental Biology*, *199*(1), 201–209. https://doi.org/10.1242/jeb.199.1.201

Etienne, Ariane S., Teroni, E., Hurni, C., & Portenier, V. (1990). The effect of a single light cue on homing behaviour of the golden hamster. *Animal Behaviour*, *39*(1), 17–41. https://doi.org/10.1016/S0003-3472(05)80723-7

Foster, T. C., Castro, C. A., & McNaughton, B. L. (1989). Spatial selectivity of rat hippocampal neurons: Dependence on preparedness for movement. *Science*, *244*(4912), 1580–1582. https://doi.org/10.1126/science.2740902

Fyhn, M., Molden, S., Witter, M. P., Moser, E. I., & Moser, M. B. (2004). Spatial representation in the entorhinal cortex. *Science*, *305*(5688), 1258–1264. https://doi.org/10.1126/science.1099901

Gabrieli, J. D. E., Cohen, N. J., & Corkin, S. (1988). The impaired learning of semantic knowledge following bilateral medial temporal-lobe resection. *Brain and Cognition*, *7*(2), 157–177. https://doi.org/10.1016/0278-2626(88)90027-9

Gaffan, D. (1979). Acquisition and forgetting in monkeys' memory of informational object-reward associations. *Learning and Motivation*, *10*(4), 419–444. https://doi.org/10.1016/0023-9690(79)90056-0

Gallistel, C. R., & Cramer, A. E. (1996). Computations on metric maps in mammals: Getting oriented and choosing a multi-destination route. *Journal of Experimental Biology*, *199*(1), 211–217. https://doi.org/10.1242/jeb.199.1.211

Geva-Sagiv, M., Romani, S., Las, L., & Ulanovsky, N. (2016). Hippocampal global remapping for different sensory modalities in flying bats. *Nature Neuroscience*, *19*(7), 952–958. https://doi.org/10.1038/nn.4310

Gil, M., Ancau, M., Schlesiger, M. I., Neitz, A., Allen, K., De Marco, R. J., & Monyer, H. (2018). Impaired path integration in mice with disrupted grid cell firing. *Nature Neuroscience*, *21*(1), 81–93. https://doi.org/10.1038/s41593-017-0039-3

Go, M. A., Rogers, J., Gava, G. P., Davey, C. E., Prado, S., Liu, Y., & Schultz, S. R. (2021). Place Cells in Head-Fixed Mice Navigating a Floating Real-World Environment. *Frontiers in Cellular Neuroscience*, *15*. https://doi.org/10.3389/fncel.2021.618658

Góis, Z. H. T. D., & Tort, A. B. L. (2018). Characterizing Speed Cells in the Rat Hippocampus. *Cell Reports*, *25*(7), 1872-1884.e4. https://doi.org/10.1016/j.celrep.2018.10.054

Gothard, K. M., Skaggs, W. E., Moore, K. M., & McNaughton, B. L. (1996a). Binding of hippocampal CA1 neural activity to multiple reference frames in a landmark-based navigation task. *Journal of Neuroscience*, *16*(2), 823–835. https://doi.org/10.1523/jneurosci.16-02-00823.1996

Gothard, K. M., Skaggs, W. E., Moore, K. M., & McNaughton, B. L. (1996b). Binding of hippocampal CA1 neural activity to multiple reference frames in a landmark-based navigation task. *Journal of Neuroscience*, *16*(2), 823–835. https://doi.org/10.1523/JNEUROSCI.16-02-00823.1996

Hafting, T., Fyhn, M., Molden, S., Moser, M. B., & Moser, E. I. (2005). Microstructure of a spatial map in the entorhinal cortex. *Nature*, *436*(7052), 801–806. https://doi.org/10.1038/nature03721

Hardcastle, K., Ganguli, S., & Giocomo, L. M. (2015). Environmental Boundaries as an Error Correction Mechanism for Grid Cells. *Neuron*, *86*(3), 827–839. https://doi.org/10.1016/j.neuron.2015.03.039

Høydal, Ø. A., Skytøen, E. R., Andersson, S. O., Moser, M. B., & Moser, E. I. (2019). Object-vector coding in the medial entorhinal cortex. *Nature*, *568*(7752), 400–404. https://doi.org/10.1038/s41586-019-1077-7

Jacob, P. Y., Casali, G., Spieser, L., Page, H., Overington, D., & Jeffery, K. (2017). An independent, landmark-dominated head-direction signal in dysgranular retrosplenial cortex. *Nature Neuroscience*, *20*(2), 173–175. https://doi.org/10.1038/nn.4465

Jarrard, L. E. (1995). What does the hippocampus really do? *Behavioural Brain Research*, *71*(1–2), 1–10. https://doi.org/10.1016/0166-4328(95)00034-8

Jayakumar, R. P., Madhav, M. S., Savelli, F., Blair, H. T., Cowan, N. J., & Knierim, J. J. (2019). Recalibration of path integration in hippocampal place cells. *Nature*, *566*(7745), 533–537. https://doi.org/10.1038/s41586-019-0939-3

Jeewajee, A., Barry, C., O'Keefe, J., & Burgess, N. (2008). Grid cells and theta as oscillatory interference: Electrophysiological data from freely moving rats. *Hippocampus*, *18*(12), 1175–1185. https://doi.org/10.1002/hipo.20510

Kitamura, T., Pignatelli, M., Suh, J., Kohara, K., Yoshiki, A., Abe, K., & Tonegawa, S. (2014). Supplementary Materials - Island Cells Control Temporal Association Memory. *Science*, *343*(6173), 896–901. https://doi.org/10.1126/science.1244634

Koenig, S., Wolf, R., & Heisenberg, M. (2016). Vision in flies: Measuring the attention span. *PLoS ONE*, *11*(2), 1–16. https://doi.org/10.1371/journal.pone.0148208

Kropff, E., Carmichael, J. E., Moser, M. B., & Moser, E. I. (2015). Speed cells in the medial entorhinal cortex. *Nature*, *523*(7561), 419–424. https://doi.org/10.1038/nature14622

Maaswinkel, H., Jarrard, L. E., & Whishaw, I. Q. (1999). Hippocampectomized rats are impaired in homing by path integration. *Hippocampus*, *9*(5), 553–561. https://doi.org/10.1002/(SICI)1098-1063(1999)9:5<553::AID-HIPO9>3.0.CO;2-G

Markus, E. J., Qin, Y.-L., Leonard, B., Skaggs, W. E., Mcnaughton, B. L., & Barnes1, C. A. (1995). Interactions between Location and Task Affect the Spatial and Directional Firing of Hippocampal Neurons. In *The Journal of Neuroscience* (Vol. 15, Issue 11).

Maurer, A. P., VanRhoads, S. R., Sutherland, G. R., Lipa, P., & McNaughton, B. L. (2005). Self-motion and the origin of differential spatial scaling along the septo-temporal axis of the hippocampus. *Hippocampus*, *15*(7), 841–852. https://doi.org/10.1002/hipo.20114

Mcnaughton, B. L., Barnes, C. A., Gerrard, J. L., Gothard, K., Jung, M. W., Knierim, J. J., Kudrimoti, H., Qin, Y., Skaggs, W. E., Suster, M., & Weaver, K. L. (1996). Deciphering the hippocampal polyglot: The hippocampus as a path integration system. *Journal of Experimental Biology*, *199*(1), 173–185. https://doi.org/10.1242/jeb.199.1.173

McNaughton, B. L., Barnes, C. A., & O'Keefe, J. (1983). The contributions of position, direction, and velocity to single unit activity in the hippocampus of freely-moving rats. *Experimental Brain Research*, *52*(1), 41–49. https://doi.org/10.1007/BF00237147

McNaughton, Bruce L., Battaglia, F. P., Jensen, O., Moser, E. I., & Moser, M. B. (2006a). Path integration and the neural basis of the "cognitive map." *Nature Reviews Neuroscience*, *7*(8), 663–678. https://doi.org/10.1038/nrn1932

McNaughton, Bruce L., Battaglia, F. P., Jensen, O., Moser, E. I., & Moser, M. B. (2006b). Path integration and the neural basis of the "cognitive map." *Nature Reviews Neuroscience*, *7*(8), 663–678. https://doi.org/10.1038/NRN1932

Mittelstaedt, M. L., & Mittelstaedt, H. (1980). Homing by path integration in a mammal. *Naturwissenschaften*, *67*(11), 566–567. https://doi.org/10.1007/BF00450672

Mizumori, S. J. Y., McNaughton, B. L., Barnes, C. A., & Fox, K. B. (1989). Preserved spatial coding in hippocampal CA1 pyramidal cells during reversible suppression of CA3c output: Evidence for pattern completion in hippocampus. *Journal of Neuroscience*, *9*(11), 3915–3928. https://doi.org/10.1523/jneurosci.09-11-03915.1989

Morris, R., Garrud, P., Rawlins, J. et al. Place navigation impaired in rats with hippocampal lesions. Nature 297, 681–683 (1982). https://doi.org/10.1038/297681a0

Moser, E. I., Moser, M. B., & McNaughton, B. L. (2017). Spatial representation in the hippocampal formation: A history. *Nature Neuroscience*, *20*(11), 1448–1464. https://doi.org/10.1038/nn.4653

Muir, G. M., & Taube, J. S. (2002). The neural correlates of navigation: do head direction and place cells guide spatial behavior? *Behavioral and Cognitive Neuroscience Reviews*, *1*(4), 297–317. https://doi.org/10.1177/1534582302238339

Müller, M., & Wehner, R. (1988). Path integration in desert ants, Cataglyphis fortis . *Proceedings of the National Academy of Sciences*, *85*(14), 5287–5290. https://doi.org/10.1073/pnas.85.14.5287

Muller, R. U., Kubie, J. L., & Ranck, J. B. (1987). Spatial firing patterns of hippocampal complex-spike cells in a fixed environment. *Journal of Neuroscience*, *7*(7), 1935–1950. https://doi.org/10.1016/S0301-0082(96)00019-6

Naber, P. A., Lopes Da Silva, F. H., & Witter, M. P. (2001). Reciprocal connections between the entorhinal cortex and hippocampal fields CA1 and the subiculum are in register with the projections from CA1 to the subiculum. *Hippocampus*, *11*(2), 99–104. https://doi.org/10.1002/hipo.1028

Neves, G., Cooke, S. F., & Bliss, T. V. P. (2008). Synaptic plasticity, memory and the hippocampus: A neural network approach to causality. *Nature Reviews Neuroscience*, *9*(1), 65–75. https://doi.org/10.1038/nrn2303

Neylan, T. C., Editor, S., & Scoville, W. B. (2000). NEUROPSYCHIATRY CLASSICS Memory and the Medial Temporal Lobe : Patient H . M . Loss of Recent Memory After Bilateral Hippocampal Lesions. *Journal Of Neuropsychiatry*, *253*(5026), 1380–1386.

O'Keefe, J. O., & Nades, L. (1979). *OKeefe&Nadel (1979) The hippocampus as a cognitive map*. 487–533.

O'Keefe, J., & Burgess, N. (1996). Geometric determinants of the neurons. *Nature*, *381*(May), 425–428.

O'Keefe, J., Dostrovsky, J., & J. O'Keefe, J. D. (1971). Short Communications The hippocampus as a spatial map . Preliminary evidence from unit activity in the freely-moving rat. *Brain Research*, *34*(1), 171–175. http://www.ncbi.nlm.nih.gov/pubmed/5124915

O'Keefe, J., & Speakman, A. (1987). Single unit activity in the rat hippocampus during a spatial memory task. *Experimental Brain Research*, *68*(1), 1–27. https://doi.org/10.1007/BF00255230

Olton, D. S., & Paras, B. C. (1979). Spatial memory and hippocampal function. *Neuropsychologia*, *17*(6), 669–682. https://doi.org/10.1016/0028-3932(79)90042-3

Parron, C., Poucet, B., & Save, E. (2004). Entorhinal cortex lesions impair the use of distal but not proximal landmarks during place navigation in the rat. *Behavioural Brain Research*, *154*(2), 345–352. https://doi.org/10.1016/j.bbr.2004.03.006

Patel, J. (2015). Network mechanisms underlying the initiation and generation of sharp-wave-associated ripple oscillations. *Journal of Neuroscience*, *35*(6), 2323–2325. https://doi.org/10.1523/JNEUROSCI.4215-14.2015

Pérez-Escobar, J. A., Kornienko, O., Latuske, P., Kohler, L., & Allen, K. (2016). Visual landmarks sharpen grid cell metric and confer context specificity to neurons of the medial entorhinal cortex. *ELife*, *5*(JULY), 1–21. https://doi.org/10.7554/eLife.16937

Quirk, G. J., Muller, R. U., & Kubie, J. L. (2008). The Firing of Hippocampal Rat ' s Recent Experience Place Cells in the Dark Depends on the. *The Journal of Neuroscience*, *7*(June 1990), 2008–2017.

Radvansky, B. A., Oh, J. Y., Climer, J. R., & Dombeck, D. A. (2021). Behavior determines the hippocampal spatial mapping of a multisensory environment. *Cell Reports*, *36*(5), 109444. https://doi.org/10.1016/j.celrep.2021.109444

Ravassard, P., Kees, A., Willers, B., Ho, D., Aharoni, D., Cushman, J., Aghajan, Z. M., Mehta, M. R., Text, S., & References, F. (2013). Supplementary Materials for Multisensory control of hippocampal spatiotemporal selectivity. *Science (New York, N.Y.)*, *May*, 1342–1347. https://doi.org/10.1126/science1232655

Rawlins, J. N. P. (1985). Associations across time: The hippocampus as a temporary memory store. *Behavioral and Brain Sciences*, *8*(3), 479–497. https://doi.org/10.1017/S0140525X00001291

Rivard, B., Li, Y., Lenck-Santini, P. P., Poucet, B., & Muller, R. U. (2004). Representation of objects in space by two classes of hippocampal pyramidal cells. *Journal of General Physiology*, *124*(1), 9–25. https://doi.org/10.1085/jgp.200409015

Sargolini, F., Fyhn, M., Hafting, T., McNaughton, B. L., Witter, M. P., Moser, M. B., & Moser, E. I. (2006). Conjunctive representation of position, direction, and velocity in entorhinal cortex. *Science*, *312*(5774), 758–762. https://doi.org/10.1126/science.1125572

Save, E., Cressant, A., Thinus-Blanc, C., & Poucet, B. (1998). Spatial firing of hippocampal place cells in blind rats. *Journal of Neuroscience*, *18*(5), 1818–1826. https://doi.org/10.1523/jneurosci.18-05-01818.1998

Senova, S., Fomenko, A., Gondard, E., & Lozano, A. M. (2020). Anatomy and function of the fornix in the context of its potential as a therapeutic target. *Journal of Neurology, Neurosurgery and Psychiatry*, *91*(5), 547–559. https://doi.org/10.1136/jnnp-2019-322375

Skaggs, W. E., McNaughton, B. L., Wilson, M. A., & Barnes, C. A. (1996). Theta phase precession in hippocampal neuronal populations and the compression of temporal sequences. *Hippocampus*, *6*(2), 149–172. https://doi.org/10.1002/(SICI)1098-1063(1996)6:2<149::AID-HIPO6>3.0.CO;2-K

Solstad, T., Boccara, C. N., Kropff, E., Moser, M.-B., & Moser, E. I. (2008). Representation of Geometric Borders in the Entorhinal Cortex. *Science*, *322*(5909), 1865–1868. https://doi.org/10.1126/science.1166466

Solstad, T., Moser, E. I., & Einevoll, G. T. (2006). From grid cells to place cells: A mathematical model. *Hippocampus*, *16*(12), 1026–1031. https://doi.org/10.1002/hipo.20244

Stackman, R. W., & Taube, J. S. (1998). Firing properties of rat lateral mammillary single units: Head direction, head pitch, and angular head velocity. *Journal of Neuroscience*, *18*(21), 9020–9037. https://doi.org/10.1523/jneurosci.18-21-09020.1998

Stangl, M., Kanitscheider, I., Riemer, M., Fiete, I., & Wolbers, T. (2020). Sources of path integration error in young and aging humans. *Nature Communications*, *11*(1). https://doi.org/10.1038/s41467-020-15805-9

Taube JS. Head direction cells recorded in the anterior thalamic nuclei of freely moving rats. J Neurosci. 1995 Jan;15(1 Pt 1):70-86. doi: 10.1523/JNEUROSCI.15-01-00070.1995.

Taube, J. S. (2007). The head direction signal: Origins and sensory-motor integration. *Annual Review of Neuroscience*, *30*(May), 181–207. https://doi.org/10.1146/annurev.neuro.29.051605.112854

Terrazas, A., Krause, M., Lipa, P., Gothard, K. M., Barnes, C. A., & McNaughton, B. L. (2005). Self-motion and the hippocampal spatial metric. *Journal of Neuroscience*, *25*(35), 8085–8096. https://doi.org/10.1523/JNEUROSCI.0693-05.2005

Valerio, S., & Taube, J. S. (2012). Path integration: How the head direction signal maintains and corrects spatial orientation. *Nature Neuroscience*, *15*(10), 1445–1453. https://doi.org/10.1038/nn.3215

Van Cauter, T., Camon, J., Alvernhe, A., Elduayen, C., Sargolini, F., & Save, E. (2013). Distinct roles of medial and lateral entorhinal cortex in spatial cognition. *Cerebral Cortex*, *23*(2), 451–459. https://doi.org/10.1093/cercor/bhs033

Vanderwolf CH. Hippocampal electrical activity and voluntary movement in the rat. Electroencephalogr Clin Neurophysiol. 1969 Apr;26(4):407-18.. 10.1016/0013-4694(69)90092-3. PMID: 4183562.

Van Strien, N. M., Cappaert, N. L. M., & Witter, M. P. (2009). The anatomy of memory: An interactive overview of the parahippocampal- hippocampal network. *Nature Reviews Neuroscience*, *10*(4), 272–282. https://doi.org/10.1038/nrn2614

Walker, S. F. (1992). Book review. *Animal Behaviour*, *43*(2), 357. https://doi.org/10.1016/s0003-3472(05)80233-7

Wan, X., Wang, R. F., & Crowell, J. A. (2012). The effect of landmarks in human path integration. *Acta Psychologica*, *140*(1), 7–12. https://doi.org/10.1016/j.actpsy.2011.12.011

Wang, C., Chen, X., Lee, H., Deshmukh, S. S., Yoganarasimha, D., Savelli, F., & Knierim, J. J. (2018). Egocentric coding of external items in the lateral entorhinal cortex. *Science*, *362*(6417), 945–949. https://doi.org/10.1126/science.aau4940

Wehner, R., & Srinivasan, M. V. (1981). Searching behaviour of desert ants, genus Cataglyphis (Formicidae, Hymenoptera). *Journal of Comparative Physiology □ A*, *142*(3), 315–338. https://doi.org/10.1007/BF00605445

Whishaw, I. Q. (n.d.). *Hippocampal lesions and path integration John E McKenna and Hans Maaswinkel*. 228–234.

Whishaw, I. Q., & Tomie, J. A. (1997). Piloting and dead reckoning dissociated by fimbria-fornix lesions in a rat food carrying task. *Behavioural Brain Research*, *89*(1–2), 87–97. https://doi.org/10.1016/S0166-4328(97)00068-5

Witter, M. P., & Amaral, D. G. (1991). Entorhinal cortex of the monkey: V. Projections to the dentate gyrus, hippocampus, and subicular complex. *Journal of Comparative Neurology*, *307*(3), 437–459. https://doi.org/10.1002/cne.903070308

Witter, M. P., Doan, T. P., Jacobsen, B., Nilssen, E. S., & Ohara, S. (2017). Architecture of the entorhinal cortex a review of entorhinal anatomy in rodents with some comparative notes. *Frontiers in Systems Neuroscience*, *11*(June), 1–12. https://doi.org/10.3389/fnsys.2017.00046

Witter, M. P., Wouterlood, F. G., Naber, P. A., & Van Haeften, T. (2000). Anatomical organization of the parahippocampal-hippocampal network. *Annals of the New York Academy of Sciences*, *911*, 1–24. https://doi.org/10.1111/j.1749-6632.2000.tb06716.x

Yoder, R. M., & Taube, J. S. (2014). The vestibular contribution to the head direction signal and navigation. *Frontiers in Integrative Neuroscience*, *8*(APR), 1–13. https://doi.org/10.3389/fnint.2014.00032

Zhang, S. J., Ye, J., Couey, J. J., Witter, M., Moser, E. I., & Moser, M. B. (2014). Functional connectivity of the entorhinal - Hippocampal space circuit. *Philosophical Transactions of the Royal Society B: Biological Sciences*, *369*(1635), 1–8. https://doi.org/10.1098/rstb.2012.0516

Zhang, S., Schönfeld, F., Wiskott, L., & Manahan-Vaughan, D. (2014). Spatial representations of place cells in darkness are supported by path integration and border information. *Frontiers in Behavioral Neuroscience*, *8*(JUNE), 1–12. https://doi.org/10.3389/fnbeh.2014.00222

7. Supplementary figures

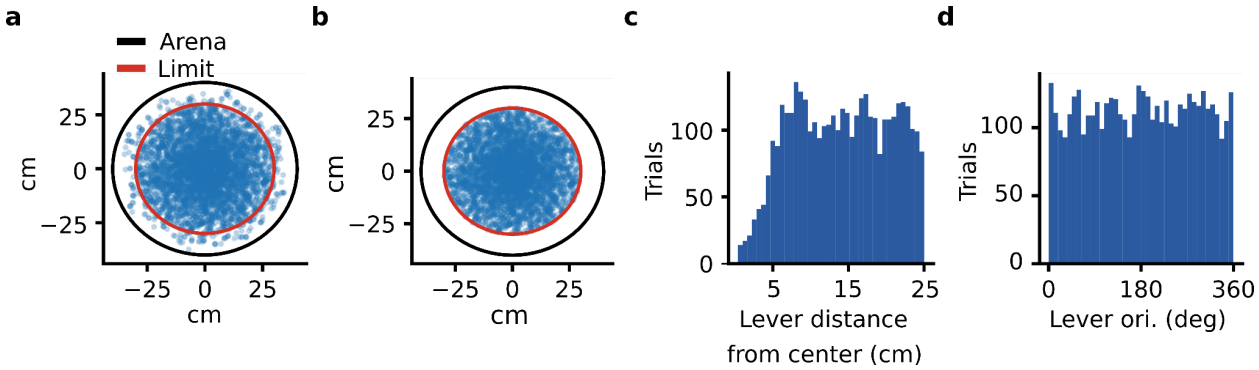

Supplementary Fig. 1. Position and orientation of the lever box on the arena. a, Distribution of lever box position on the arena for trials of the test sessions. The red circle indicated the maximal distance (25 cm) between the lever box centre and the arena centre for a trial to be included in the analysis. **b**, The lever box position distribution for trials included in the analysis. **c**, Distribution of distance between the lever box and the centre of the arena for all trials of the test sessions. **d**, Distribution of lever box orientation for all trials of the test sessions.

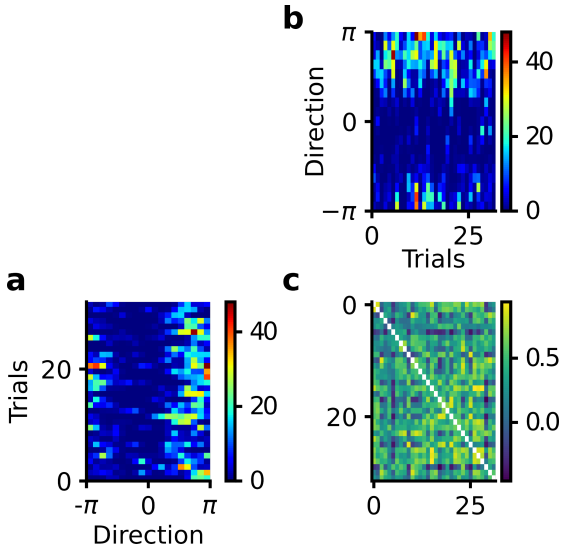

Supplementary Fig. 2. Procedure to calculate the trial matrix correlation. a, Trial matrix showing the firing rate of a neuron on each trial as a function of a behavioural variable, here the

direction of the mouse around the lever box. **b**, Same trial matrix as in **a** but rotated by 90° anti-clockwise. **c**, Correlation matrix showing the Pearson correlation coefficients between all pairs of trials. The trial matrix correlation is the mean of the correlation matrix after excluding the values of the main diagonal.

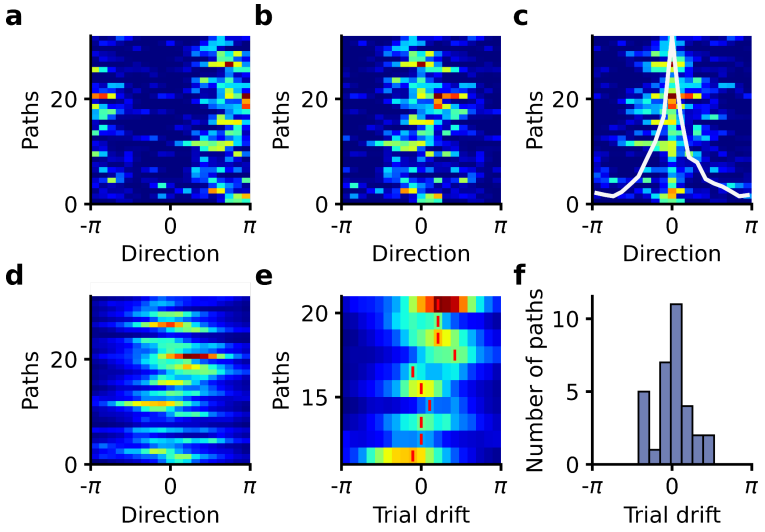

Supplementary Fig. 3. Procedure to calculate the directional trial drift of lever-box-anchored fields. a, Trial matrix showing the firing rate of a neuron on every trial as a function of the direction of the mouse relative to the lever box. **b**, Trial matrix after shifting all trials together so that the highest mean firing rate is aligned to 0. This preserves the relative direction of firing across trials. **c**, Trial matrix after aligning the firing rate on each trial so that its peak is at 0. This eliminates the potential drift of the preferred direction on each trial. It was calculated the mean firing rate as a function of direction (white line), which served as an idealised tuning curve of the neuron. **d**, Cross-correlation between the firing rate on each trial (matrix shown in **b**) and the idealised tuning curve of the neuron (white line in **c**). **e,** Same as in **d,** but fewer trials are shown. The vertical red bars, which are aligned to the peak of each trial's cross-correlation, represent the neuron's directional trial driftthe cross-correlation of each trial, represent the directional trial drift of the neuron. **f**, Distribution of directional trial drift for a lever-box-anchored neuron during the dark trials of a single session.

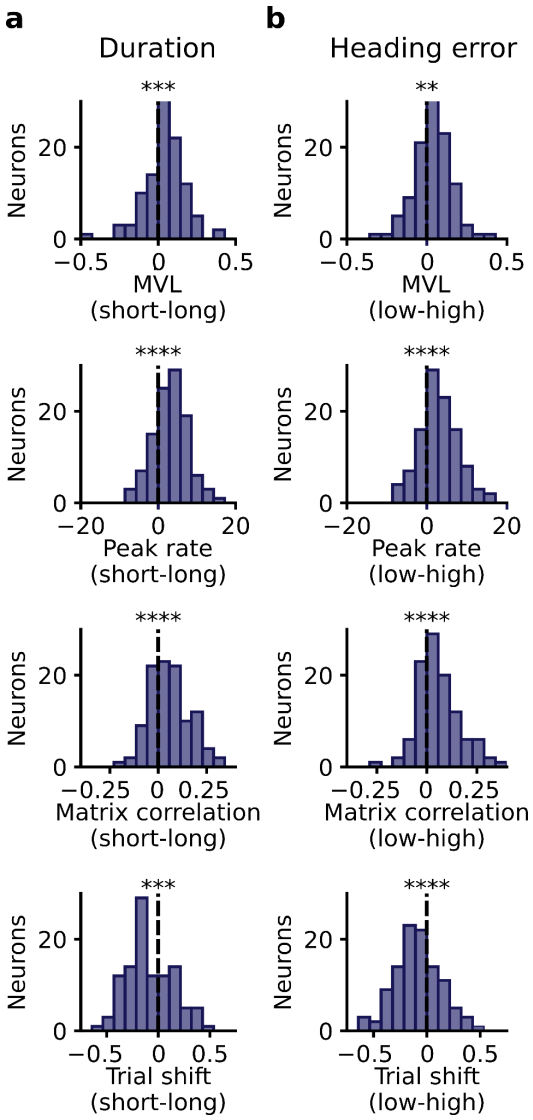

Supplementary Fig. 4. Effect of search path duration and search heading error on the directional selectivity of lever-box-anchored firing fields. a, Change in directional selectivity between trials with short and long search path duration. Trials were divided into two equal-sized groups containing short and long search duration trialstrials with short and long search duration. Spatial directionality was assessed using the mean vector length (MVL) and peak rate of the directional firing rate histogram, the trial matrix correlation and the directional trial drift. The plots show the difference in these four measures of directional selectivity between trials with short and long search paths ([(Short) - (Long)], Wilcoxon signed-rank tests, MVL: $P = 4.0 \times 10^{-5}$, peak rate: $P = 4.13 \times 10^{-9}$, trial matrix correlation: $P = 1.35 \times 10^{-7}$, and trial drift: $P = 1.36 \times 10^{-4}$). **b**, Same as **a** but for search heading error instead of search path duration. The plots show the difference in directional selectivity between trials with low and high heading errors during the search path ([(Short) - (Long)]). Heading error during the search path was defined as the angle

between a vector pointing in the direction of movement of the mouse and a vector from the animal head to the center of the lever box. The angle was calculated at 30 Hz, and the median of each trial was calculated. Trials were classified as low and high heading errors based on whether their heading error was lower or higher than the median of each recording session (Wilcoxon signed-rank tests, MVL: $P = 0.0012$, peak rate: $P = 8.14 \times 10^{-9}$, trial matrix correlation: $P = 1.35 \times 10^{-7}$, and trial drift: $P = 5.42 \times 10^{-5}$). $^{**}P < 0.01$, $^{***}P < 0.001$, $^{****}P < 0.0001$.

8. List of figures

9. List of abbreviations

ADN	Anterior dorsal thalamic nucleus
AutoPI	Automated path integration task
CA	Cornu Ammonis
HD	Head-direction
IFR	Instantaneous firing rate
LDA	linear discriminant analysis
LEC	lateral entorhinal cortex
MEC	Medial entorhinal cortex
MVL	Mean vector length
PCA	Principal components analysis
PI	Path integration
PRC	Perirhinal cortex
ROS	Robot Operating System
SWR	Sharp wave ripple
VR	Virtual reality

10. Contributions

The work described here was conducted in the Department of Clinical Neurobiology of the Medical Faculty of the Heidelberg University and the German Cancer Research Center (DKFZ, Heidelberg) under the supervision of Prof. Hannah Monyer and Dr. Kevin Allen. The daily scientific supervision was provided by Dr. Kevin Allen.

The Material and Method section and the result section is based on a manuscript that is under consideration at Nature Neuroscience journal (also in bioRxiv). The title of the manuscript is “Hippocampal firing fields anchored to a moving object predict homing direction during path-integration-based behavior”.

Adrian Tymorek developed the AutoPIRos package which enabled us to automatize the setup. He also trained the first three mice which we trained in this task.

Ting-Yun Yen updated the behavioral setup which then reduced the time we had to spend fixing the setup. She also helped training of some mice for this task.

Felix Jose Kavarayil, helped me for training of the mice and developed a new arena which then eased the troubleshooting of the setup.

Moritz Stingl, Sherman Richard Chau, Benay Baskurt, Celia García Vilela were master students under my supervision that helped me train mice both for the behaviour and the recording part of the thesis.

11. Acknowledgement:

I want to thank my supervisor, **Dr. Kevin Allen**, for allowing me to conduct my PhD in his group. Thank you for being there whenever I reached you, even during weekends or public holidays. Also, thank you so much for teaching me the scientific way of problem-solving, and for the help with troubleshooting recording setups or python code. Thanks for growing as a supervisor and mentor with me along this way. I want to thank **Prof. Hannah Monyer** for accepting to be my first supervisor and supporting me during these years. I want to thank **Dr. Elke Fuchs** for reading and proofreading this thesis. Thank you for providing and breeding the mice for this experiment whenever we needed it. I want to thank **Dr. Antonio Caputi** for providing valuable feedback on the manuscript. Thanks for allowing having scientific and real-world discussions in the lab.

I thank **Isabel Barriuso** for being my friend and colleague during my PhD. Thanks for providing mental support whenever I needed it. Thanks for reading and proofreading this thesis. Also, I would like to thank you for introducing me to the world of card games. I want to thank **Beate Throm** for being my colleague and friend during my PhD. Thanks for listening to me even when you have to do three experiments simultaneously. Thank you for reading and proofreading this thesis. Also thank you for playing tennis with me although my tennis skills are not as advanced as yours. I want to thank **Marcel Weinreich** for being my friend and colleague. Thank you so much for helping me fix the setup whenever I was lost, even when you were so busy with your experiments. Thank you for providing the mental support during these years and listening to my complaints even when It was not making sense. I want to thank **Felix Jose Kavarayil** for being a friend and colleague in the last year of my PhD. Thanks for having the tea time breaks with me. Also, thank you for changing the arena and helping me training mice. I would also like to thank my master's students **Moritz Stingl, Sherman Richard Chau, Benay Baskurt, and Celia García Vilela.** Thank you so much for helping me train mice for this experiment. Without your help, I would not have done training or recording from enough mice for this thesis.